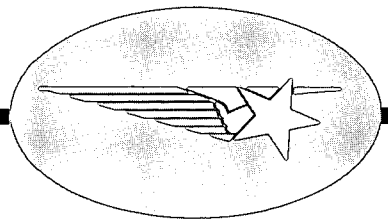

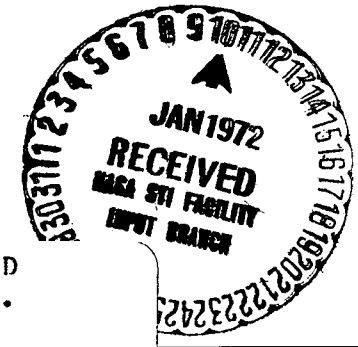

N72-14363 (NASA-CR-114379) AIRBORNE AURORAL DATA AND SATELLITE DATA ANALYSIS Final Report S.B. Mende, et al (Lockheed Missiles and Space Co.) Oct. 1971 94 p CSCL 03B
Unclas 11361 G3/13
FACILITY (NASA CR OR TMX OR AD NUMBER) (CATEGORY)

Reproduced by
NATIONAL TECHNICAL
INFORMATION SERVICE
Springfield, Va. 22151

NASA CR 114379

AVAILABLE TO THE PUBLIC

AIRBORNE AURORAL DATA AND SATELLITE DATA ANALYSIS FINAL REPORT

By S.B. Mende and R.H. Eather

Distribution of this report is provided in the interest of information exchange. Responsibility for the contents resides in the author or organization that prepared it.

October 1971

Prepared Under Contract No. NAS2-6299

By

Lockheed Palo Alto Research Laboratories

For

Ames Research Center

National Aeronautics and Space Administration

SUMMARY

The photometric data taken during the 1969 CV990 expedition were analyzed in more detail. It was found that the so-called soft auroral zone extends right through the night side auroral zone. The soft precipitation is a permanent feature of the night side auroral zone and probably signifies the position of the plasma sheet. The harder auroras which include the conventional visible auroras occur less frequently. The intensity and mean energy of auroral electrons is correlated suggesting that the fluctuation in auroral intensity comes primarily from the variability of the acceleration mechanism rather than the variations in the particle population densities. The results were published in a number of oral presentations and in scientific journals. During the 1969 CV990 expedition, coordinated data was taken with the Lockheed particle experiments on OV1-18 and ATS-5 satellites. The satellite data was reduced to facilitate coordinated investigations with the airborne experimenters. The airborne photometric λ5200 NI data were analyzed and the effective life time was found to be 4.5 minutes.

OBJECTIVE

To provide a final summary of the work accomplished in the program entitled "Satellite Data Analysis" under Contract Number NAS2-6299.

INTRODUCTION

In the framework of a previous program entitled "6 Channel Photometric Observations from the CV990 Aircraft" (NASw 1997), Lockheed instrumentation and scientific personnel took part in the 1969 NASA CV990 auroral aircraft expedition.

The data taken during this expedition was combined with the data taken during the 1968 expedition and was analyzed during the present program.

The data obtained during the two expeditions constitutes an extremely fine body of absolute photometric observations of the aurora. No comparable body of data having such extensive coverage, high sensitivity, and high resolution exists. The absolute calibration permits the direct interpretation of the measurements. The regularity and frequency of the observations permits the use of statistical methods. The zenithal total column intensity measurements can be very simply interpreted as absolute particle intensities. The high altitude aircraft platform permitted the spatial scanning of the aurora. The uncertainties normally introduced by lower atmospheric scattering and absorption are minimized by the high altitude aircraft platform.

The analysis of the data did produce some very significant results in the understanding of the auroras. Further analysis of this type of data still promises great returns and there are a large number of questions which could be answered by the more detailed analysis of these data.

There have been a number of observations during the 1969 aircraft expedition which were coordinated with the Lockheed experiments on OV1-18 and ATS-5 satellites. One of the purposes of this contract was to reduce the satellite data into a form which is amenable for analysis and comparison with the airborne data.

ACCOMPLISHMENTS

New Results From Photometric Data

The Lockheed airborne data was analyzed in more detail and a number of new discoveries were made during the period of this contract as regards to the properties of the aurora.

1. The dayside soft-zone is associated with the dayside cusp region and the particles are soft being of magnetosheath energies (Eather and Mende, 1971a).
2. In the nightside auroral zone, two types of electron auroras occurred; namely, the hard aurora generated by electrons in the keV range and the softer aurora, often subvisual, generated by electrons in the 100-1000 eV range (Eather and Mende, 1971b).
3. The occurrence of soft auroras are very widespread and occur continuously within the nightside of the oval. The hard types occur less frequently. The nightside soft zone at higher latitude is caused by the absence of the hard components (Eather and Mende, 1971c).
4. The soft precipitation is related to the plasma sheet, both in mean energy and flux of electrons (Eather and Mende, 1971b).
5. The intensity of auroras are correlated with mean energy. The ratio of 6300 and 4278 intensities decreases with increasing 4278 intensity. The 5577 to 4278 intensity ratio also follows this same tendency, but to a lesser extent (Eather and Mende, 1971c).
6. The mean electron energy at precipitation fluctuates very largely in the aurora while the number flux is relatively constant (Eather and Mende, 1971b,c).
7. A technique was developed in which a rough measurement of auroral primary parameters could be obtained from ground based observations. These parameters are: proton flux, electron energy flux,

mean electron energy parameter. This provides a technique of monitoring these quantities without the use of a spacecraft (Eather and Mende, 1971c).

Reduction of Satellite Data

The satellite data were reduced to absolute calibrated particle fluxes for the coordination periods listed. The satellite data are included in this report as Appendix 2.

Dissemination of the Airborne Photometer Data

The Lockheed photometric airborne data was distributed in March 1971 in a format requested by the other experimenters. The program was rerun and the required number of output copies were generated by Lockheed.

λ5200 NI Analysis

λ5200 NI is a forbidden line from atomic nitrogen with a very long upper-level lifetime of 26 hours. Hence, quenching is severe, but the line still appears in auroral spectra with appreciable intensity, implying that the excitation rate to the upper level must be exceedingly large.

We have previously reported statistical plots of the rates of λ5200/λ4278 as a function of latitude, and shown that such a plot confirms the existence of soft-electron precipitation at high latitudes (Eather and Mende, 1971).

We have also attempted to determine the effective lifetime of the ^2D upper level. Fig. 1 shows a plot of λ5200, λ6300 and λ5577 during about 1 hour of active aurora. It may be seen that λ5200 and λ6300 show very similar behavior, and both are sluggish compared to λ5577. This implies λ5200 and λ6300 have quite similar effective lifetimes. We filtered the λ5577 signal with a t = 100 sec filter, using digital computer techniques and got the curve labeled "filtered 5577". From this we see that during the first 20 minutes of the event, 100 sec is a fair estimate of effective lifetime of both λ6300 and λ5200.

We used data from all flights to determine the fractional change in λ5200 intensity and λ6300 intensity for a given fractional change in the excitation rate (proportional to λ4278 N_2^+ intensity), and these results are shown in Figure 2. It may be seen that, on the average, λ5200 is more sluggish then λ6300 and does not follow changes in the excitation rate as quickly as does λ6300. To a first approximation, the ratio of slopes on the graph gives ratios of effective upper-level lifetimes.

i.e. NI ^2D effective lifetime $\simeq$ 2.7 x OI ^1D effective lifetime

Most λ6300 emission comes from ≥ 250 km with effectife lifetimes of 100 sec, so we imply the NI ^2D effective lifetime is 4-1/2 minutes. This agrees well with an independent determination from airglow measurements (Weill, 1969).

Any further analysis (such as deriving excitation rates and height of emission) involves a knowledge of excitation and quenching processes, and we do not know enough about these to make this a profitable exercise. Dr. M.H. Rees is considering if he can use his measurements of NI (^2P - ^4S) at λ3466 to further this investigation.

PUBLICATIONS

In accordance with the contract, the results were published and the project scientists attended meetings where they read papers.

Dr. S. B. Mende and Dr. R. H. Eather were both at the AGU meeting in Washington in April 1971 and both gave related papers.

Dr. R. H. Eather presented a paper at the Advanced Study Institut, Dalseter, Norway, April 1971.

Dr. S. B. Mende attended the IUGG meeting in Moscow in August 1971 where a paper was given. Similarly, he attended the Cortina Advanced Study Institut in September 1971 and presented another short paper.

Complete list of publications of this year's work arising from this contract is in Appendix 1 of this report.

CONCLUSIONS

The satellite data have been reduced into a suitable form for coordinated investigation. There are a number of interesting possibilities in coordinating with airborne experimenters. Quantitative comparisons can be made so that the absolute efficiencies generating the visible and infrared emissions could be evaluated.

The Lockheed photometric data should be analyzed further and substorm times introduced into the data. All the data analysis so far took large averages regardless of the status of the magnetosphere. The substorm occurrence times should be established for all flights from world wide magnetograms. This then has to be introduced into the statistical analysis.

The conclusions of the airborne photometer experiment are summarized in the review paper entitled "High Latitude Particle Precipitation and Source Regions in the Magnetosphere." A preprint of this paper is attached to this report as Appendix 3.

REFERENCES

1. Eather, R. H., S. B. Mende, Airborne Observations of Auroral Precipitation Patterns. J. Geophys. Res. 76, pp. 1746-1755, 1971a.

2. Eather, R. H., S. B. Mende, High Latitude Precipitation and Source Regions in the Magnetosphere. Magnetosphere Ionosphere Interactions, Dalseter, Norway, April 1971b.

3. Eather, R. H., S. B. Mende, "Systematics in Auroral Energy Spectra." J. Geophys. Res. Accepted for publication, 1971e.

4. Weill, G. M., NI(^{4}S - ^{2}D). Radiation in the night airglow and low latitude aurora. Atmospheric Emissions Ed. B. M. McCormac, Van Norstad, pp. 449-470.

5. Reed, R. D., E. G. Shelley, J. C. Bakke, T. C. Sanders and J. D. McDaniel, IEEE Trans. Nucl. Sci-NS-16, 359, 1969.

6. Sharp, R. D., E. G. Shelley, R. G. Johnson, G. Paschman, J. Geophys. Res. 75, 6092, 1970.

7. Paschman, G., Untersuchungen des Elektroneneinfalls in die polare atmosphare, Doctor's Thesis, Max Planck Institut fur Physik und Astrophysik, Munich, Germany, March 1971.

8. Sharp, R. D., R. G. Johnson, Low energy auroral particle measurements from polar satellites, in "The Radiating Atmosphere" Ed. by B. M. McCormac, Reidel Publ. Co., Dordrecht, Holland, 1971.

9. Sharp, R. D., D. L. Carr, R. G. Johnson, E. G. Shelley, Coordinated Auroral Electron Observations from a Synchronous and a Polar Satellite, J. Geophys. Res., Nov. 1971 (in press).

FIGURE CAPTIONS

Figure 1. Active aurora as observed in 5200A, 6300A and 5577A. The curve labeled filtered 5577 includes an assumed filter with a time constant of 100 sec.

Figure 2. Fractional change in 5200A and 6300A as a function of fractional change in 4278A.

Figure 3-56. Satellite data of Appendix 2.

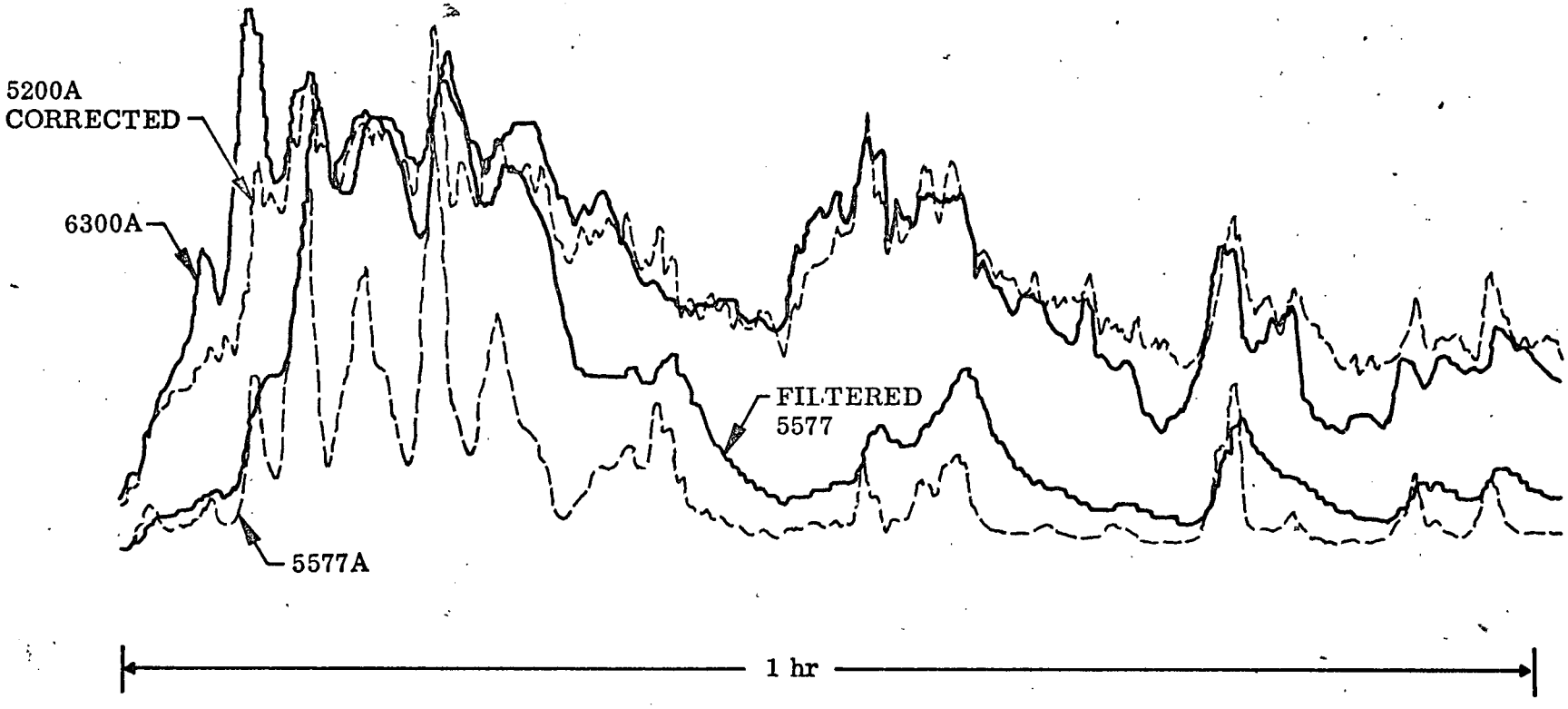

Figure 1.

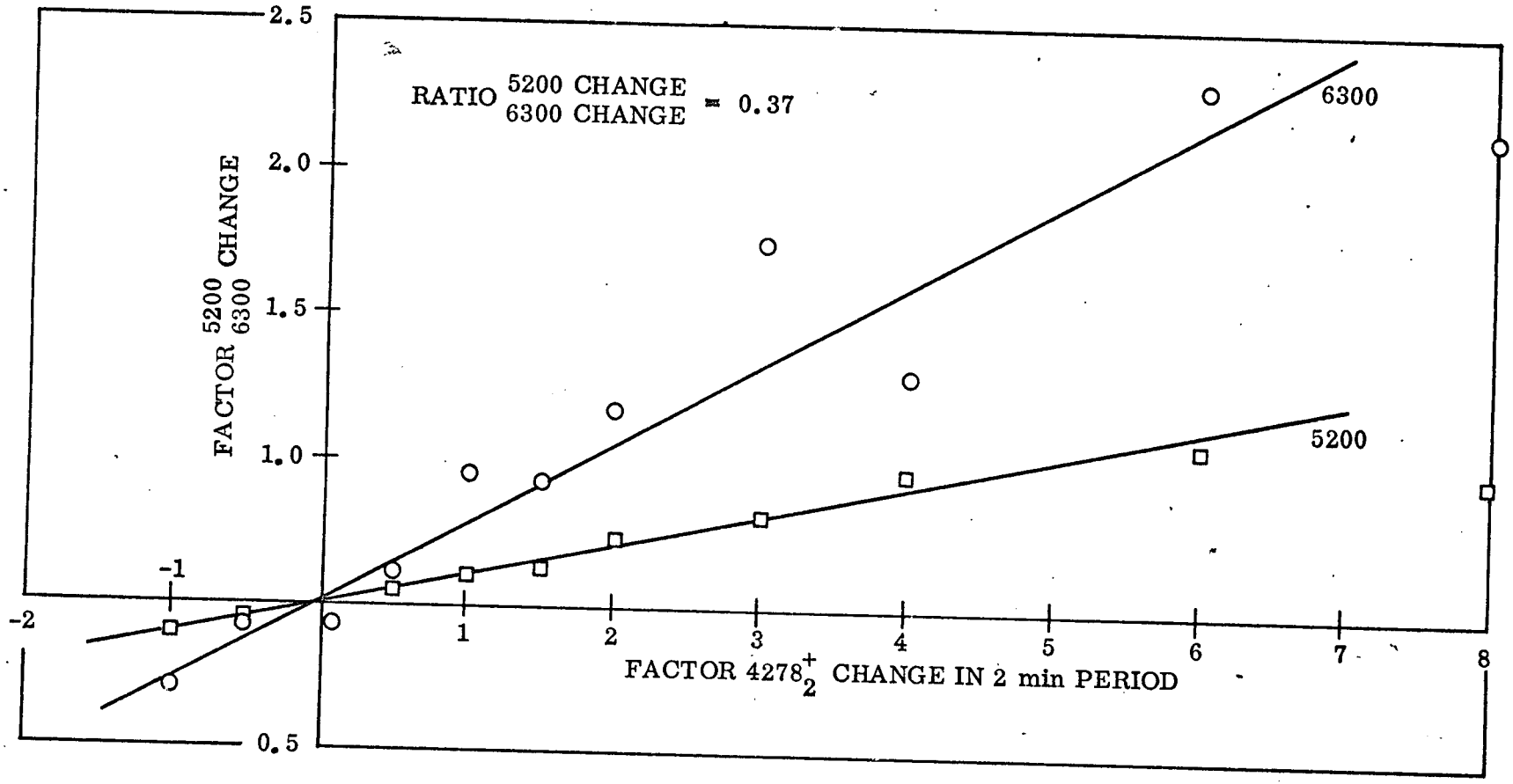
RATIO 5200 CHANGE / 6300 CHANGE = 0.37
6300
5200
FACTOR 5200 / 6300 CHANGE
2.5
2.0
1.5
1.0
0.5
-2
-1
1
2
3
4
5
6
7
8
FACTOR 4278$_2^+$ CHANGE IN 2 min PERIOD

figure 2.

APPENDIX 1

LIST OF PUBLICATIONS THIS YEAR (1971) FROM CONTRACT NAS2-6299

Mende, S.B., R.H. Eather, Auroral Intensity Ratios Related to the Energy of Precipitating Particles. Trans. A.G.U., pp. 305, April 1971.

Eather, R.H., High Latitude Dayside Aurora. Trans. A.G.U., pp. 319, April 1971.

Eather, R.H., S.B. Mende, High Latitude Particle Precipitation and Source Regions in the Magnetosphere, Magnetosphere Ionosphere Interaction, Dalseter, Norway, April 1971. To be published in the conference proceedings.

Mende, S.B., R.H. Eather, Auroral Intensity Ratios Related to the Energy of Precipitating Particles. Presented at Moscow meeting of IUGG August 1971.

Mende, S.B., R.H. Eather, "Systematics in Auroral Intensity Ratios," presented at Advanced Study Institut, Cortina, September 1971, Italy. To be published in the proceedings of the Institut.

Eather, R.H., and S.B. Mende, "Systematics in Auroral Energy Spectra". Accepted for publication. J. Geophys. Res.

SATELLITE DATA:

Coordinated observations with the ATS-5 synchronous satellite were acquired on five nights and with the OV1-18 polar satellite on one night as indicated in Table I. Both of these satellites contained similar experiments designed to measure the fluxes of auroral electrons and protons in the keV range. The experiments and some typical results have been described in references 5 through 9. They utilize channel multiplier sensors and either magnetic analyses or foil threshold techniques to define the energy ranges. The ATS-5 experiment provides a measurement of the trapped electron fluxes at 6.6 RE in four energy intervals and the trapped proton fluxes (integral) above three thresholds as indicated in Table II. The OV1-18 experiment provides a measurement of precipitating particles. The energy ranges of the OV1-18 detectors utilized for this study are indicated in Table III. Data will be presented at two pitch angles; one for the group 1 detectors, (CME-1A, CFP-1B, etc.) and one for the group 2 and 3 detectors (CME-2A, CME-3B, CMP-3A, CFP-2C, etc.).

The ATS-5 data for the times of interest are given in Figures 3 - 54 on two different time scales - twenty-four-hour plots of the fluxes are shown in Figures 3 - 44 in order to present the data in the context of the substorm activity of the entire day. Then an expanded scale plot of the fluxes at the specific times of the coordination are presented in Figures 45 - 54. The ATS-5 satellite throughout this period was maintained with latitude ≤ 2.40, and a geocentric distance of 6.61 RE. The longitude varied from 104.7° east on November 24 to 103.9° east on December 6.

The OV1-18 ephemeris data for the coordinated overpass is given in Table IV and the fluxes as measured by the various detectors every one second are presented in Table V for a 200-second

period approximately centered on the time of the overpass of the aircraft. Figures 55 and 56 show the integral electron fluxes and the average electron energy (for electrons in the energy range 0.8 - 16.3 keV) as well as the pitch angle at which the measurements were acquired (180° corresponds to the detector looking up the field line) for the two sets of detectors, group 1 (Fig. 55) and groups 2 and 3 (Fig. 56). The integral proton detectors were at their background levels throughout the period of the overpass. The CMP-3B and CMP-3C proton detectors were responding at satellite times near 905,300 seconds and the measured flux levels are tabulated in Table V. The CMP flux values should be multiplied by the following scale factors: CMPA x 1.88; CMPB x 1.92; CMPC x 1.30. The appropriate pitch angle is given in Fig. 56 as a function of satellite time.

Table I

COORDINATION WITH ATS-5 AND OV1-18 SATELLITE

Flight No.	Date 1969	Time U.T.	Aircraft Latitude (N)	Aircraft Longitude (W)	Satellite Coordination
2	Nov. 24	12:15	52°52'	96°34'	ATS-5
3	Nov. 26	01:05	55°25'	96°38'	ATS-5
4	Nov. 27 Nov. 27	00:46 05:21	55°45' 55°45'	96°27' 96°24'	ATS-5
5	Nov. 29	03:41 to 06:39	(Grid Pattern About Conjugate Point)		ATS-5
8	Dec. 5	10:51	55°45'	96°24'	ATS-5
9	Dec. 7	08:32 08:56	55°45' 55°37'	96°21' 96°28'	ATS-5
10	Dec. 8	10:18	59°29'	103°12'	OV1-18

Table II

ENERGY RANGE OF THE ATS-5 DETECTORS

Detector	Particle	Energy Range (keV)
CME-A	e	0.65- 1.9
CME-B	e	1.8 - 5.4
CME-C	e	5.9 -17.8
CME-D	e	17.4 -53
CFP-A	p	> 5
CFP-B	p	> 15
CFP-C	p	> 38

Table III

ENERGY RANGES OF THE OV1-18 DETECTORS

Detector	Particle	Energy Range (keV)
CME-1A	e	0.8 - 1.5
CME-1B	e	1.75- 3.3
CME-1C	e	3.75- 7.0
CME-1D	e	8.3 -16.3
CME-1E	e	17.3 -37.0
CME-2A	e	0.8 - 1.5
CME-3B	e	1.8 - 3.25
CME-3C	e	3.7 - 7.0
CME-2D	e	8.4--16.3
CMP-3A	p	0.40 - 1.2
CMP-3B	p	.88 - 2.6
CMP-3C	p	2.9 - 8.7
CFP-1B	p	> 9
CFP-1D	p	> 38
CFP-2A	p	> 5
CFP-3B	p	> 7.7
CFP-2C	p	>24
CFP-3D	p	>38

Table IV

OV1-18 EPHEMERIS DATA DEC. 8, 1969 (ACQ 4027)

Satellite Time (seconds)	UT (seconds)	Geodetic Latitude	Geocentric Latitude	East Longitude	Altitude (km)
905200	36921	65.68	65.55	262.36	532
905250	36971	62.74	62.60	259.59	534
905300	37021	59.77	59.61	257.29	536
905350	37071	56.76	56.60	255.34	538
905400	37121	53.74	53.57	25.36	540

TABLE V.

WRITE DIFFERENTIAL FLUX

ST	CME1A	CME1B	CME1C	CME1D	CME1E	CME2A
22905200.	.629+06	.205+06	.991+05	.121+05	.286+04	.484+06
22905201.	.629+06	.205+06	.991+05	.121+05	.286+04	.484+06
22905202.	.629+06	.205+06	.991+05	.121+05	.286+04	.484+06
22905203.	.629+06	.205+06	.991+05	.121+05	.286+04	.484+06
22905204.	.629+06	.205+06	.991+05	.121+05	.286+04	.484+06
22905205.	.629+06	.205+06	.991+05	.121+05	.286+04	.484+06
22905206.	.629+06	.205+06	.991+05	.121+05	.286+04	.484+06
22905207.	.629+06	.205+06	.991+05	.121+05	.286+04	.484+06
22905208.	.629+06	.205+06	.991+05	.121+05	.286+04	.484+06
22905209.	.629+06	.205+06	.991+05	.121+05	.286+04	.484+06
22905210.	.629+06	.205+06	.991+05	.121+05	.286+04	.484+06
22905211.	.629+06	.205+06	.991+05	.121+05	.286+04	.484+06
22905212.	.629+06	.205+06	.991+05	.121+05	.286+04	.484+06
22905213.	.629+06	.205+06	.991+05	.121+05	.286+04	.484+06
22905214.	.629+06	.205+06	.991+05	.121+05	.286+04	.484+06
22905215.	.629+06	.205+06	.991+05	.121+05	.286+04	.484+06
22905216.	.629+06	.205+06	.991+05	.121+05	.286+04	.484+06
22905217.	.629+06	.205+06	.991+05	.121+05	.286+04	.484+06
22905218.	.629+06	.205+06	.991+05	.121+05	.286+04	.484+06
22905219.	.629+06	.205+06	.991+05	.121+05	.286+04	.484+06
22905220.	.629+06	.205+06	.991+05	.121+05	.286+04	.484+06
22905221.	.629+06	.205+06	.991+05	.121+05	.286+04	.484+06
22905222.	.629+06	.205+06	.991+05	.121+05	.286+04	.484+06
22905223.	.629+06	.205+06	.991+05	.121+05	.286+04	.484+06
22905224.	.629+06	.205+06	.991+05	.121+05	.286+04	.484+06
22905225.	.629+06	.205+06	.991+05	.121+05	.286+04	.484+06
22905226.	.629+06	.205+06	.991+05	.121+05	.286+04	.484+06
22905227.	.629+06	.205+06	.991+05	.121+05	.286+04	.484+06
22905228.	.629+06	.205+06	.991+05	.121+05	.286+04	.484+06
22905229.	.964+07	.205+06	.991+05	.121+05	.286+04	.857+07
22905230.	.612+08	.972+07	.244+06	.121+05	.286+04	.318+08
22905231.	.457+08	.114+08	.159+06	.121+05	.286+04	.297+08
22905232.	.495+08	.483+07	.991+05	.121+05	.286+04	.184+08
22905233.	.221+08	.156+07	.991+05	.121+05	.286+04	.857+07
22905234.	.579+07	.587+06	.991+05	.121+05	.286+04	.441+07
22905235.	.964+07	.807+06	.991+05	.121+05	.286+04	.592+07
22905236.	.456+07	.205+06	.991+05	.121+05	.286+04	.484+06
22905237.	.245+07	.205+06	.991+05	.121+05	.286+04	.104+07
22905238.	.159+07	.205+06	.991+05	.121+05	.286+04	.484+06
22905239.	.629+06	.205+06	.991+05	.121+05	.286+04	.484+06
22905240.	.629+06	.205+06	.991+05	.121+05	.286+04	.484+06
22905241.	.629+06	.205+06	.991+05	.121+05	.286+04	.484+06
22905242.	.120+07	.205+06	.991+05	.121+05	.286+04	.484+06
22905243.	.245+07	.205+06	.991+05	.121+05	.286+04	.104+07
22905244.	.159+07	.205+06	.991+05	.121+05	.286+04	.104+07
22905245.	.159+07	.205+06	.991+05	.121+05	.286+04	.150+07
22905246.	.629+06	.205+06	.991+05	.121+05	.286+04	.484+06
22905247.	.629+06	.205+06	.991+05	.121+05	.286+04	.104+07
22905248.	.629+06	.205+06	.991+05	.121+05	.286+04	.484+06
22905249.	.629+06	.205+06	.991+05	.121+05	.286+04	.484+06
22905250.	.840+06	.205+06	.991+05	.121+05	.286+04	.484+06
22905251.	.629+06	.205+06	.991+05	.121+05	.286+04	.150+07
22905252.	.851+07	.807+06	.991+05	.121+05	.286+04	.441+07
22905253.	.293+07	.205+06	.991+05	.121+05	.286+04	.150+07
22905254.	.120+07	.205+06	.991+05	.121+05	.286+04	.254+07

ST	CMEIA	CMEIB	CMEIC	CMEID	CMEIE	CMEZA
22905255.	.704+08	.697+07	.159+06	.121+05	.286+04	.550+08
22905256.	.866+08	.589+08	.496+07	.372+05	.286+04	.775+08
22905257.	.809+08	.478+08	.422+07	.260+05	.286+04	.775+08
22905258.	.238+08	.825+07	.539+06	.121+05	.286+04	.168+08
22905259.	.106+08	.156+07	.991+05	.121+05	.286+04	.105+08
22905260.	.293+07	.587+06	.991+05	.121+05	.286+04	.254+07
22905261.	.629+06	.205+06	.991+05	.121+05	.286+04	.484+06
22905262.	.629+06	.205+06	.991+05	.121+05	.286+04	.484+06
22905263.	.629+06	.205+06	.991+05	.121+05	.286+04	.484+06
22905264.	.629+06	.205+06	.991+05	.121+05	.286+04	.484+06
22905265.	.629+06	.205+06	.991+05	.121+05	.286+04	.484+06
22905266.	.344+07	.104+07	.991+05	.121+05	.286+04	.676+07
22905267.	.879+07	.216+07	.991+05	.121+05	.286+04	.592+07
22905268.	.722+07	.129+07	.991+05	.121+05	.286+04	.952+07
22905269.	.879+07	.507+06	.244+06	.121+05	.286+04	.218+08
22905270.	.299+08	.355+07	.336+06	.121+05	.286+04	.257+08
22905271.	.257+08	.395+07	.244+06	.121+05	.286+04	.297+08
22905272.	.169+08	.438+07	.244+06	.121+05	.286+04	.218+08
22905273.	.126+08	.282+07	.336+06	.121+05	.286+04	.105+08
22905274.	.651+07	.185+07	.159+06	.121+05	.286+04	.952+07
22905275.	.161+08	.318+07	.434+06	.121+05	.286+04	.297+08
22905276.	.299+08	.638+07	.105+07	.121+05	.286+04	.257+08
22905277.	.204+08	.583+07	.539+06	.121+05	.286+04	.168+08
22905278.	.137+08	.318+07	.244+06	.121+05	.286+04	.128+08
22905279.	.148+08	.395+07	.336+06	.121+05	.286+04	.342+08
22905280.	.755+08	.166+08	.167+07	.121+05	.286+04	.952+08
22905281.	.809+08	.363+08	.357+07	.121+05	.882+04	.889+08
22905282.	.612+08	.274+08	.299+07	.121+05	.286+04	.515+08
22905283.	.299+08	.896+07	.134+07	.121+05	.286+04	.257+08
22905284.	.137+08	.438+07	.134+07	.121+05	.286+04	.116+08
22905285.	.106+08	.129+07	.434+06	.121+05	.286+04	.128+08
22905286.	.148+08	.282+07	.775+06	.121+05	.286+04	.237+08
22905287.	.174+08	.483+07	.775+06	.121+05	.286+04	.257+08
22905288.	.964+07	.483+07	.906+06	.121+05	.286+04	.257+08
22905289.	.106+08	.436+07	.434+06	.121+05	.286+04	.141+08
22905290.	.516+07	.395+07	.434+06	.121+05	.286+04	.116+08
22905291.	.584+07	.483+07	.336+06	.121+05	.286+04	.857+07
22905292.	.398+07	.483+07	.539+06	.121+05	.286+04	.116+08
22905293.	.456+07	.532+07	.653+06	.121+05	.286+04	.123+08
22905294.	.293+07	.483+07	.336+06	.121+05	.286+04	.184+08
22905295.	.201+07	.318+07	.336+06	.121+05	.286+04	.200+08
22905296.	.245+07	.318+07	.336+06	.121+05	.286+04	.237+08
22905297.	.201+07	.318+07	.159+06	.121+05	.286+04	.257+08
22905298.	.159+07	.282+07	.336+06	.121+05	.286+04	.200+08
22905299.	.629+06	.185+07	.991+05	.121+05	.286+04	.168+08

ST	CME1A	CME1B	CME1C	CME1D	CME1E	CME2A
22905355.	.245+07	.205+06	.991+05	.121+05	.286+04	.484+06
22905356.	.640+06	.205+06	.991+05	.121+05	.286+04	.484+06
22905357.	.629+06	.587+06	.991+05	.121+05	.286+04	.618+06
22905358.	.629+06	.205+06	.991+05	.121+05	.286+04	.150+07
22905359.	.120+07	.205+06	.991+05	.121+05	.286+04	.484+06
22905360.	.201+07	.205+06	.991+05	.121+05	.286+04	.150+07
22905361.	.629+06	.205+06	.991+05	.121+05	.286+04	.484+06
22905362.	.629+06	.205+06	.991+05	.121+05	.286+04	.484+06
22905363.	.629+06	.205+06	.991+05	.121+05	.286+04	.484+06
22905364.	.629+06	.205+06	.991+05	.121+05	.286+04	.484+06
22905365.	.629+06	.205+06	.991+05	.121+05	.286+04	.484+06
22905366.	.629+06	.205+06	.991+05	.121+05	.286+04	.484+06
22905367.	.629+06	.205+06	.991+05	.121+05	.286+04	.484+06
22905368.	.629+06	.205+06	.991+05	.121+05	.286+04	.618+06
22905369.	.629+06	.205+06	.991+05	.121+05	.286+04	.484+06
22905370.	.629+06	.205+06	.991+05	.121+05	.286+04	.484+06
22905371.	.629+06	.205+06	.991+05	.121+05	.286+04	.484+06
22905372.	.629+06	.205+06	.991+05	.121+05	.286+04	.484+06
22905373.	.629+06	.205+06	.991+05	.121+05	.286+04	.484+06
22905374.	.629+06	.205+06	.991+05	.121+05	.286+04	.484+06
22905375.	.629+06	.205+06	.991+05	.121+05	.286+04	.484+06
22905376.	.629+06	.205+06	.991+05	.121+05	.286+04	.484+06
22905377.	.629+06	.205+06	.991+05	.121+05	.286+04	.484+06
22905378.	.629+06	.205+06	.991+05	.121+05	.286+04	.484+06
22905379.	.629+06	.205+06	.991+05	.121+05	.286+04	.484+06
22905380.	.629+06	.205+06	.991+05	.121+05	.286+04	.484+06
22905381.	.629+06	.205+06	.991+05	.121+05	.286+04	.484+06
22905382.	.629+06	.205+06	.991+05	.121+05	.286+04	.484+06
22905383.	.629+06	.205+06	.991+05	.121+05	.286+04	.484+06
22905384.	.629+06	.205+06	.991+05	.121+05	.286+04	.484+06
22905385.	.629+06	.205+06	.991+05	.121+05	.286+04	.484+06
22905386.	.629+06	.205+06	.991+05	.121+05	.286+04	.484+06
22905387.	.629+06	.205+06	.991+05	.121+05	.286+04	.484+06
22905388.	.629+06	.205+06	.991+05	.121+05	.286+04	.484+06
22905389.	.629+06	.205+06	.991+05	.121+05	.286+04	.484+06
22905390.	.629+06	.205+06	.991+05	.121+05	.286+04	.484+06
22905391.	.629+06	.205+06	.991+05	.121+05	.286+04	.484+06
22905392.	.629+06	.205+06	.991+05	.121+05	.286+04	.484+06
22905393.	.629+06	.205+06	.991+05	.121+05	.286+04	.484+06
22905394.	.629+06	.205+06	.991+05	.121+05	.286+04	.484+06
22905395.	.629+06	.205+06	.991+05	.121+05	.286+04	.484+06
22905396.	.629+06	.205+06	.991+05	.121+05	.286+04	.484+06
22905397.	.629+06	.205+06	.991+05	.121+05	.286+04	.484+06
22905398.	.629+06	.205+06	.991+05	.121+05	.286+04	.484+06
22905399.	.629+06	.205+06	.991+05	.121+05	.286+04	.484+06

ST	CMP3A	CMP3B	CMP3C	CME3B	CME3C	CME2D
22905300.	.551+05	.535+05	.124+06	.642+07	.160+07	.177+06
22905301.	.551+05	.206+05	.107+06	.589+07	.131+07	.347+06
22905302.	.551+05	.710+05	.480+05	.589+07	.160+07	.907+05
22905303.	.551+05	.360+05	.346+05	.589+07	.212+07	.131+06
22905304.	.551+05	.360+05	.138+05	.589+07	.231+07	.282+06
22905305.	.551+05	.206+05	.138+05	.642+07	.160+07	.177+06
22905306.	.551+05	.206+05	.138+05	.332+07	.117+07	.177+06
22905307.	.551+05	.206+05	.138+05	.492+07	.131+07	.110+06
22905308.	.551+05	.206+05	.138+05	.406+07	.145+07	.153+06
22905309.	.551+05	.206+05	.138+05	.332+07	.131+07	.226+06
22905310	551+05	206+05	221+05	.332+07	.117+07	.282+06
22905311	551+05	206+05	138+05	.208+07	.145+07	.226+06
22905312.	.551+05	.206+05	.138+05	.236+07	.683+06	.153+06
22905313.	.950+05	.206+05	.138+05	.298+07	.683+06	.131+06
22905314.	.551+05	.206+05	.138+05	.208+07	.397+06	.563+05
22905315.	.551+05	.206+05	.138+05	.298+07	.793+06	.728+05
22905316	551+05	360+05	138+05	.266+07	.104+07	.907+05
22905317	551+05	535+05	138+05	298+07	104+07	408+05
22905318.	.551+05	.206+05	.138+05	236+07	683+06	158+05
22905319.	.551+05	.206+05	.138+05	.208+07	.581+06	.158+05
22905320.	.551+05	.206+05	.138+05	.298+07	.237+06	.158+05
22905321.	.551+05	.206+05	.138+05	.182+07	.683+06	.158+05
22905322.	.551+05	.206+05	.138+05	.298+07	.683+06	.158+05
22905323.	.551+05	.206+05	.138+05	.298+07	.486+06	.728+05
22905324	551+05	206+05	138+05	236+07	581+06	158+05
22905325	551+05	206+05	138+05	182+07	314+06	265+05
22905326.	.551+05	.535+05	.138+05	.236+07	.237+06	.158+05
22905327.	.551+05	.710+05	.138+05	.208+07	.581+06	.158+05
22905328.	.551+05	.206+05	.138+05	.182+07	.237+06	.265+05
22905329.	.551+05	.206+05	.138+05	.236+07	.314+06	.563+05
22905330	551+05	206+05	138+05	.266+07	.237+06	.158+05
22905331	551+05	206+05	138+05	.113+07	.397+06	.158+05
22905332.	.551+05	.206+05	.138+05	.158+07	.397+06	.158+05
22905333.	.551+05	.206+05	.138+05	.135+07	.314+06	.158+05
22905334.	.551+05	.206+05	.221+05	.113+07	.980+05	.158+05
22905335.	.551+05	.535+05	.138+05	.158+07	.397+06	.158+05
22905336.	.551+05	.206+05	.138+05	.158+07	.165+06	.158+05
22905337.	.551+05	.360+05	.138+05	.182+07	.486+06	.158+05
22905338.	.551+05	.535+05	.138+05	.113+07	.165+06	.158+05
22905339.	.551+05	.360+05	.138+05	.208+07	.980+05	.158+05
22905340.	.551+05	.206+05	.138+05	.158+07	.732+05	.158+05
22905341.	.551+05	.206+05	.138+05	.158+07	.165+06	.158+05
22905342.	.551+05	.206+05	.138+05	.182+07	.237+06	.158+05
22905343.	.551+05	.206+05	.138+05	.158+07	.237+06	.158+05
22905344.	.551+05	.206+05	.138+05	.135+07	.732+05	.158+05
22905345.	.551+05	.206+05	.138+05	.381+06	.165+06	.158+05
22905346.	.551+05	.206+05	.138+05	.135+07	.314+06	.158+05
22905347.	.551+05	.206+05	.138+05	.208+07	.314+06	.158+05
22905348.	.551+05	.206+05	.138+05	.182+07	.732+05	.158+05
22905349.	.551+05	.206+05	.138+05	.182+07	.980+05	.158+05
22905350.	.551+05	.206+05	.138+05	.113+07	.980+05	.158+05
22905351.	.551+05	.206+05	.138+05	.929+06	.980+05	.158+05
22905352.	.551+05	.206+05	.138+05	.381+06	.732+05	.158+05
22905353.	.551+05	.206+05	.138+05	.214+06	.732+05	.158+05
22905354.	.551+05	.535+05	.138+05	.581+06	.732+05	.265+05
22905355.	.551+05	.360+05	.138+05	.381+06	.732+05	.158+05
22905356.	.551+05	.360+05	.138+05	.562+06	.980+05	.158+05

ST	CMP3A *	CMP3B *	CMP3C *	CME3B	CME3C	CME2D
22905357.	,551+05	,360+05	,138+05	,562+06	,980+05	,158+05
22905358.	,551+05	,206+05	,138+05	,740+06	,732+05	,158+05
22905359.	,551+05	,206+05	,138+05	,381+06	,732+05	,158+05
22905360.	,551+05	,206+05	,138+05	,214+06	,980+05	,158+05
22905361.	,551+05	,206+05	,138+05	,214+06	,732+05	,158+05
22905362.	,551+05	,360+05	,346+05	,214+06	,732+05	,158+05
22905363.	,551+05	,206+05	,221+05	,214+06	,732+05	,158+05
22905364.	,551+05	,206+05	,346+05	,214+06	,980+05	,158+05
22905365.	,551+05	,206+05	,138+05	,381+06	,732+05	,158+05
22905366.	,551+05	,206+05	,138+05	,562+06	,732+05	,158+05
22905367.	,551+05	,206+05	,138+05	,214+06	,732+05	,158+05
22905368.	,551+05	,206+05	,138+05	,214+06	,732+05	,158+05
22905369.	,551+05	,535+05	,138+05	,381+06	,165+06	,158+05
22905370.	,551+05	,206+05	,138+05	,214+06	,732+05	,158+05
22905371.	,551+05	,206+05	,138+05	,214+06	,732+05	,158+05
22905372.	,551+05	,206+05	,138+05	,214+06	,732+05	,158+05
22905373.	,551+05	,206+05	,480+05	,214+06	,732+05	,158+05
22905374.	,551+05	,206+05	,138+05	,214+06	,732+05	,158+05
22905375.	,551+05	,206+05	,138+05	,562+06	,732+05	,158+05
22905376.	,551+05	,206+05	,138+05	,214+06	,732+05	,158+05
22905377.	,551+05	,206+05	,138+05	,562+06	,732+05	,158+05
22905378.	,551+05	,206+05	,138+05	,214+06	,732+05	,158+05
22905379.	,551+05	,206+05	,138+05	,214+06	,732+05	,158+05
22905380.	,551+05	,206+05	,138+05	,214+06	,732+05	,158+05
22905381.	,551+05	,206+05	,221+05	,214+06	,732+05	,158+05
22905382.	,551+05	,206+05	,138+05	,214+06	,732+05	,158+05
22905383.	,551+05	,206+05	,138+05	,214+06	,732+05	,158+05
22905384.	,551+05	,360+05	,138+05	,214+06	,732+05	,158+05
22905385.	,551+05	,206+05	,138+05	,214+06	,732+05	,158+05
22905386.	,551+05	,206+05	,346+05	,214+06	,732+05	,158+05
22905387.	,551+05	,206+05	,138+05	,214+06	,732+05	,158+05
22905388.	,551+05	,206+05	,138+05	,214+06	,732+05	,158+05
22905389.	,551+05	,206+05	,138+05	,214+06	,732+05	,158+05
22905390.	,551+05	,206+05	,138+05	,214+06	,732+05	,158+05
22905391.	,551+05	,206+05	,221+05	,214+06	,732+05	,158+05
22905392.	,551+05	,206+05	,138+05	,214+06	,732+05	,158+05
22905393.	,551+05	,206+05	,138+05	,214+06	,732+05	,158+05
22905394.	,551+05	,206+05	,138+05	,214+06	,732+05	,158+05
22905395.	,551+05	,206+05	,138+05	,214+06	,732+05	,158+05
22905396.	,551+05	,206+05	,138+05	,214+06	,732+05	,158+05
22905397.	,551+05	,206+05	,138+05	,562+06	,732+05	,158+05
22905398.	,551+05	,206+05	,138+05	,214+06	,732+05	,158+05
22905399.	,551+05	,206+05	,138+05			

* MUST APPLY MULTIPLICATIVE FACTOR - SEE TEXT

ST	CMP3A *	CMP3B *	CMP3C *	CME3B	CME3C	CME2D
22905200.	.551+05	.360+05	.221+05	.214+06	.732+05	.158+05
22905201.	.551+05	.360+05	.138+05	.214+06	.732+05	.158+05
22905202.	.551+05	.206+05	.138+05	.214+06	.732+05	.158+05
22905203.	.551+05	.206+05	.138+05	.214+06	.732+05	.158+05
22905204.	.551+05	.360+05	.138+05	.214+06	.732+05	.158+05
22905205.	.551+05	.535+05	.138+05	.214+06	.732+05	.158+05
22905206.	.551+05	.206+05	.138+05	.214+06	.732+05	.158+05
22905207.	.551+05	.206+05	.138+05	.214+06	.732+05	.158+05
22905208.	.551+05	.206+05	.138+05	.214+06	.732+05	.158+05
22905209.	.551+05	.206+05	.138+05	.214+06	.732+05	.158+05
22905210.	.551+05	.206+05	.138+05	.214+06	.732+05	.158+05
22905211.	.551+05	.206+05	.138+05	.214+06	.732+05	.158+05
22905212.	.551+05	.535+05	.138+05	.214+06	.732+05	.158+05
22905213.	.551+05	.206+05	.138+05	.214+06	.732+05	.158+05
22905214.	.551+05	.206+05	.138+05	.381+06	.732+05	.158+05
22905215.	.551+05	.206+05	.138+05	.214+06	.732+05	.158+05
22905216.	.551+05	.206+05	.138+05	.214+06	.732+05	.158+05
22905217.	.551+05	.360+05	.138+05	.214+06	.732+05	.158+05
22905218.	.551+05	.206+05	.138+05	.214+06	.732+05	.158+05
22905219.	.551+05	.206+05	.138+05	.214+06	.732+05	.158+05
22905220.	.551+05	.206+05	.138+05	.214+06	.732+05	.158+05
22905221.	.551+05	.206+05	.138+05	.214+06	.732+05	.158+05
22905222.	.551+05	.206+05	.138+05	.214+06	.732+05	.158+05
22905223.	.551+05	.360+05	.138+05	.214+06	.732+05	.158+05
22905224.	.551+05	.206+05	.138+05	.214+06	.732+05	.158+05
22905225.	.551+05	.206+05	.138+05	.214+06	.732+05	.158+05
22905226.	.551+05	.206+05	.138+05	.214+06	.732+05	.158+05
22905227.	.551+05	.206+05	.138+05	.214+06	.732+05	.158+05
22905228.	.551+05	.206+05	.138+05	.214+06	.732+05	.158+05
22905229	551+05	206+05	221+05	.113+07	.732+05	.158+05
22905230:	:551+05	:206+05	:221+05	.894+07	.732+05	.158+05
22905231.	.551+05	.206+05	.346+05	.825+07	.237+06	.158+05
22905232.	.551+05	.206+05	.346+05	.406+07	.732+05	.158+05
22905233.	.551+05	.206+05	.138+05	.182+07	.732+05	.158+05
22905234.	.551+05	.206+05	.138+05	.929+06	.980+05	.158+05
22905235.	.551+05	.206+05	.138+05	.135+07	.732+05	.158+05
22905236	551+05	206+05	138+05	.929+06	.732+05	.158+05
22905237:	:551+05	:206+05	:138+05	.740+06	.732+05	.158+05
22905238.	.551+05	.206+05	.138+05	.381+06	.732+05	.158+05
22905239.	.950+05	.206+05	.138+05	.214+06	.732+05	.158+05
22905240.	.551+05	.206+05	.138+05	.381+06	.732+05	.158+05
22905241.	.551+05	.206+05	.346+05	381+06	732+05	158+05
22905242.	.551+05	.360+05	.221+05	:214+06	:732+05	:158+05
22905243.	.551+05	.535+05	.138+05	.381+06	.732+05	.158+05
22905244.	.551+05	.535+05	.221+05	.214+06	.732+05	.158+05
22905245.	.317+06	.360+05	.480+05	.562+06	.732+05	.158+05
22905246.	.551+05	.535+05	.346+05	.214+06	.732+05	.158+05
22905247.	.551+05	.899+05	.480+05	214+06	732+05	158+05
22905248.	.551+05	.360+05	.625+05	:214+06	:732+05	:158+05
22905249.	.551+05	.110+06	.480+05	.562+06	.732+05	.158+05
22905250.	.551+05	.899+05	.766+05	.562+06	.732+05	.158+05
22905251.	.551+05	.110+06	.625+05	.740+06	.732+05	.158+05
22905252.	.551+05	.360+05	.138+05	.381+06	.732+05	.158+05
22905253.	.551+05	.110+06	.221+05	562+06	314+06	158+05
22905254.	.551+05	.710+05	.221+05	:214+06	:980+05	:158+05
22905255.	.551+05	.206+05	.221+05	.122+08	.911+06	.158+05
22905256.	.551+05	.206+05	.480+05	.597+08	.820+07	.421+06

ST	CMP3A *	CMP3B *	CMP3C *	CME3B	CME3C	CME2D
22905257.	.551+05	.156+06	.143+06	.482+08	.445+07	.158+05
22905258.	.551+05	.132+06	.124+06	.642+07	.117+07	.158+05
22905259.	.551+05	.156+06	.915+05	.208+07	.314+06	.158+05
22905260.	.551+05	.710+05	.480+05	.929+06	.980+05	.158+05
22905261.	.551+05	.535+05	.138+05	.214+06	.732+05	.158+05
22905262.	.551+05	.899+05	.766+05	.214+06	.732+05	.158+05
22905263.	.551+05	.710+05	.221+05	.214+06	.732+05	.158+05
22905264.	.551+05	.535+05	.625+05	.214+06	.732+05	.158+05
22905265.	.551+05	.156+06	.107+06	.929+06	.732+05	.158+05
22905266.	.551+05	.303+06	.254+06	.298+07	.237+06	.158+05
22905267.	.551+05	.504+06	.310+06	.236+07	.314+06	.158+05
22905268.	.551+05	.504+06	.373+06	.298+07	.732+05	.158+05
22905269.	.551+05	.504+06	.408+06	.368+07	.314+06	.563+05
22905270.	.551+05	.418+06	.254+06	.642+07	.683+06	.265+05
22905271.	.551+05	.238+06	.183+06	.642+07	.683+06	.158+05
22905272.	.551+05	.238+06	.205+06	.642+07	.683+06	.158+05
22905273.	.551+05	.181+06	.205+06	.368+07	.486+06	.563+05
22905274.	.551+05	.181+06	.162+06	.266+07	.237+06	.158+05
22905275.	.551+05	.181+06	.162+06	.589+07	.793+06	.110+06
22905276.	.551+05	.238+06	.183+06	.825+07	.793+06	.158+05
22905277.	.551+05	.208+06	.124+06	.642+07	.793+06	.158+05
22905278.	.551+05	.156+06	.107+06	.406+07	.581+06	.158+05
22905279.	.551+05	.899+05	.107+06	.894+07	.104+07	.153+06
22905280.	.551+05	.206+05	.107+06	.337+08	.252+07	.131+06
22905281.	.551+05	.710+05	.766+05	.482+08	.411+07	.253+06
22905282.	.551+05	.710+05	.766+05	.252+08	.231+07	.226+06
22905283.	.551+05	.535+05	.346+05	.894+07	.793+06	.158+05
22905284.	.551+05	.156+06	.766+05	.539+07	.683+06	.728+05
22905285.	.551+05	.132+06	.107+06	.406+07	.793+06	.408+05
22905286.	.551+05	.535+05	.124+06	.699+07	.104+07	.563+05
22905287.	.551+05	.132+06	.107+06	.968+07	.145+07	.563+05
22905288.	.551+05	.132+06	.124+06	.968+07	.145+07	.177+06
22905289.	.551+05	.132+06	.107+06	.760+07	.160+07	.408+05
22905290.	.551+05	.181+06	.107+06	.589+07	.131+07	.408+05
22905291.	.198+06	.181+06	.124+06	.642+07	.104+07	.158+05
22905292.	.145+06	.535+05	.124+06	.539+07	.117+07	.265+05
22905293.	.551+05	.110+06	.766+05	.589+07	.104+07	.158+05
22905294.	.551+05	.710+05	.766+05	.589+07	.104+07	.563+05
22905295.	.551+05	.206+05	.480+05	.699+07	.117+07	.408+05
22905296.	.551+05	.206+05	.625+05	.825+07	.117+07	.201+06
22905297.	.551+05	.206+05	.766+05	.825+07	.176+07	.153+06
22905298.	.551+05	.206+05	.625+05	.760+07	.145+07	.153+06
22905299.	.551+05	.710+05	.221+05	.760+07	.176+07	.253+06

* MUST APPLY MULTIPLICATIVE FACTOR, SEE TEXT

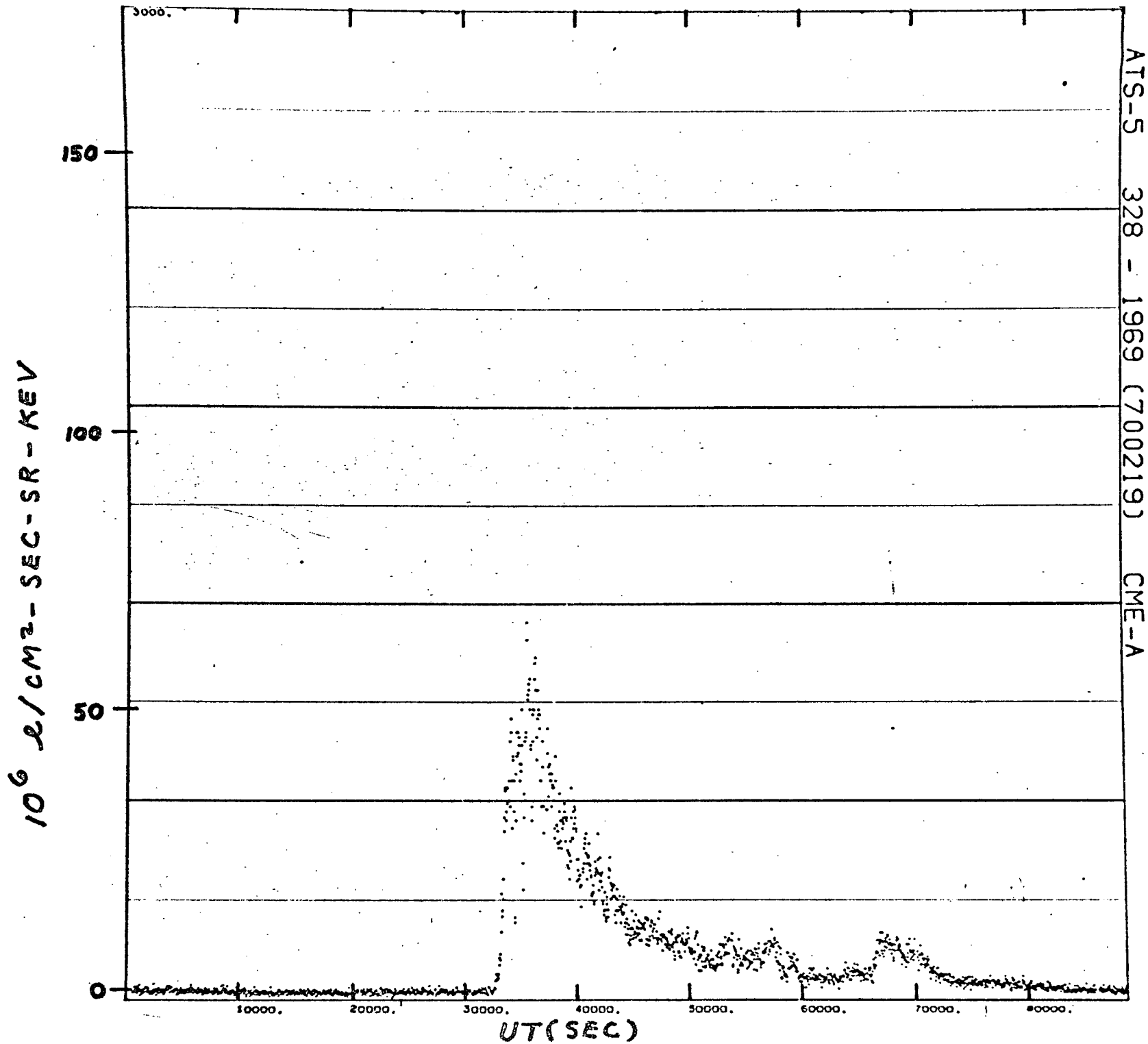
ATS-5 328 - 1969 (700219) CME-A
10^6 e/cm²-SEC-SR-KEV
150
100
50
0
10000.
20000.
30000.
40000.
50000.
60000.
70000.
80000.
UT(SEC)

Fig. 3

Fig. 4

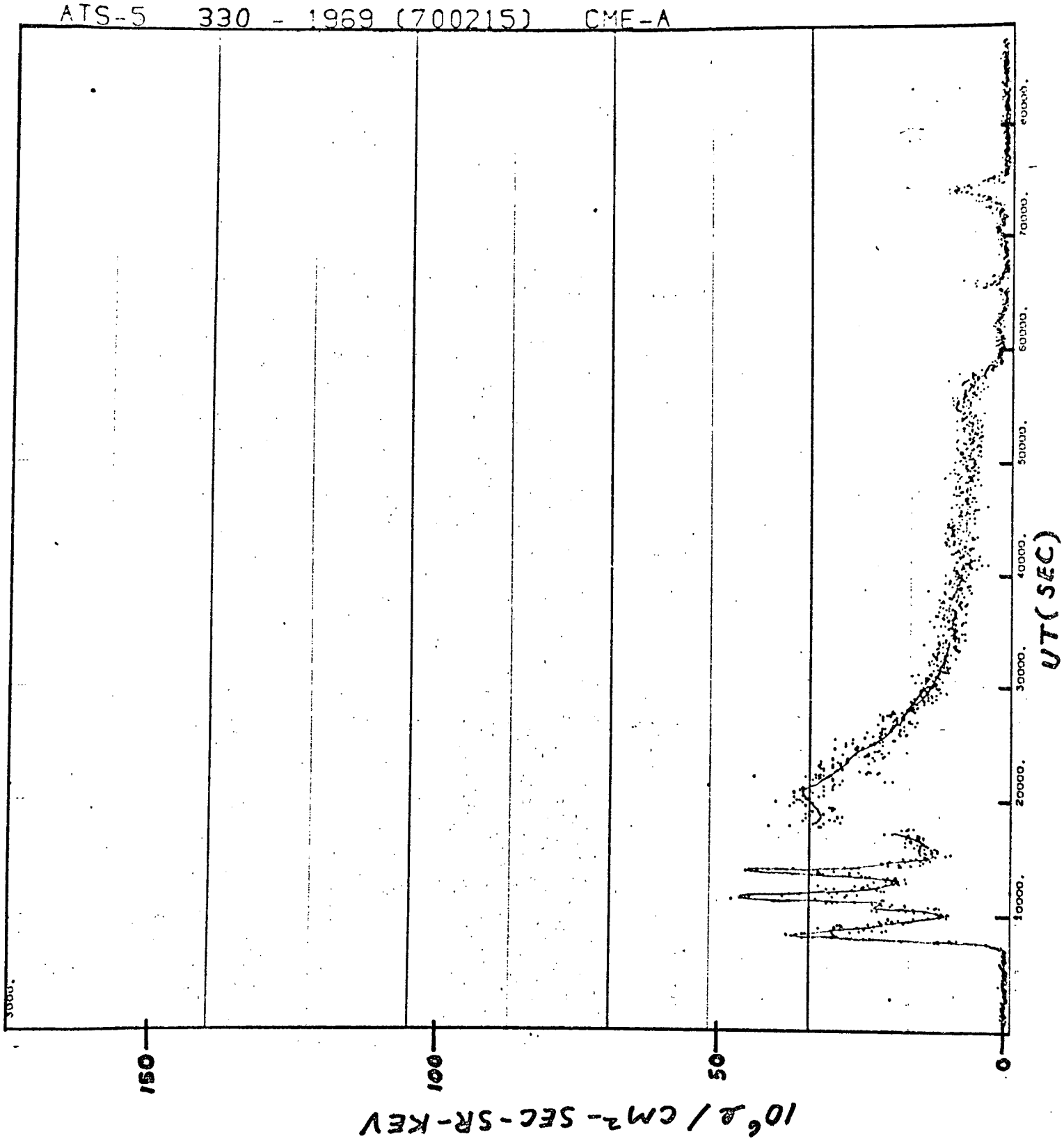
ATS-5 330 - 1969 (700215) CME-A
UT(SEC)
10000.
20000.
30000.
40000.
50000.
60000.
70000.
80000.
0
50
100
150
10⁶ Ω / CM²-SEC-SR-KEV

Fig. 5

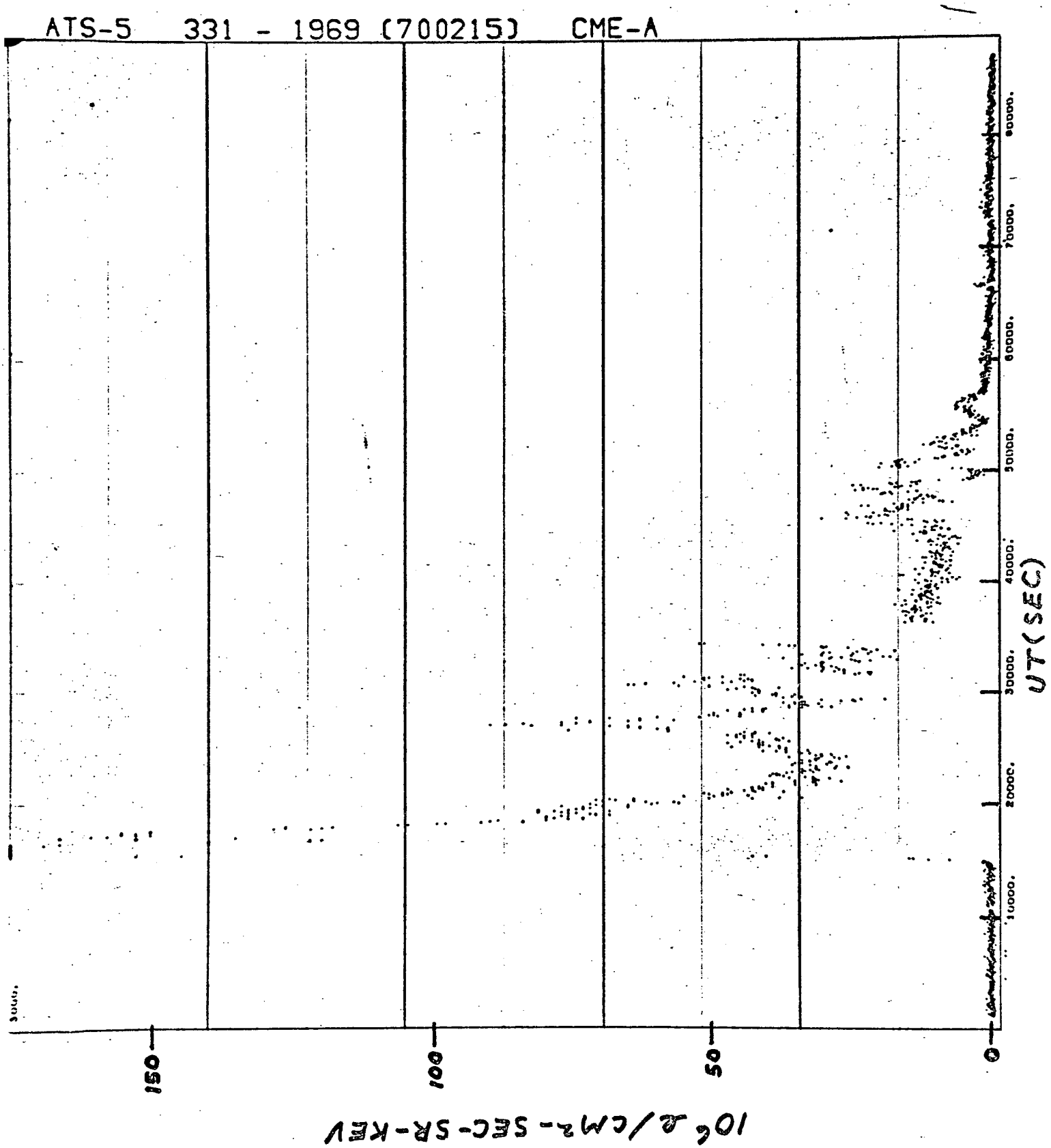
ATS-5 331 - 1969 (700215) CME-A
UT(SEC)
10000.
20000.
30000.
40000.
50000.
60000.
70000.
80000.
0
50
100
150
10^6 e/cm²-SEC-SR-KEV

Fig. 6

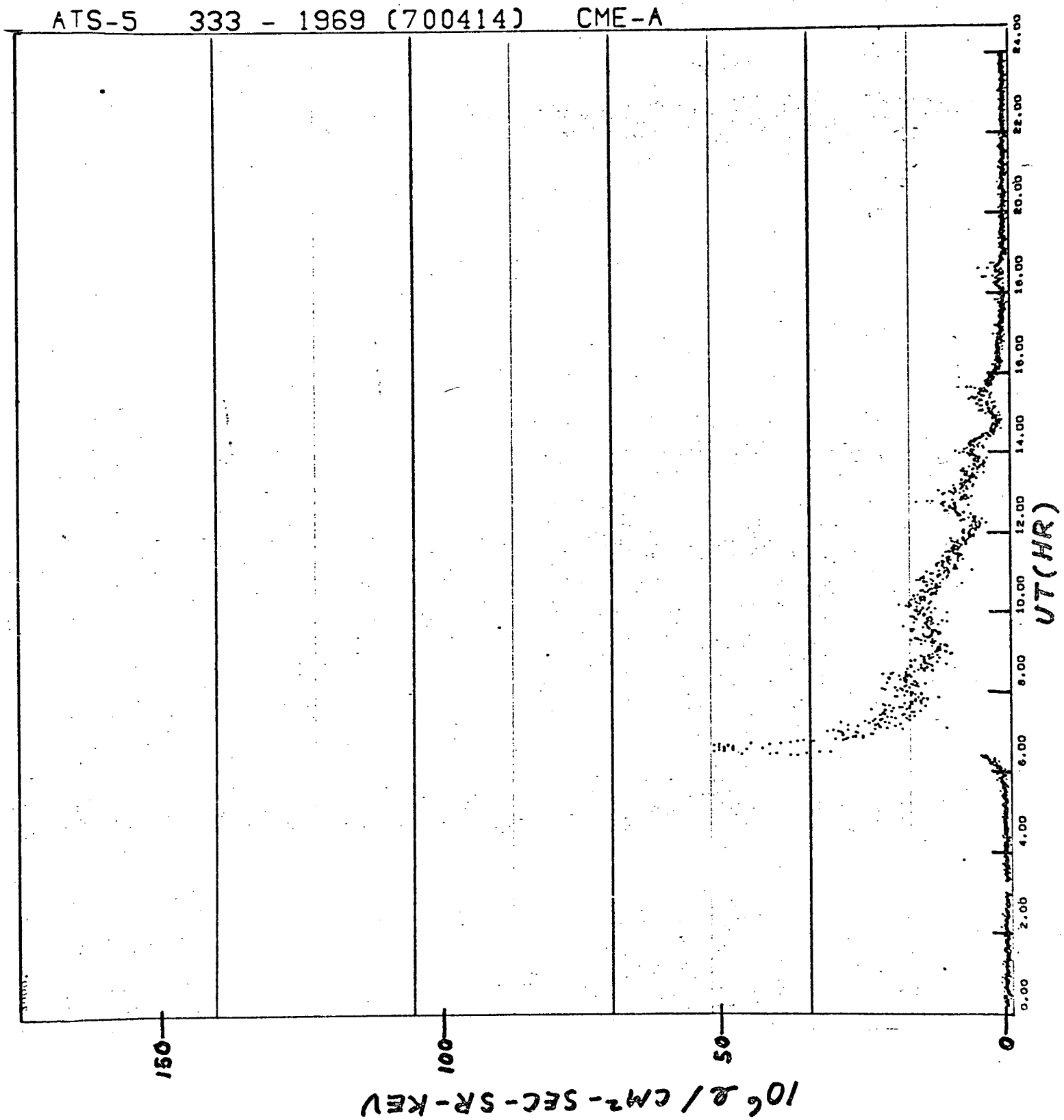
ATS-5 333 - 1969 (700414) CME-A
150
100
50
0
10^6 e / cm²- SEC- SR- KEV
0.00
2.00
4.00
6.00
8.00
10.00
12.00
14.00
16.00
18.00
20.00
22.00
24.00
UT (HR)

Fig. 7

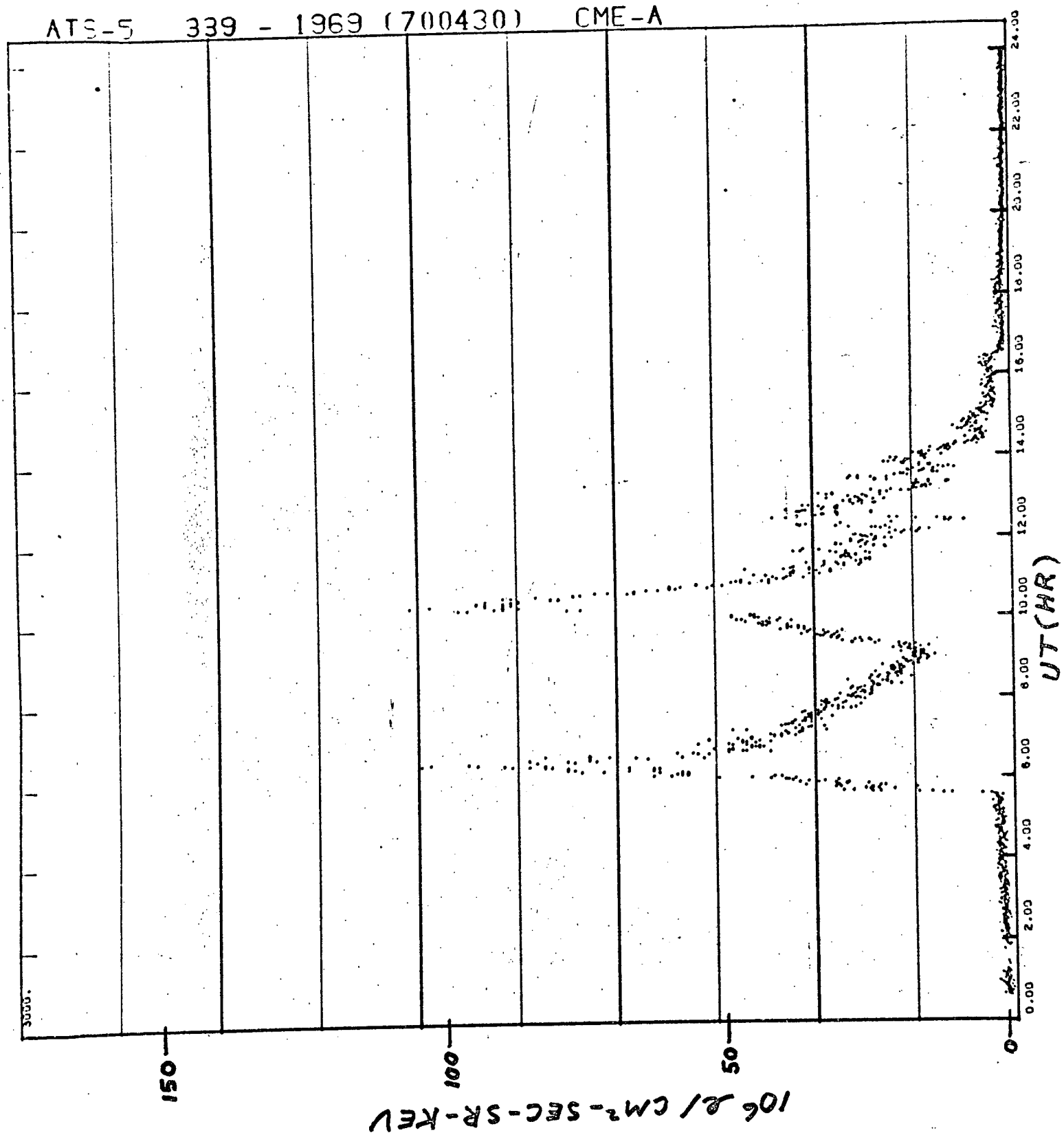
ATS-5 339 - 1969 (700430) CME-A
UT(HR)
0.00
2.00
4.00
6.00
8.00
10.00
12.00
14.00
16.00
18.00
20.00
22.00
24.00
0
50
100
150
10⁶ J/ CM²-SEC-SR-KEV

Fig. 8

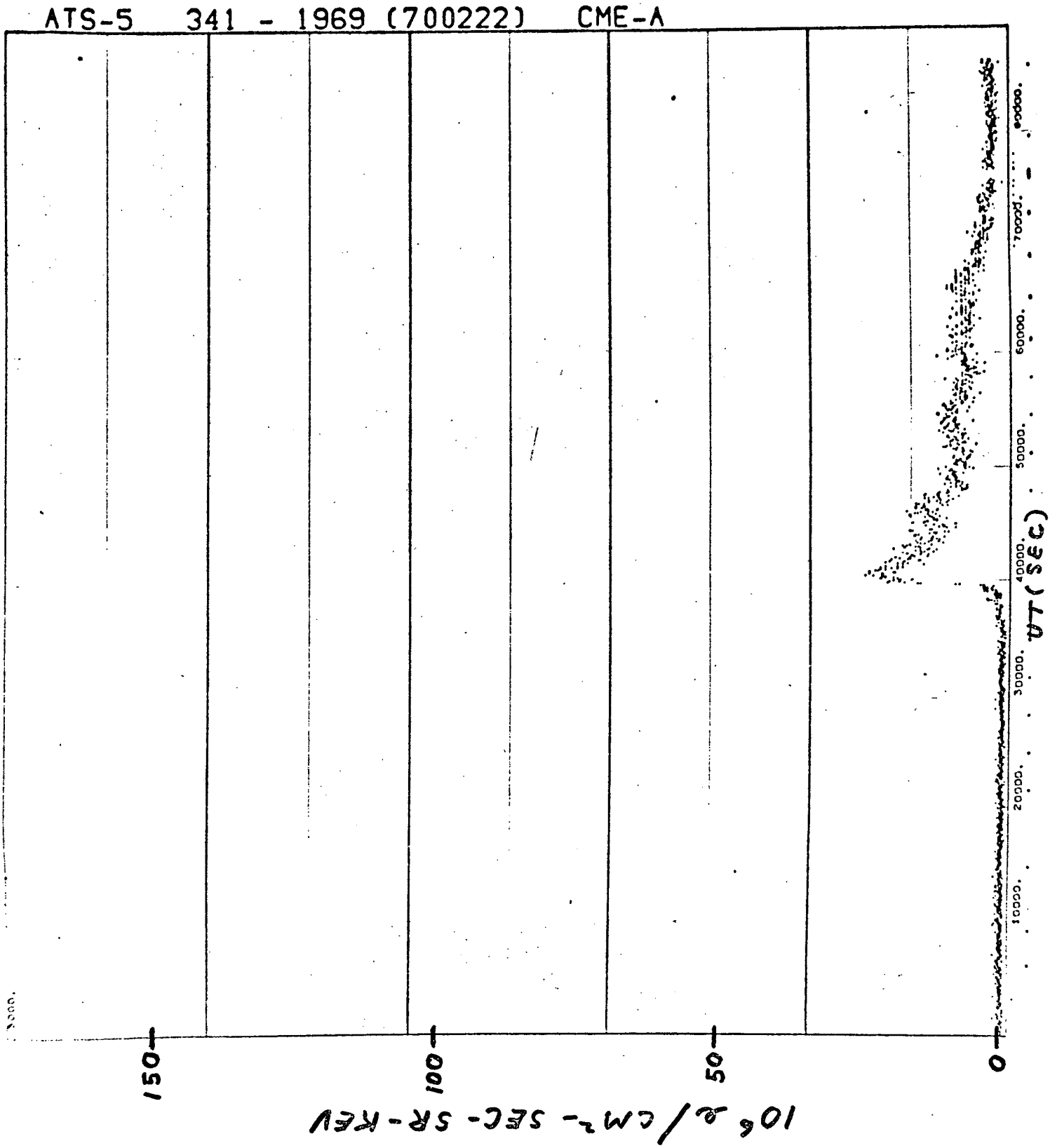
ATS-5 341 - 1969 (700222) CME-A
UT (SEC)
10000.
20000.
30000.
40000.
50000.
60000.
70000.
80000.
150
100
50
0
10⁶ e/CM²- SEC- SR- KEV

Fig. 9

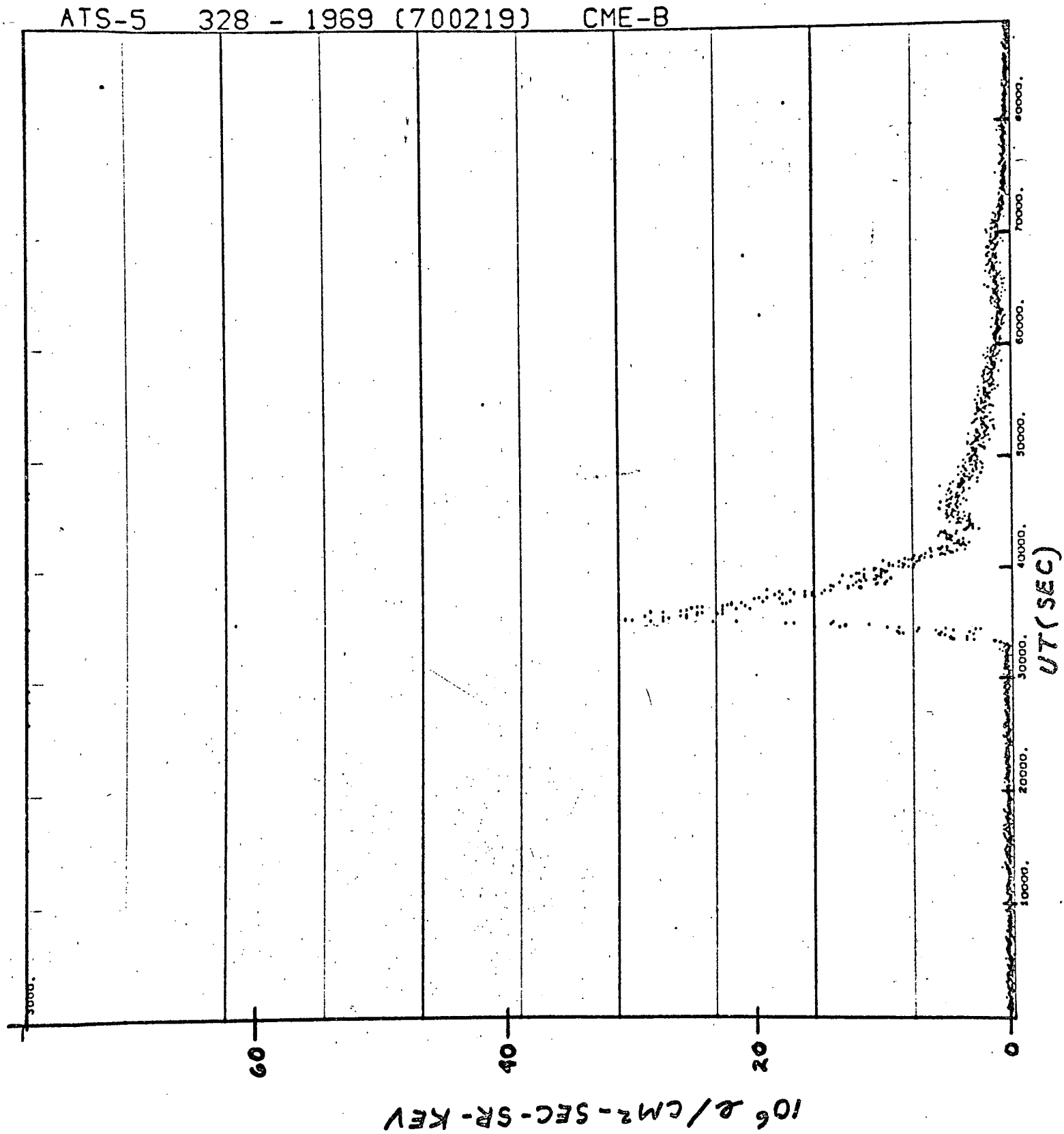

Fig. 10

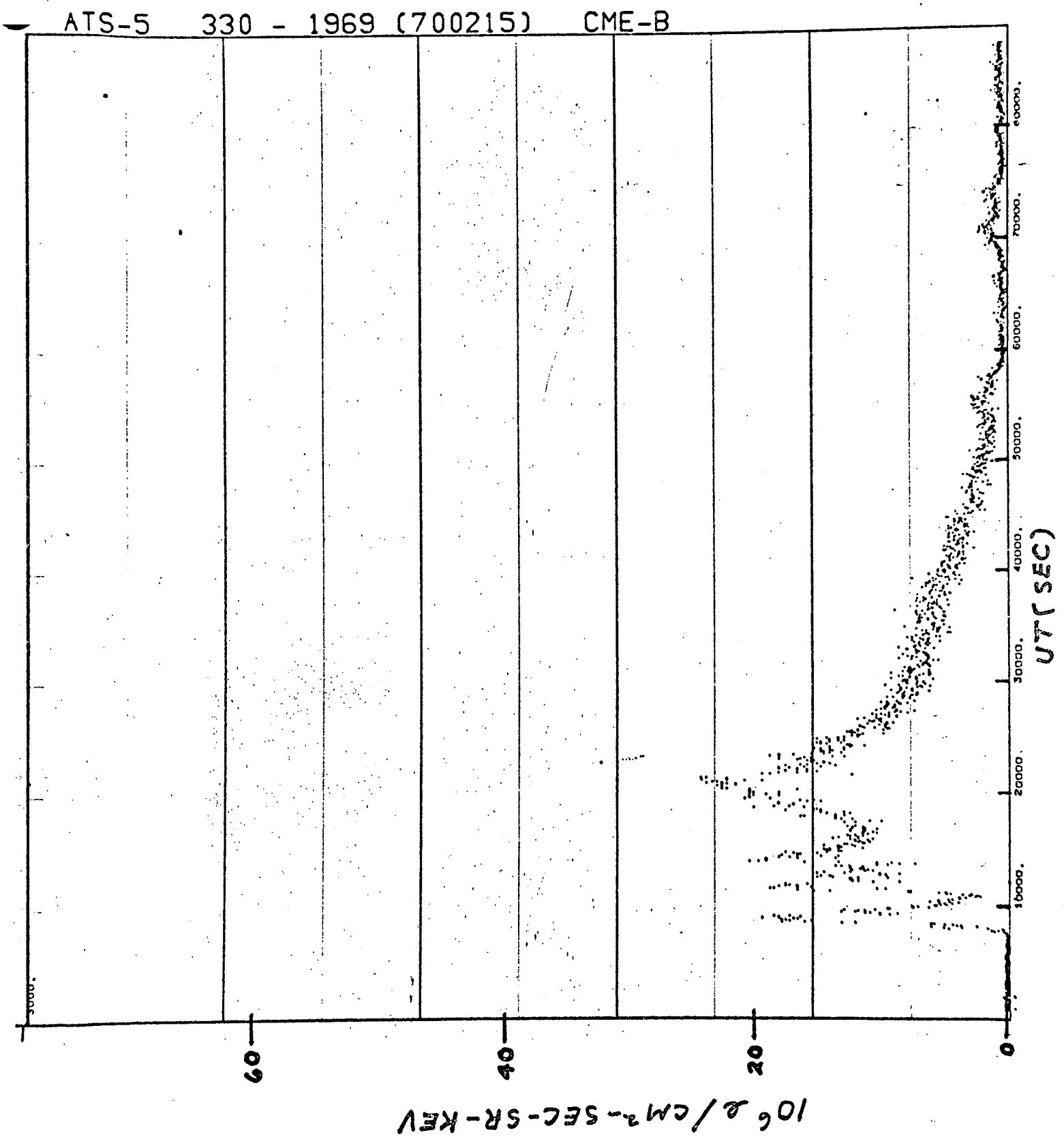

Fig. 11

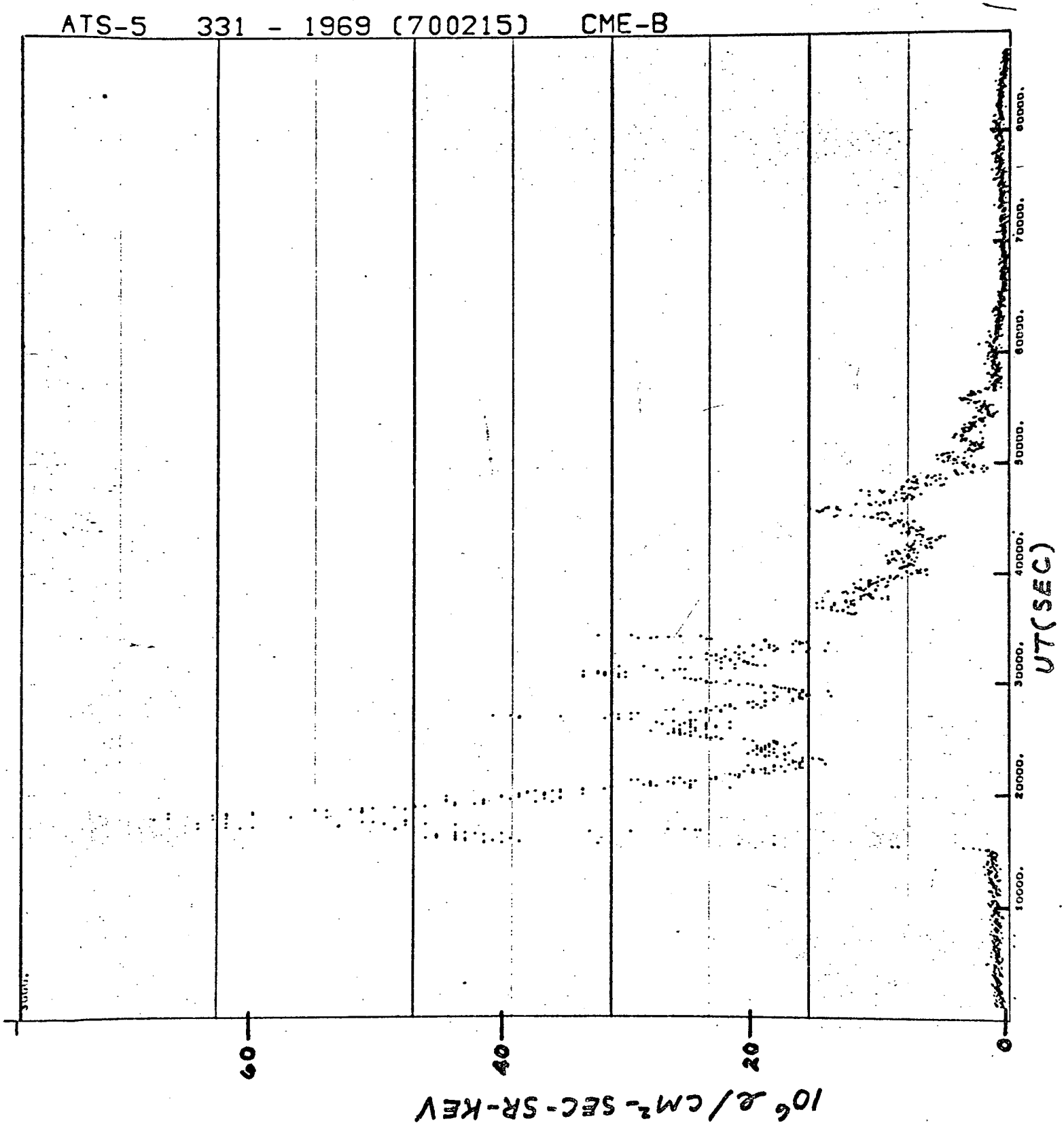
ATS-5 331 - 1969 (700215) CME-B
60
40
20
0
10^6 e/CM²-SEC-SR-KEV
UT(SEC)
10000.
20000.
30000.
40000.
50000.
60000.
70000.
80000.

Fig. 12

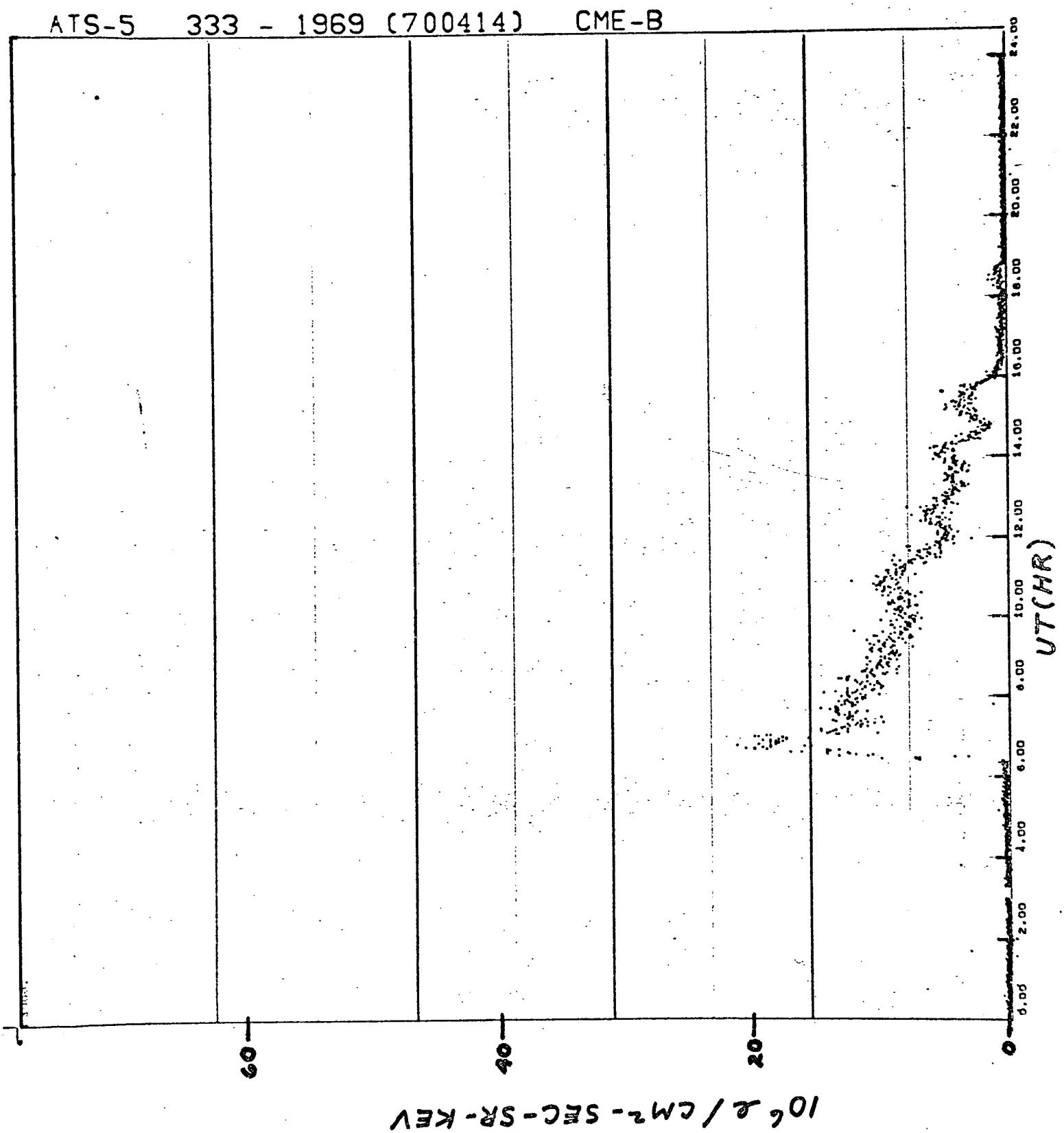
ATS-5 333 - 1969 (700414) CME-B
UT(HR)
0.00
2.00
4.00
6.00
8.00
10.00
12.00
14.00
16.00
18.00
20.00
22.00
24.00
0
20
40
60
10⁶ e / CM²- SEC-SR-KEV

Fig. 13

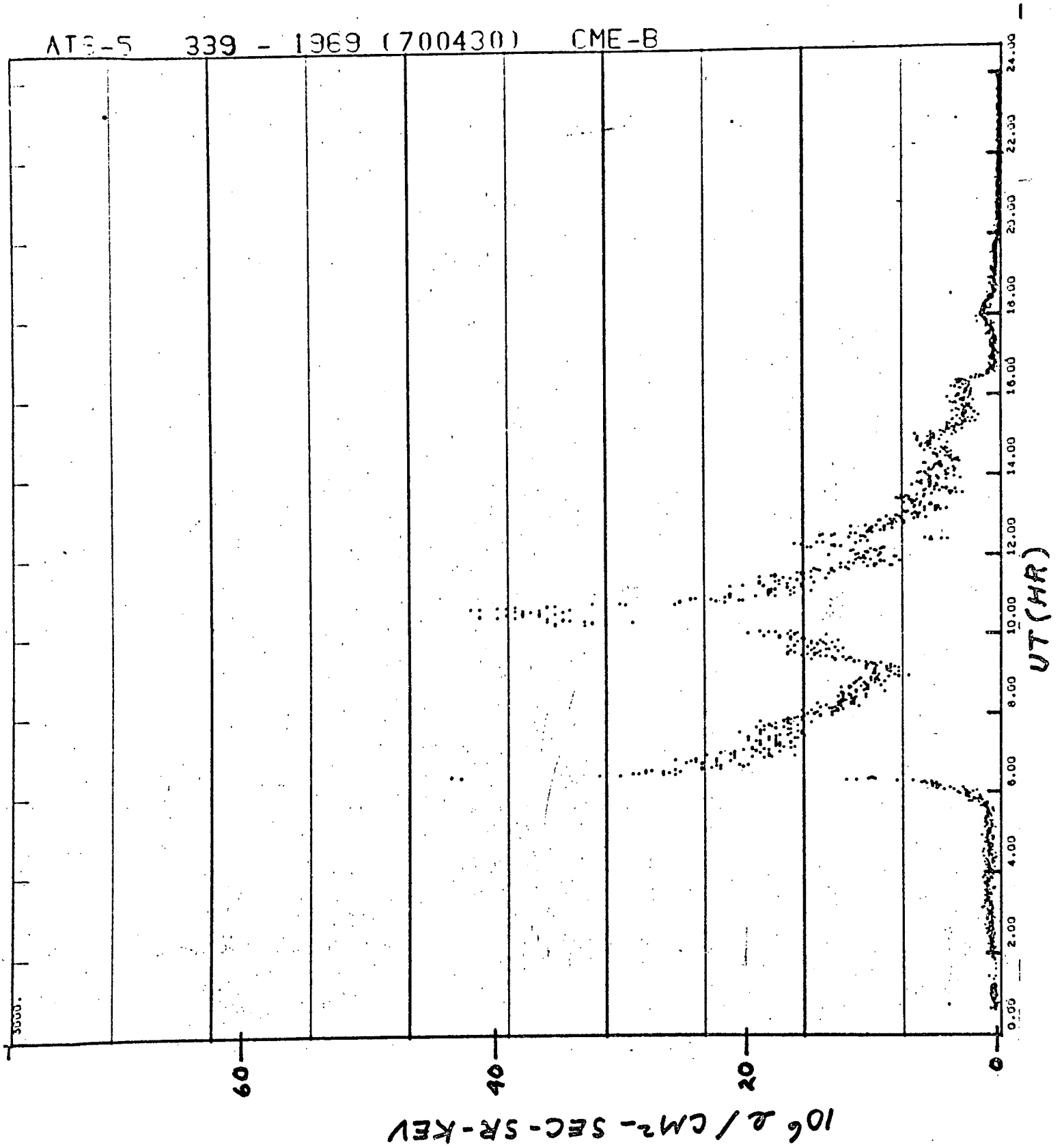
ATS-5 339 - 1969 (700430) CME-B
60
40
20
0
10^6 e / CM^2- SEC- SR- KEV
UT (HR)
0.00
2.00
4.00
6.00
8.00
10.00
12.00
14.00
16.00
18.00
20.00
22.00
24.00

Fig. 14

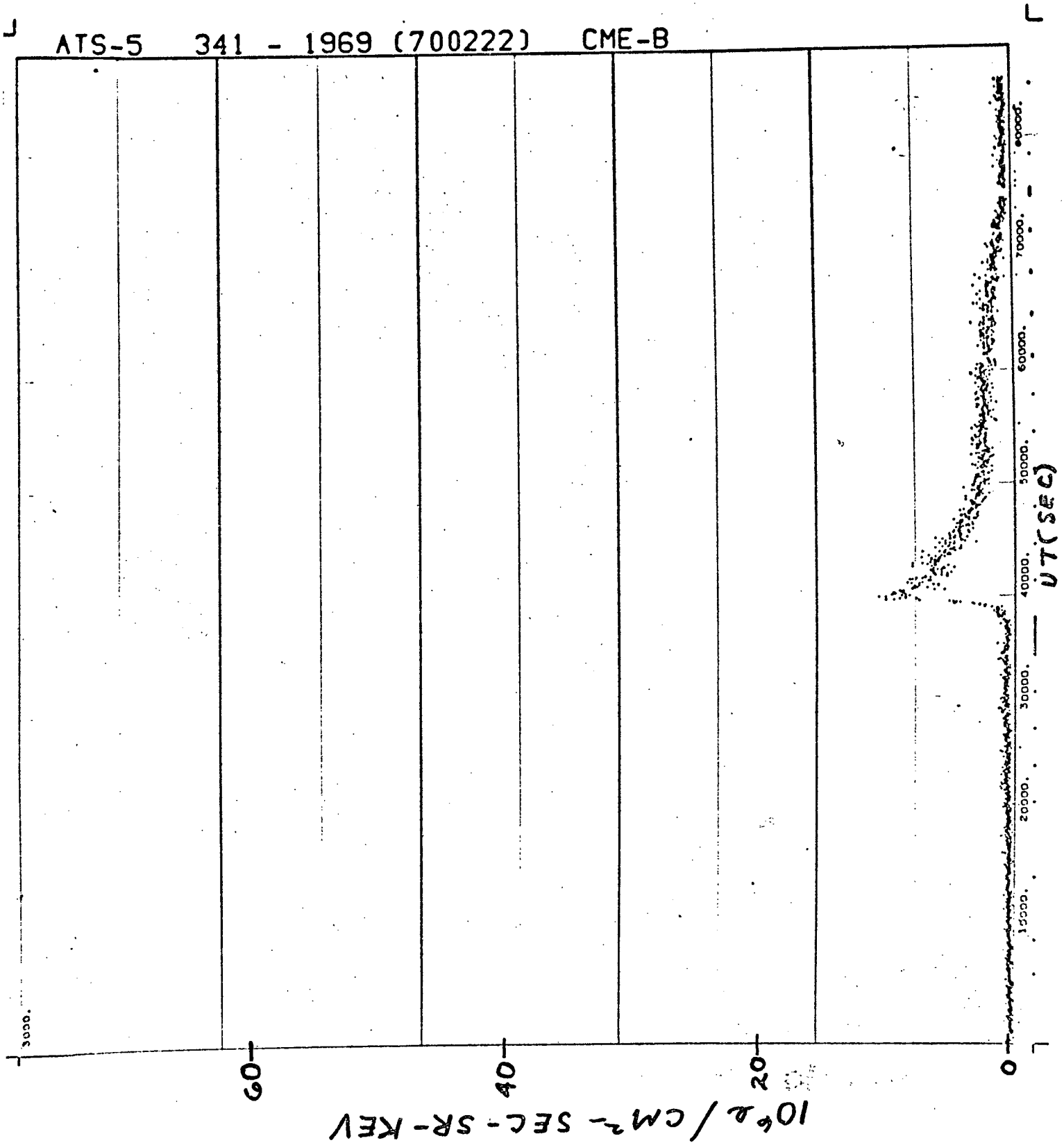

Fig. 15

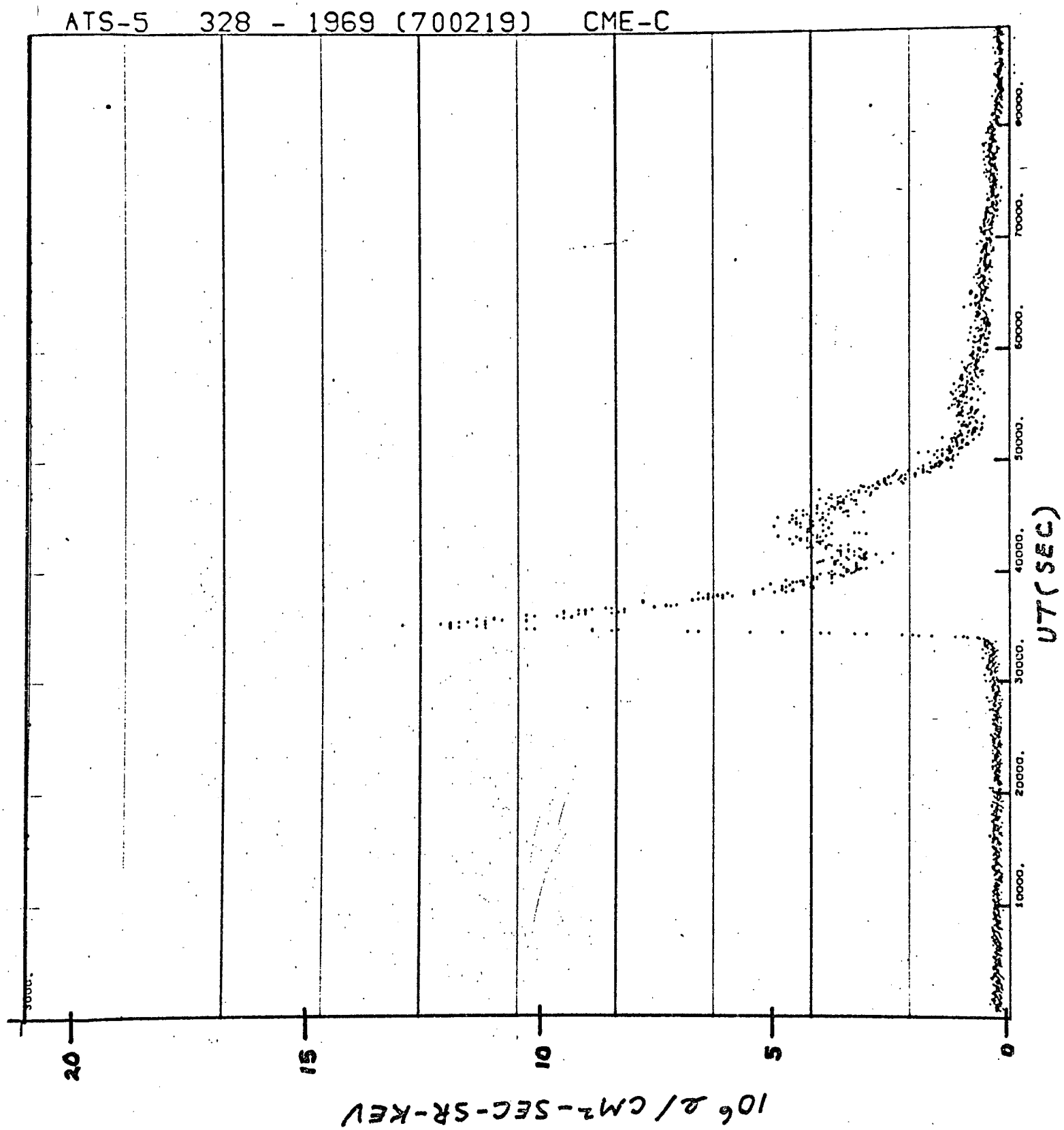

Fig. 16

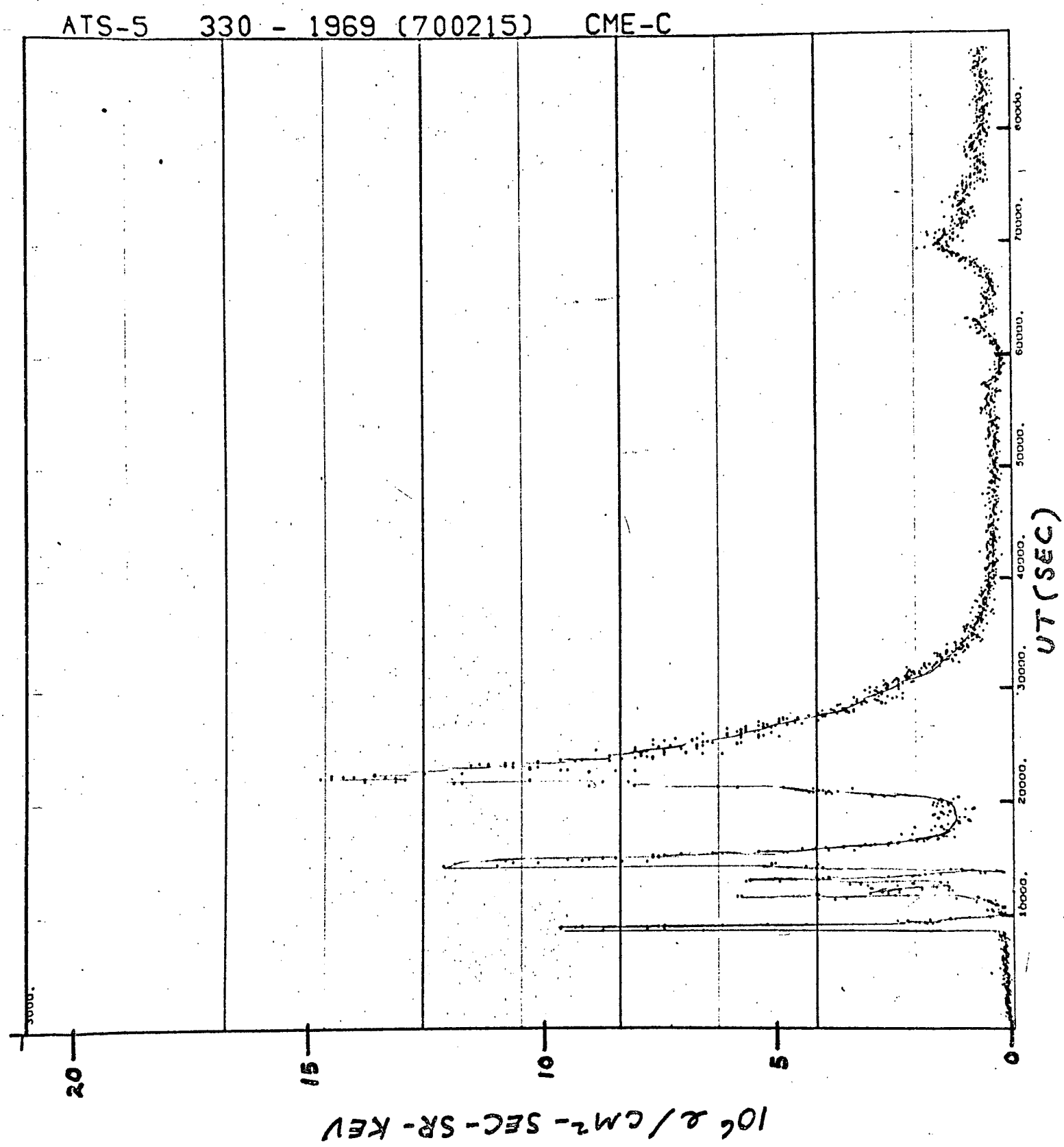

Fig. 17

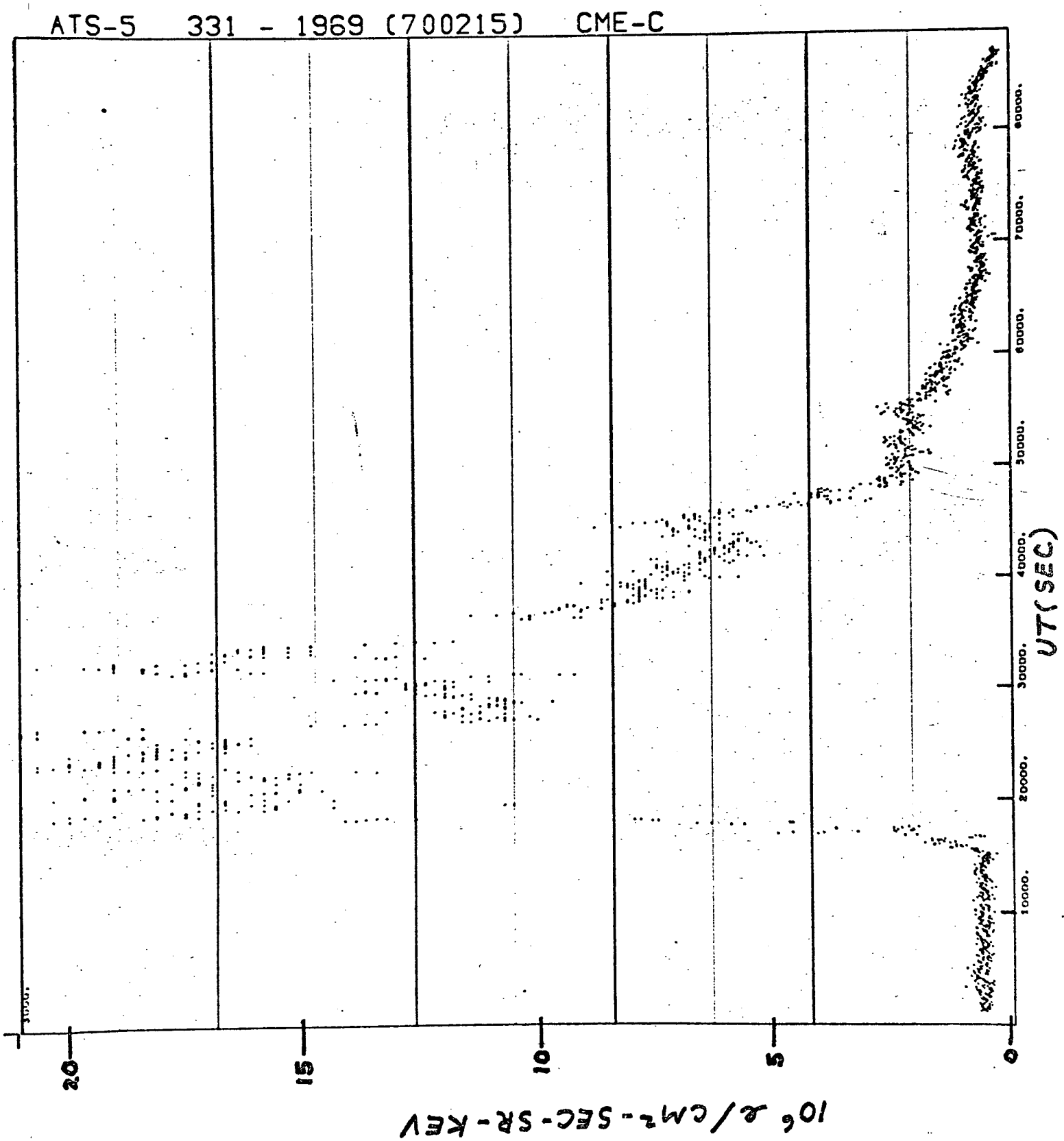
ATS-5 331 - 1969 (700215) CME-C
UT(SEC)
10000.
20000.
30000.
40000.
50000.
60000.
70000.
80000.
0
5
10
15
20
10⁶ P/CM²-SEC-SR-KEV

Fig. 18

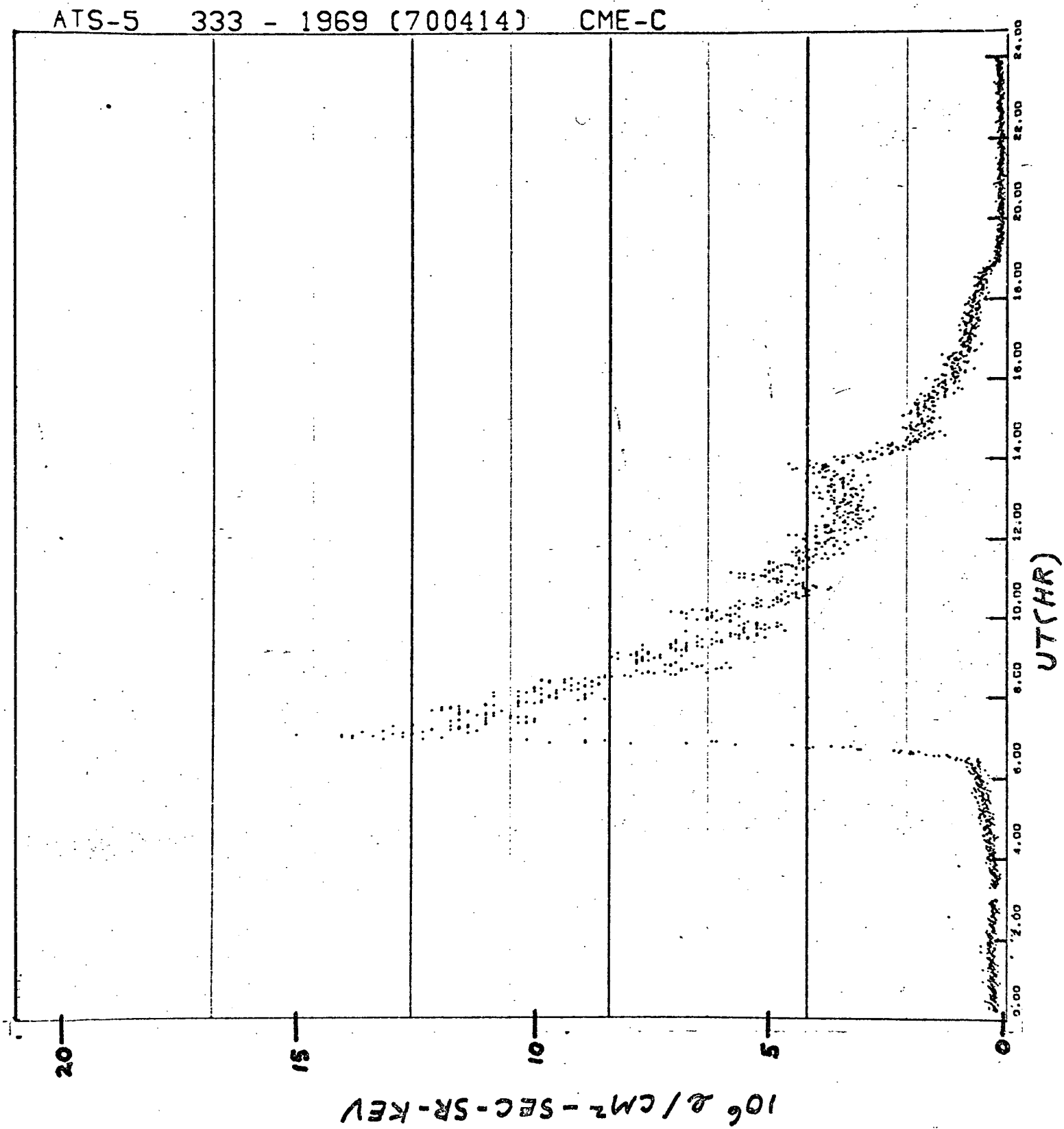
ATS-5 333 - 1969 (700414) CME-C
UT(HR)
0.00
2.00
4.00
6.00
8.00
10.00
12.00
14.00
16.00
18.00
20.00
22.00
24.00
0
5
10
15
20
10⁶ e/cm²-sec-sr-kev

Fig. 19

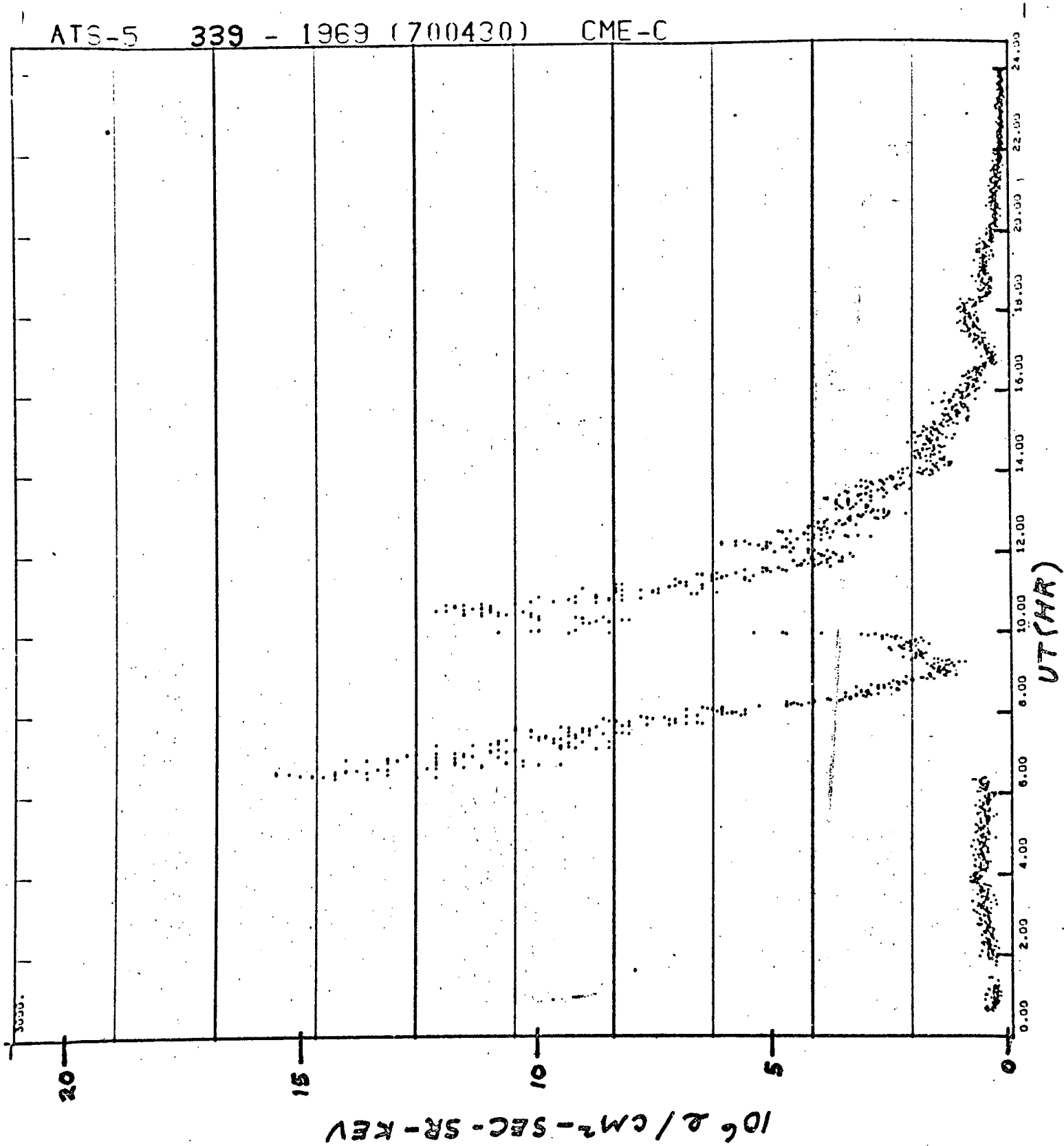
ATS-5 339 - 1969 (700430) CME-C
UT (HR)
0.00
2.00
4.00
6.00
8.00
10.00
12.00
14.00
16.00
18.00
20.00
22.00
24.00
0
5
10
15
20
10^6 e / cm^2-SEC-SR-KEV

Fig. 20

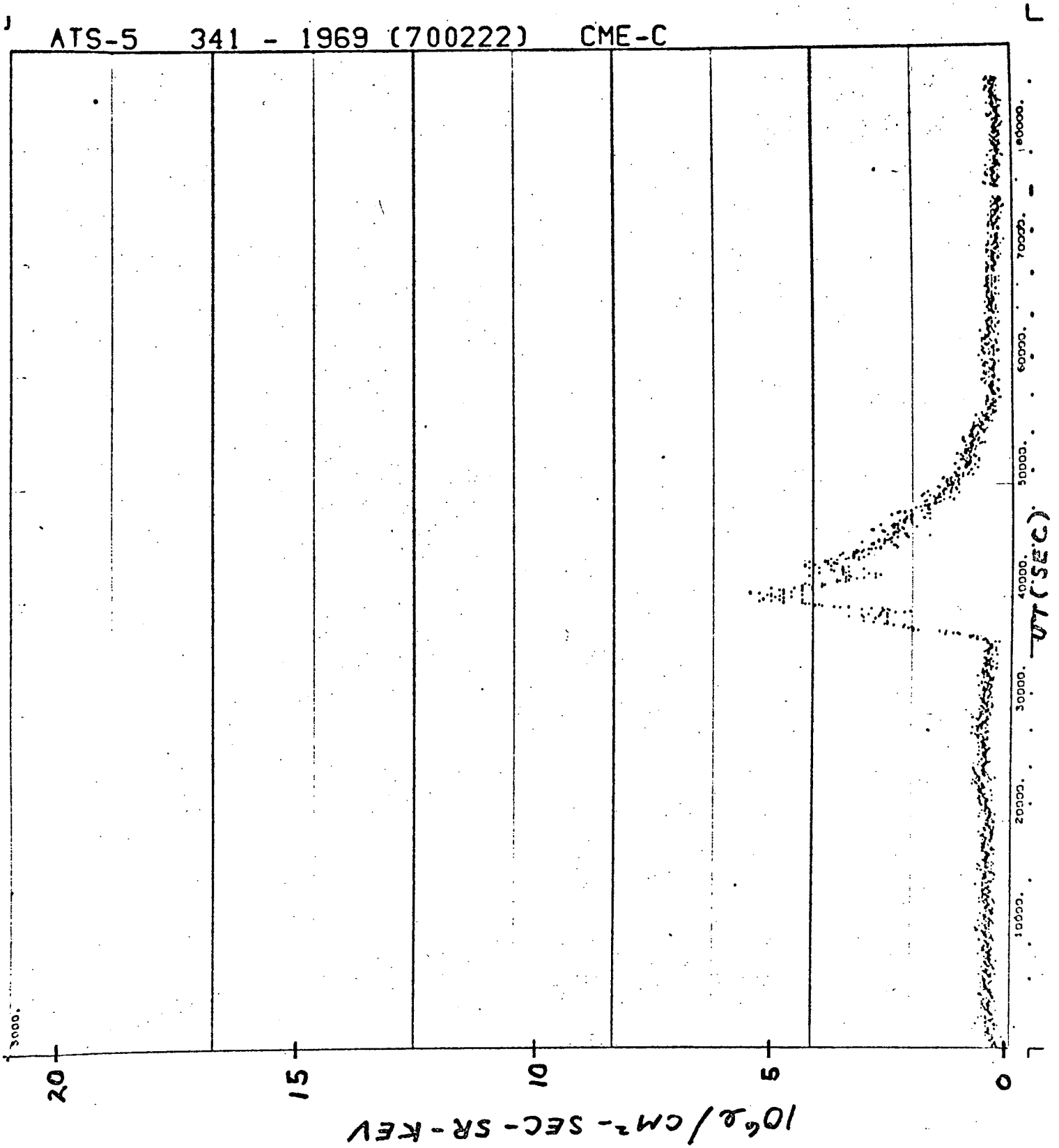

Fig. 21

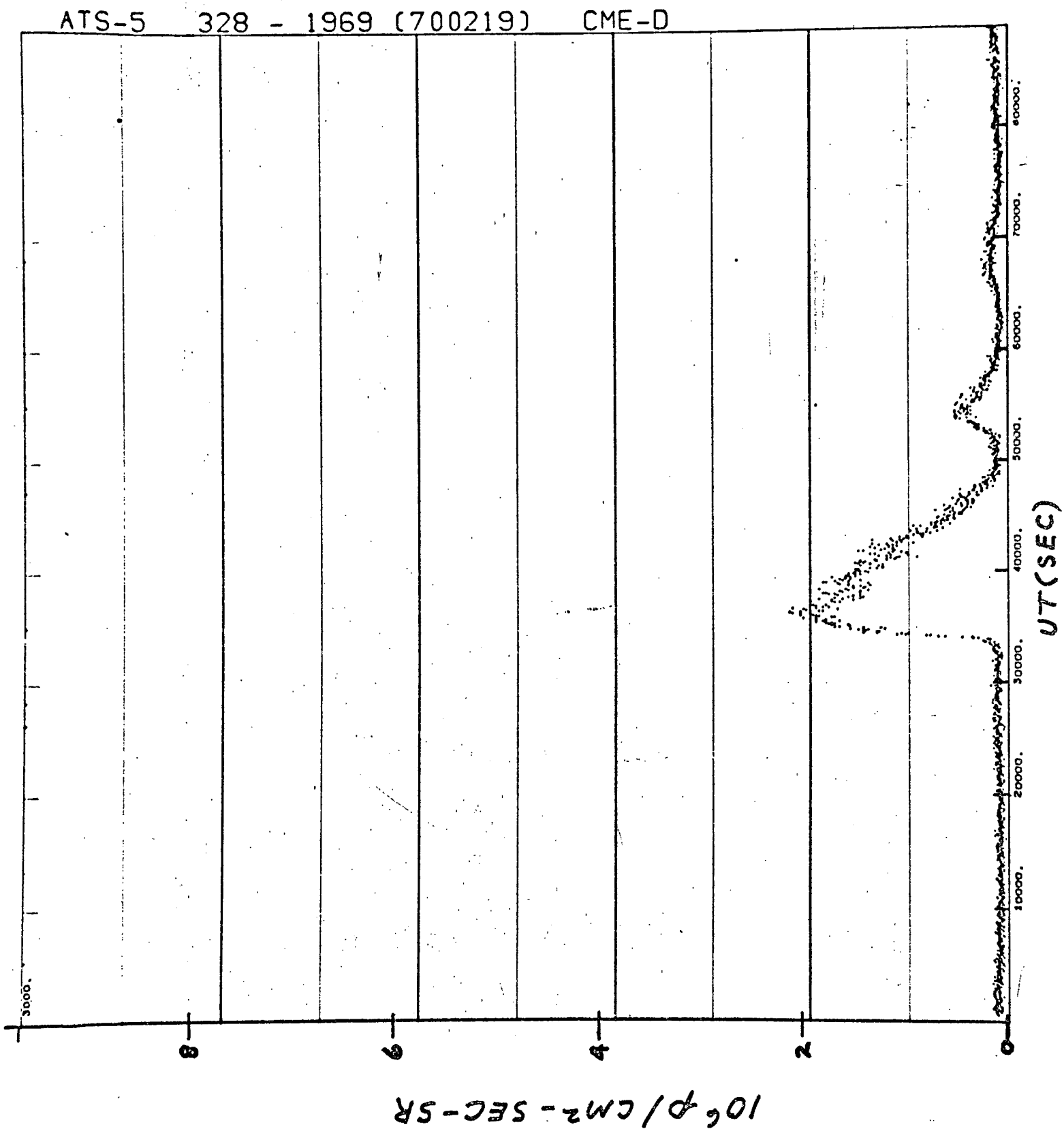

Fig. 22

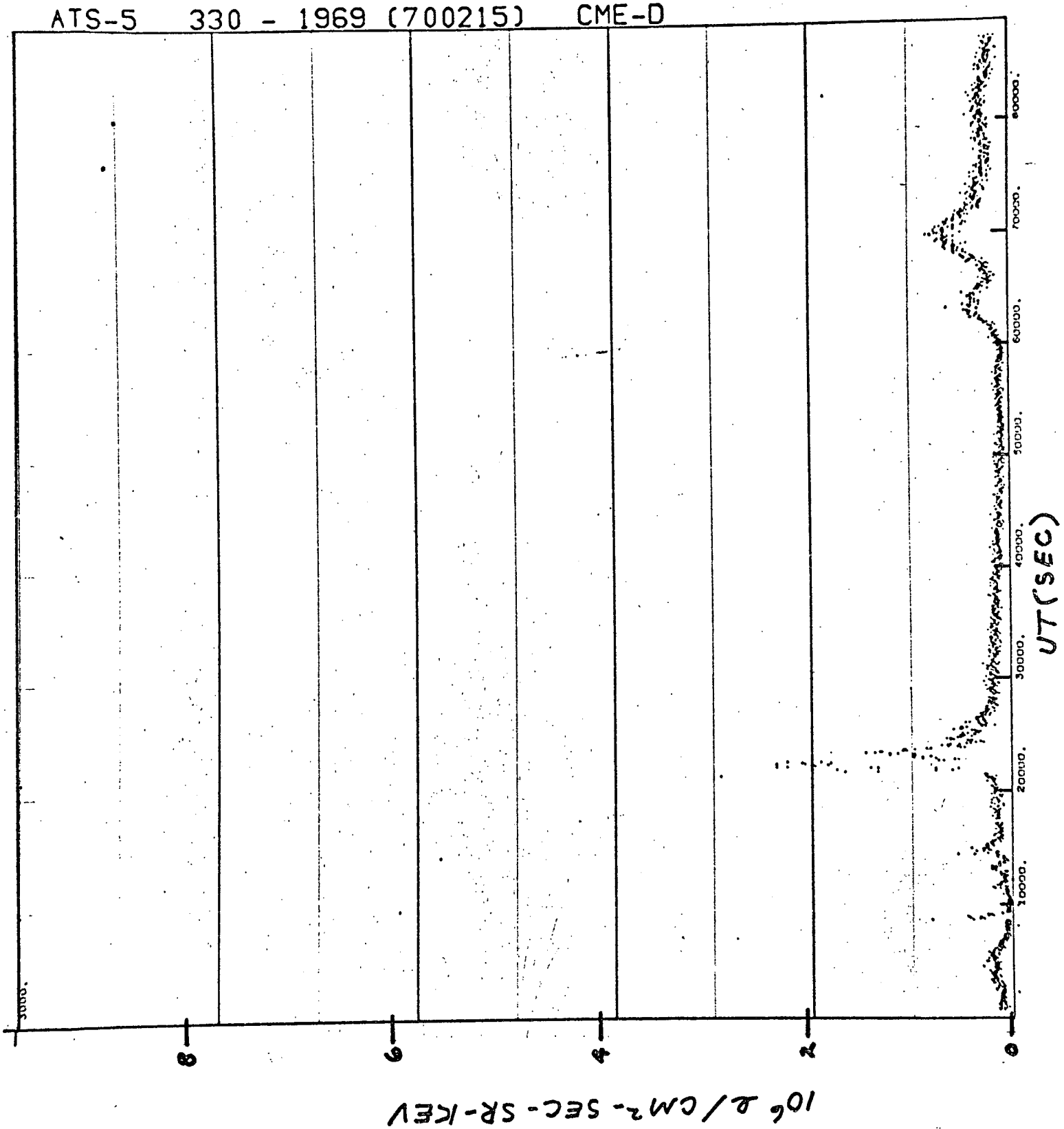

Fig. 23

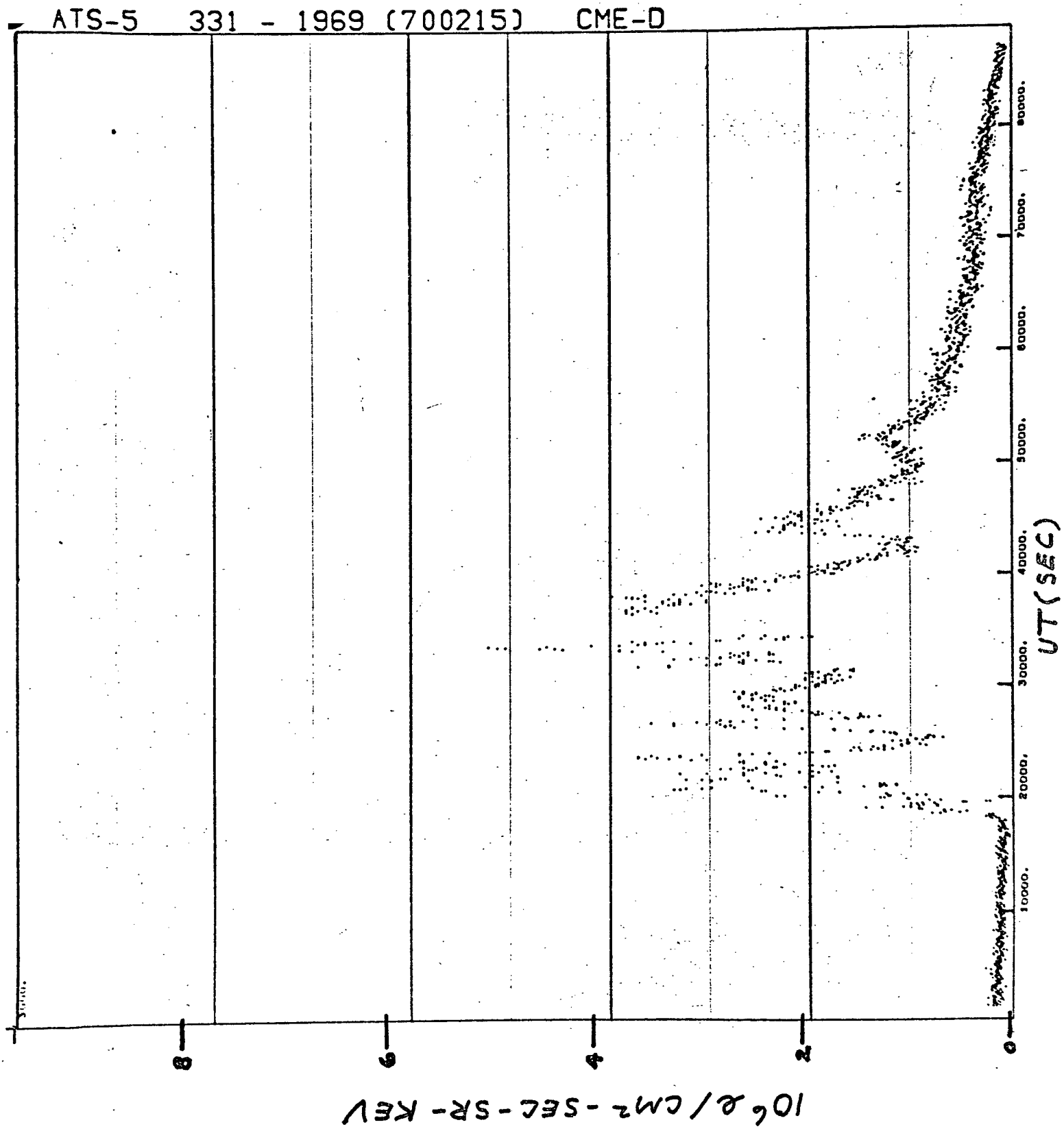
ATS-5 331 - 1969 (700215) CME-D
10000.
20000.
30000.
40000.
50000.
60000.
70000.
80000.
UT(SEC)
0
2
4
6
8
10⁶ P/CM²-SEC-SR-KEV

Fig. 24

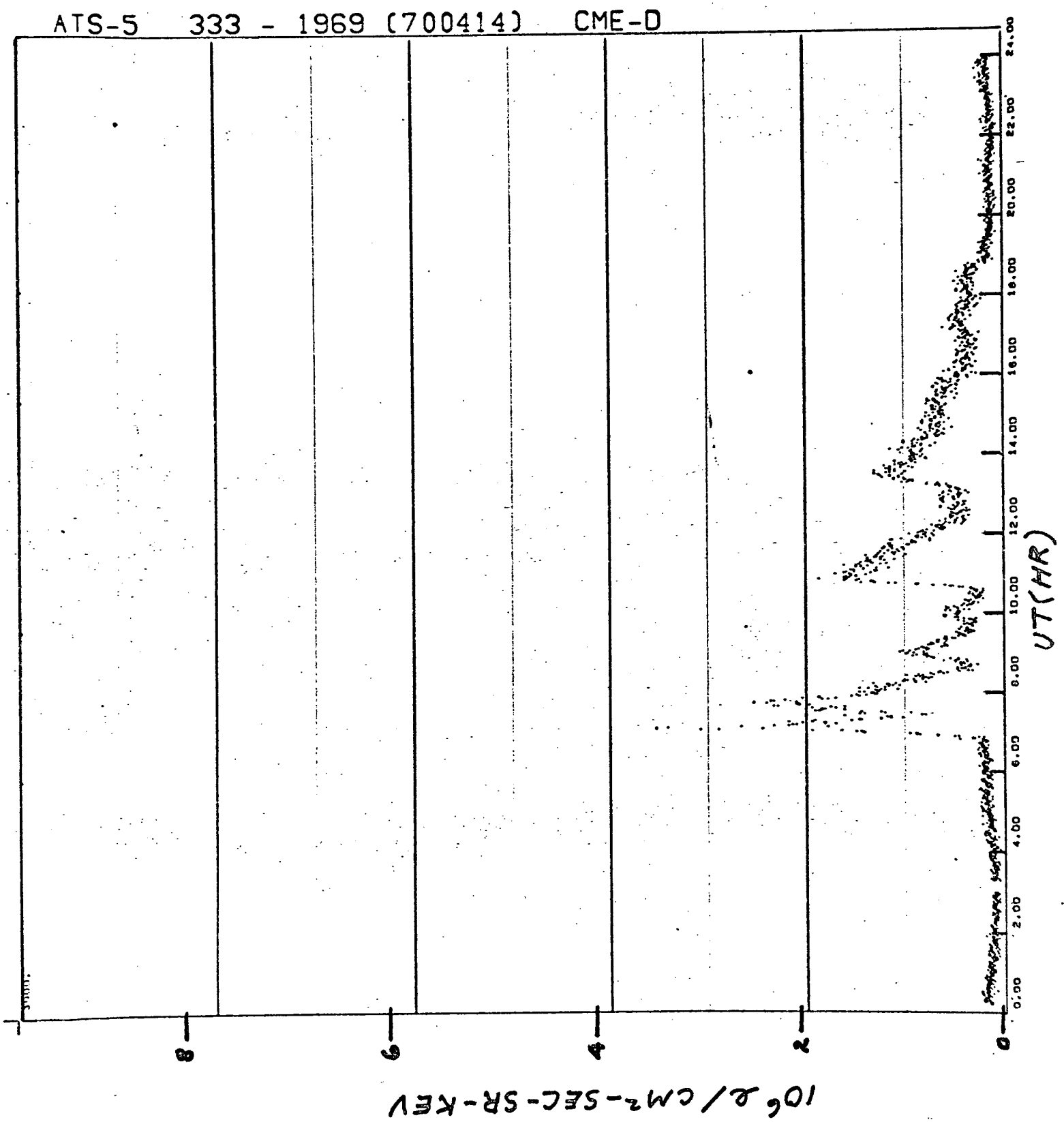
ATS-5 333 - 1969 (700414) CME-D
0.00
2.00
4.00
6.00
8.00
10.00
12.00
14.00
16.00
18.00
20.00
22.00
24.00
UT(HR)
0
2
4
6
8
10^6 P/CM²-SEC-SR-KEV

Fig. 25

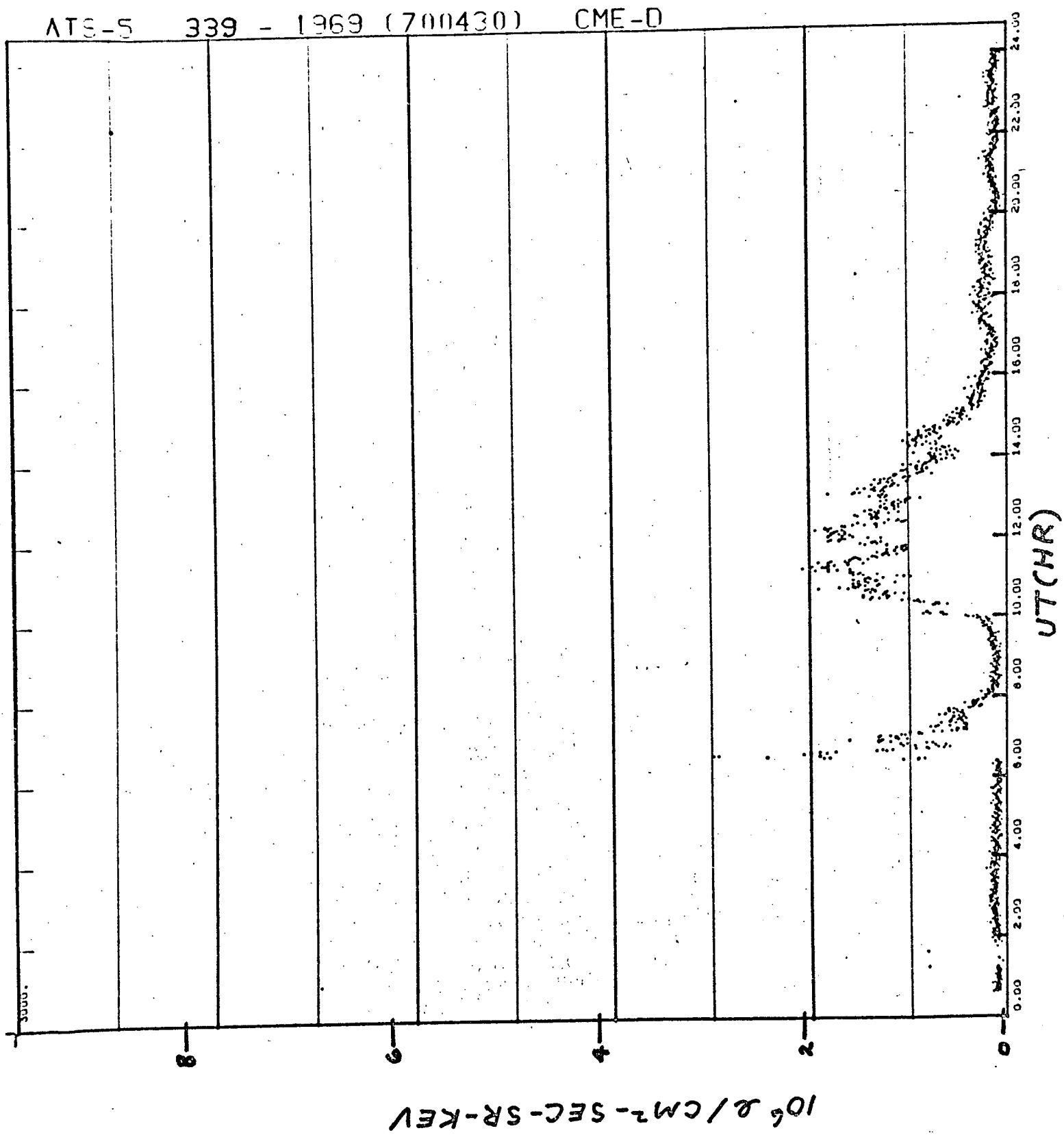

Fig. 26

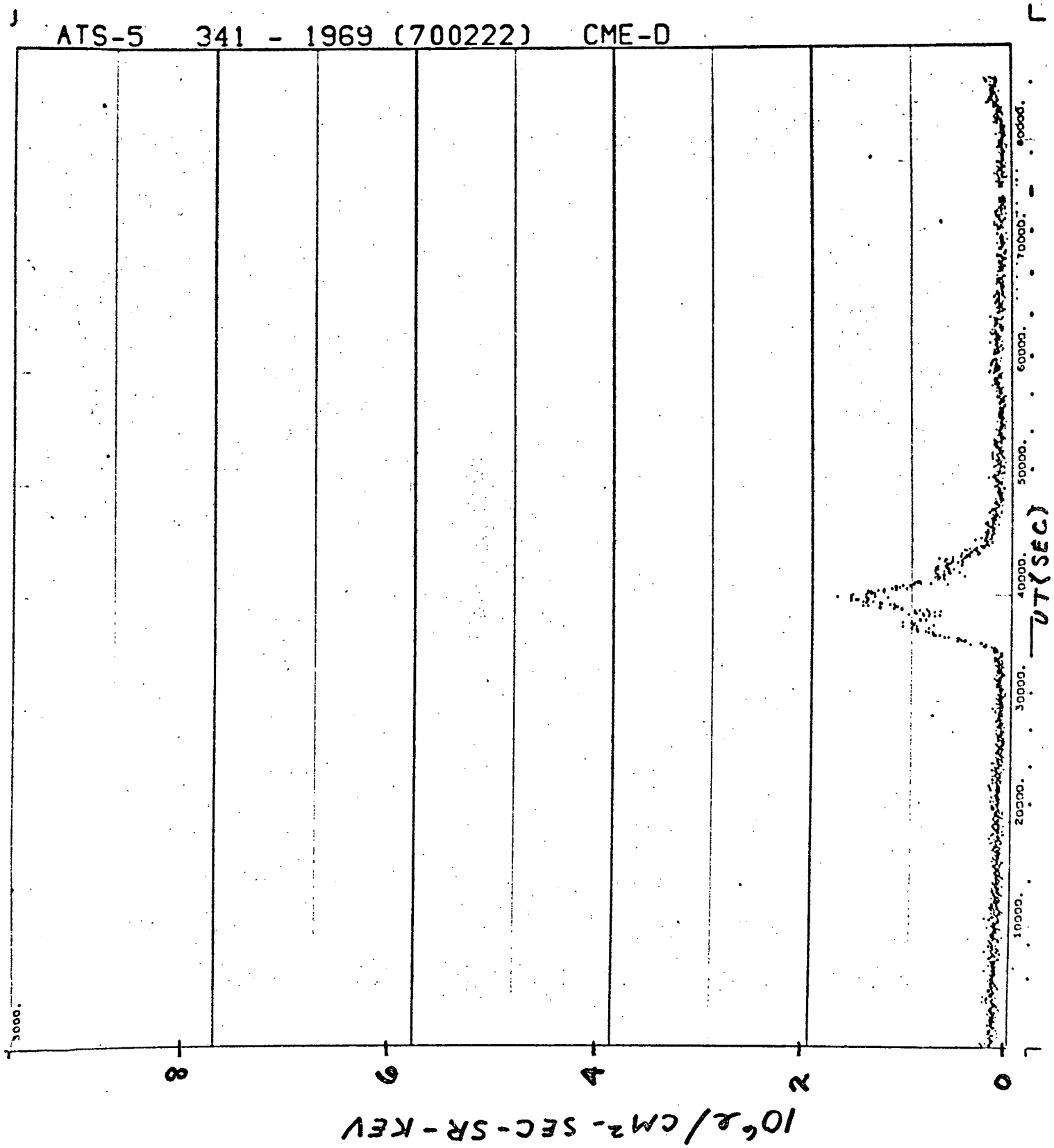

Fig. 27

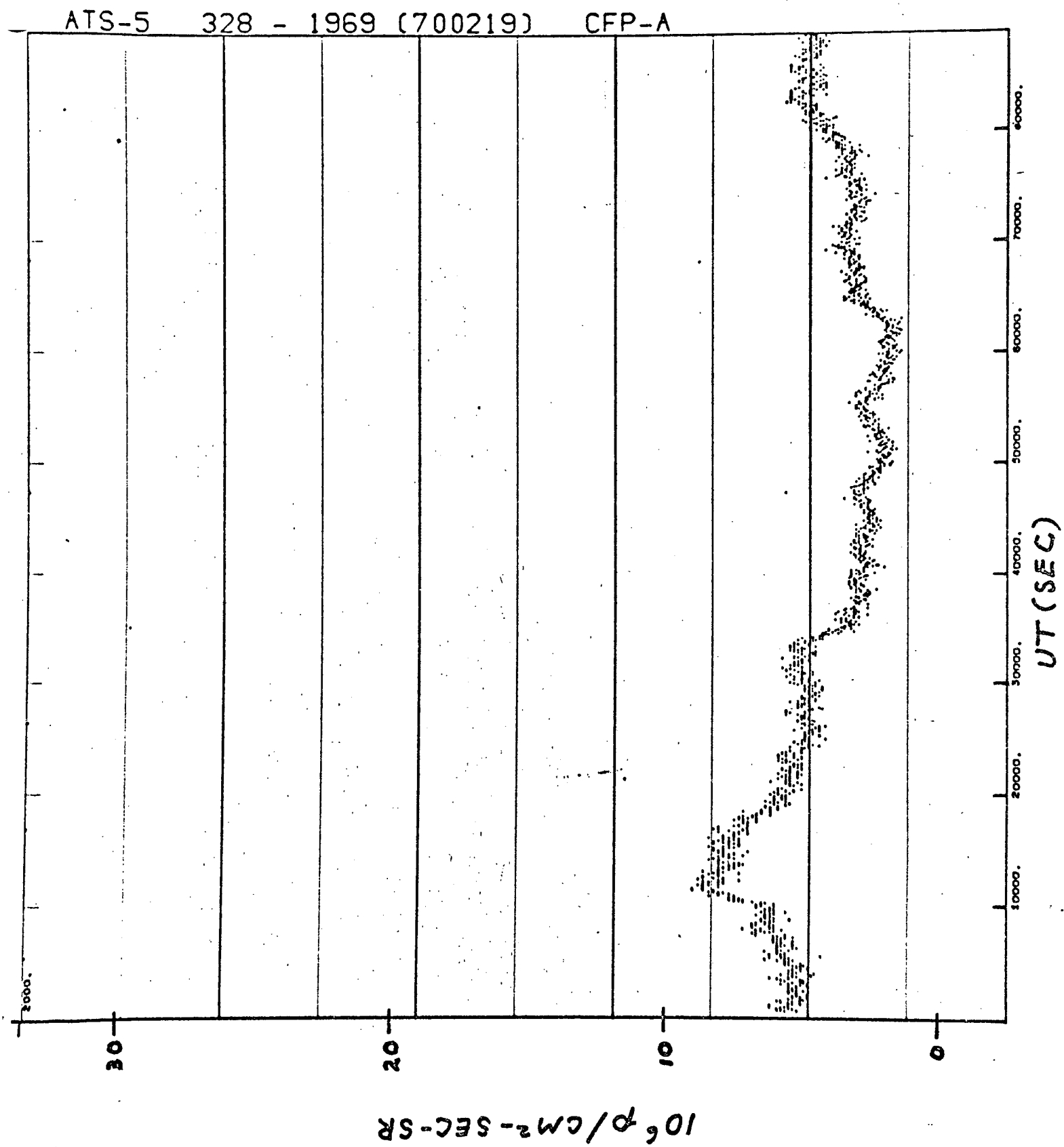

Fig. 28

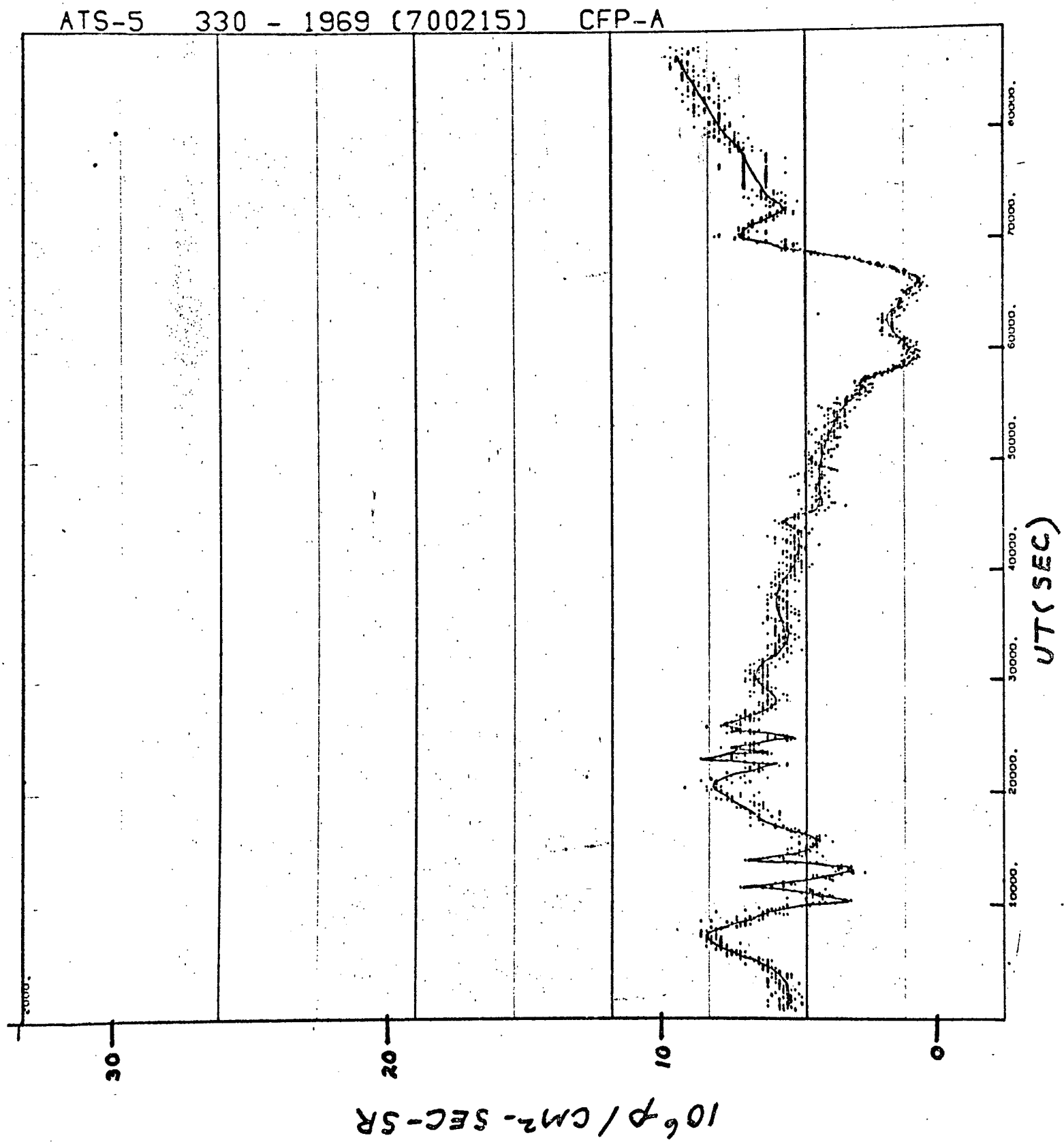

Fig. 29

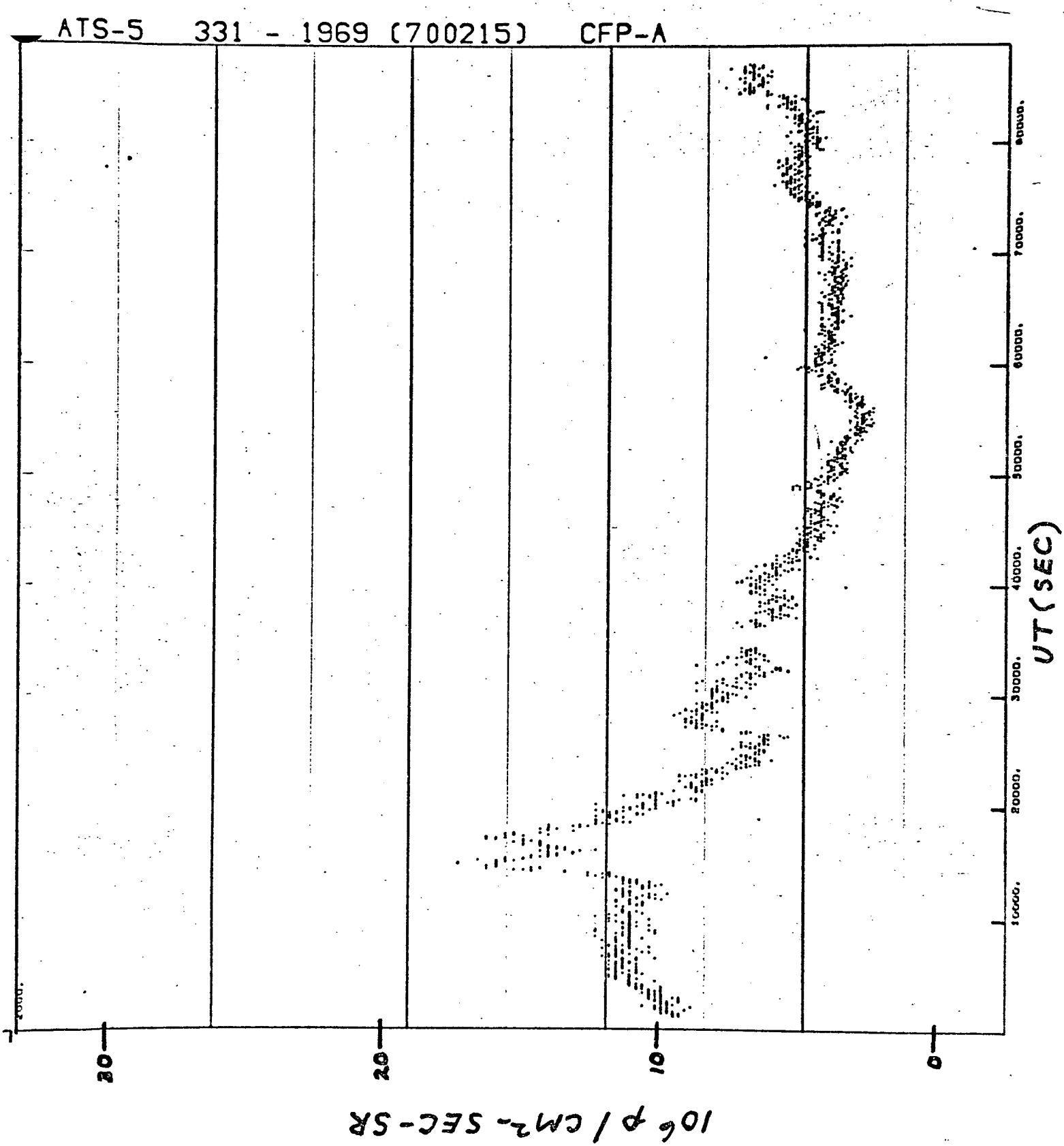

Fig. 30

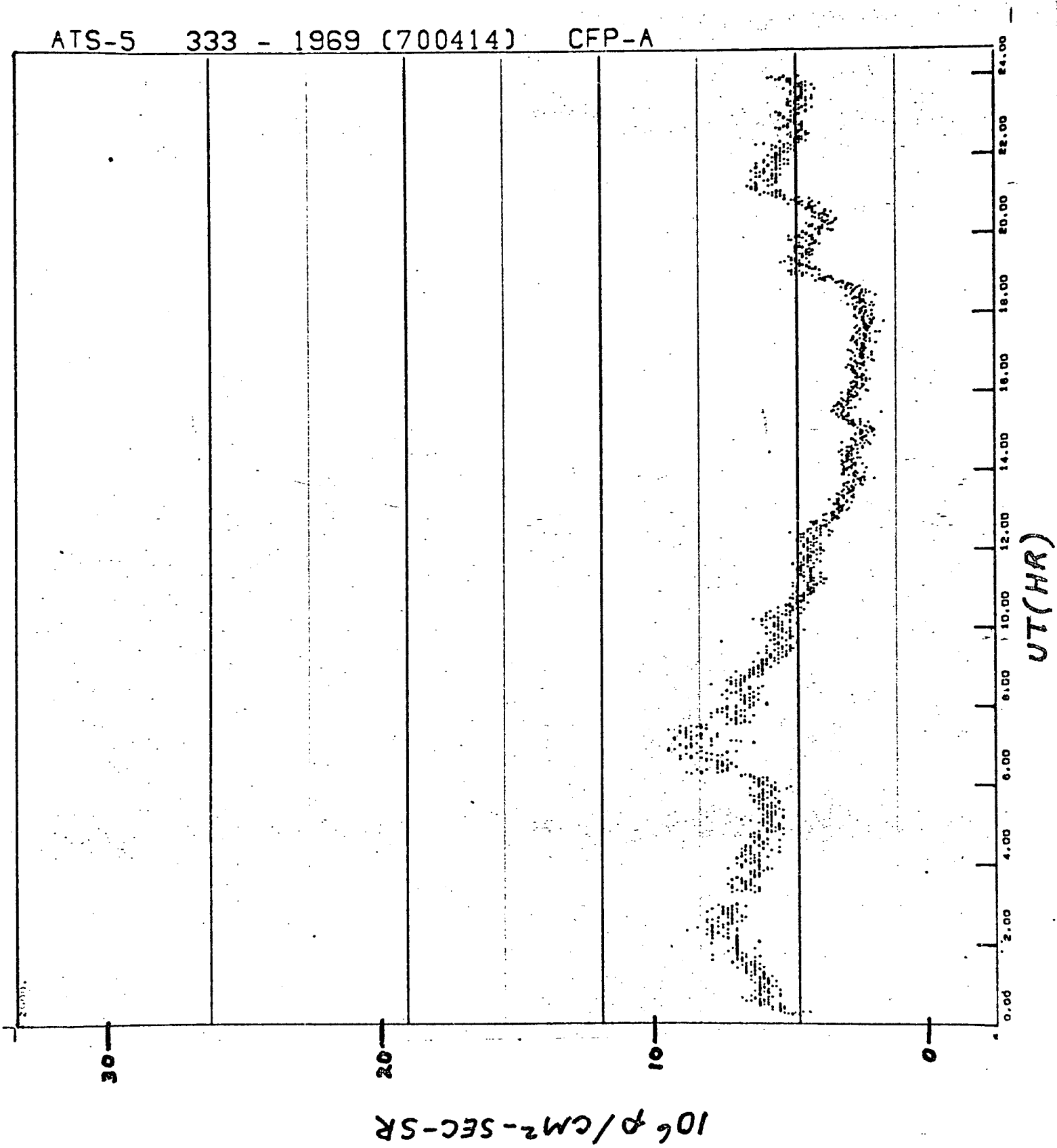
ATS-5 333 - 1969 (700414) CFP-A
0.00
2.00
4.00
6.00
8.00
10.00
12.00
14.00
16.00
18.00
20.00
22.00
24.00
UT (HR)
30
20
10
0
10⁶ P/CM²-SEC-SR

Fig. 31

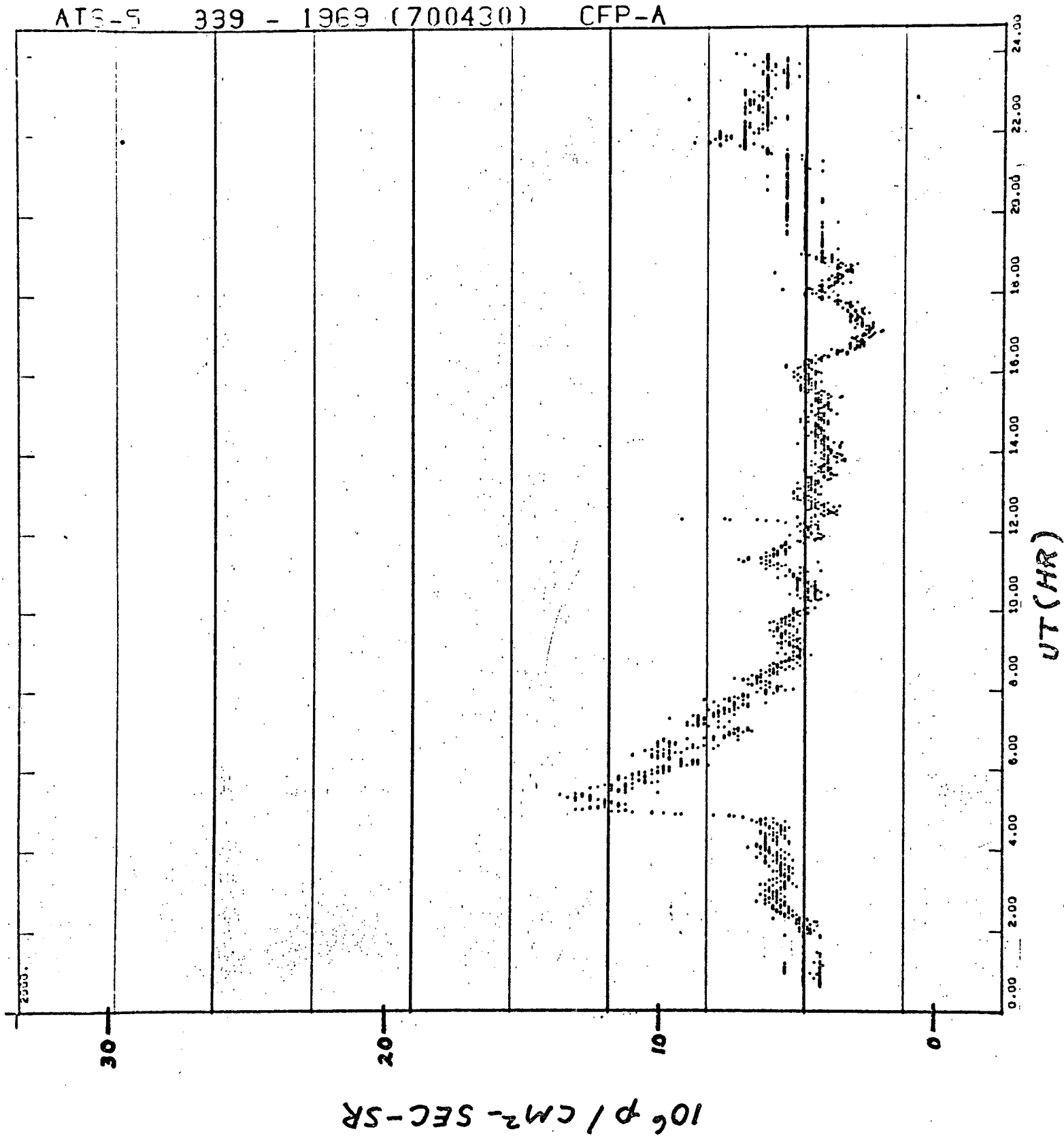
ATS-5 339 - 1969 (700430) CFP-A
0.00
2.00
4.00
6.00
8.00
10.00
12.00
14.00
16.00
18.00
20.00
22.00
24.00
UT (HR)
30
20
10
0
10⁶ P / CM²- SEC-SR

Fig. 32

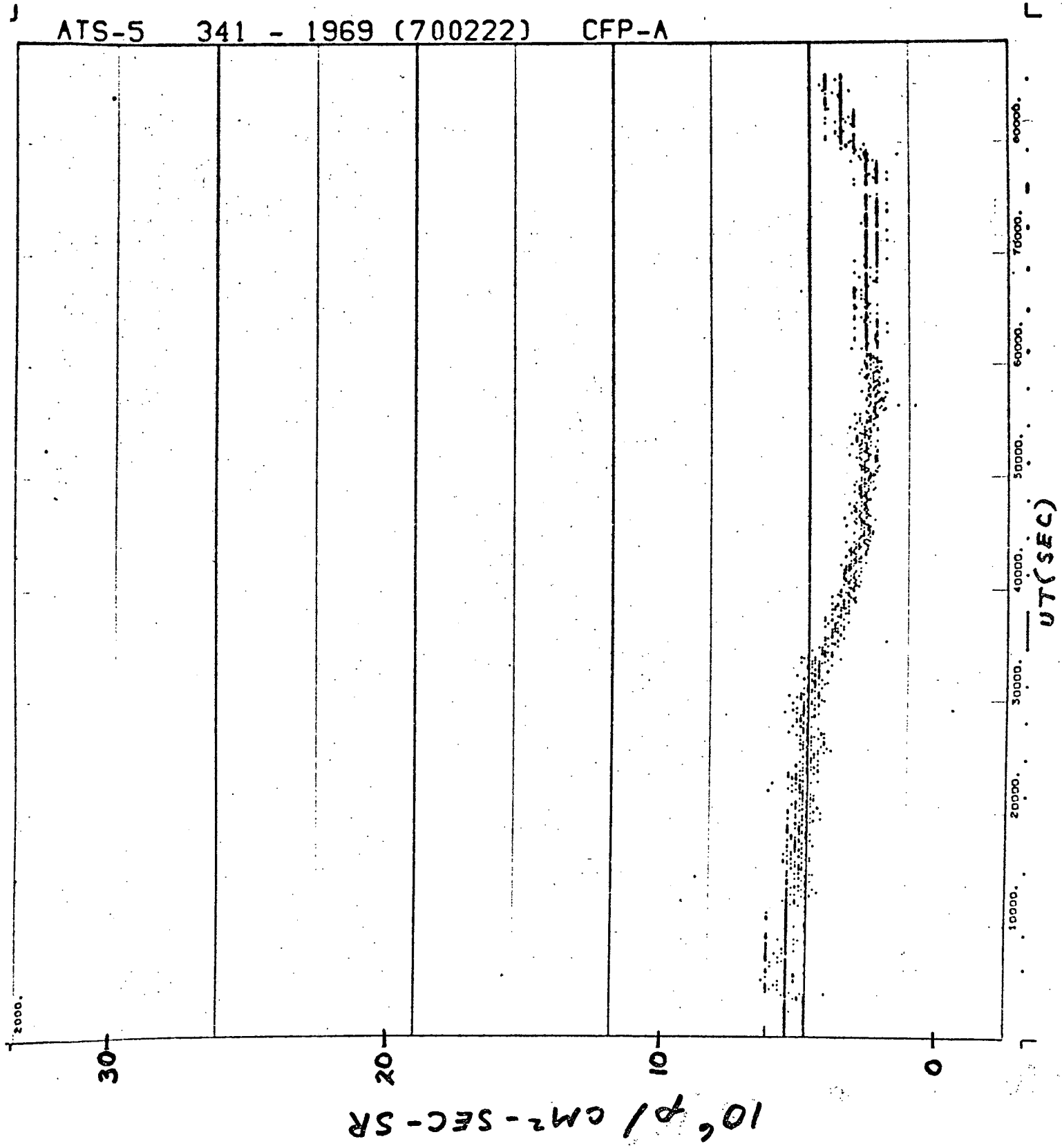
ATS-5 341 - 1969 (700222) CFP-A
UT(SEC)
10000.
20000.
30000.
40000.
50000.
60000.
70000.
80000.
2000.
30
20
10
0
10⁶ p/ CM²-SEC-SR

Fig. 33

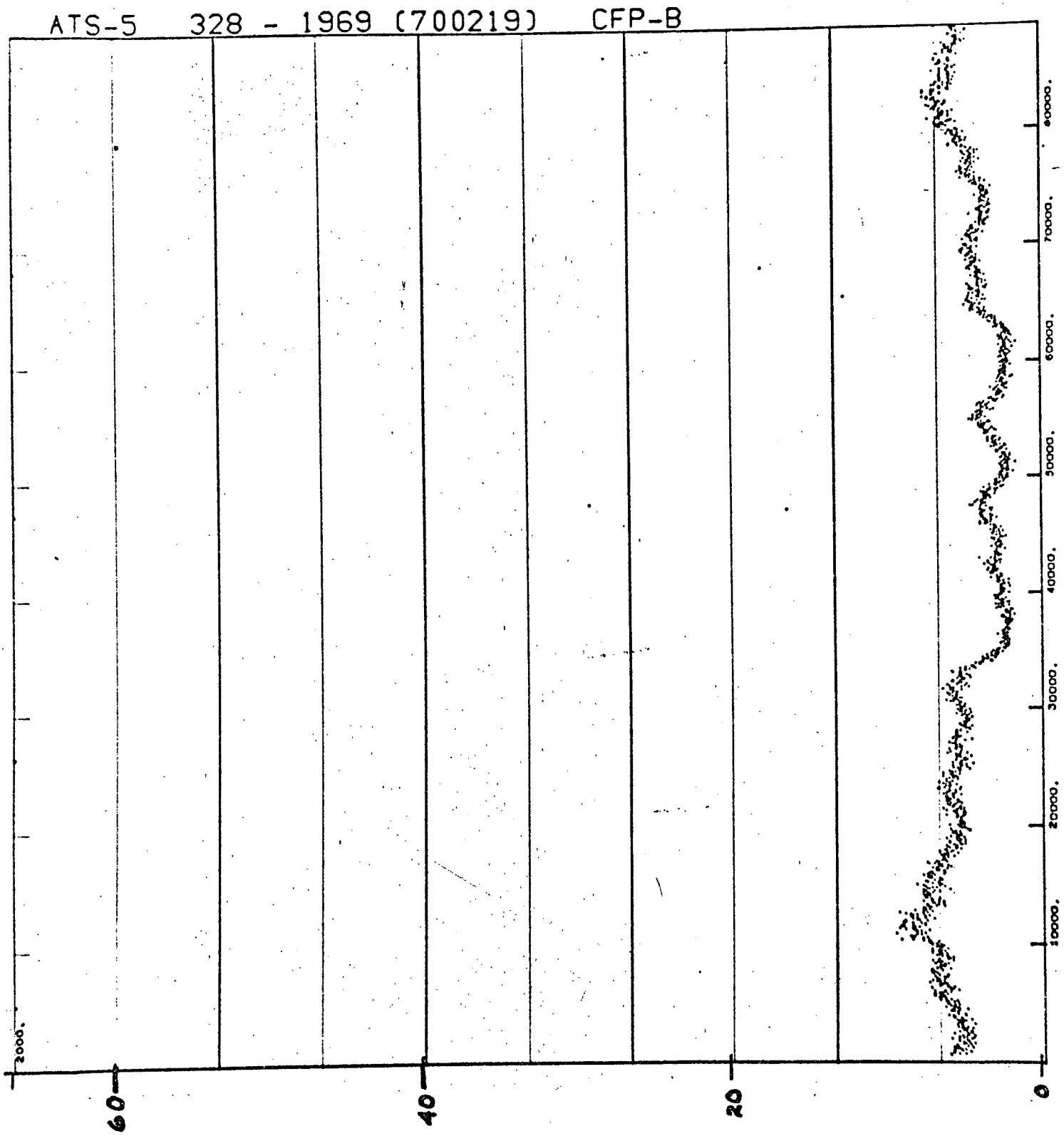

Fig. 34

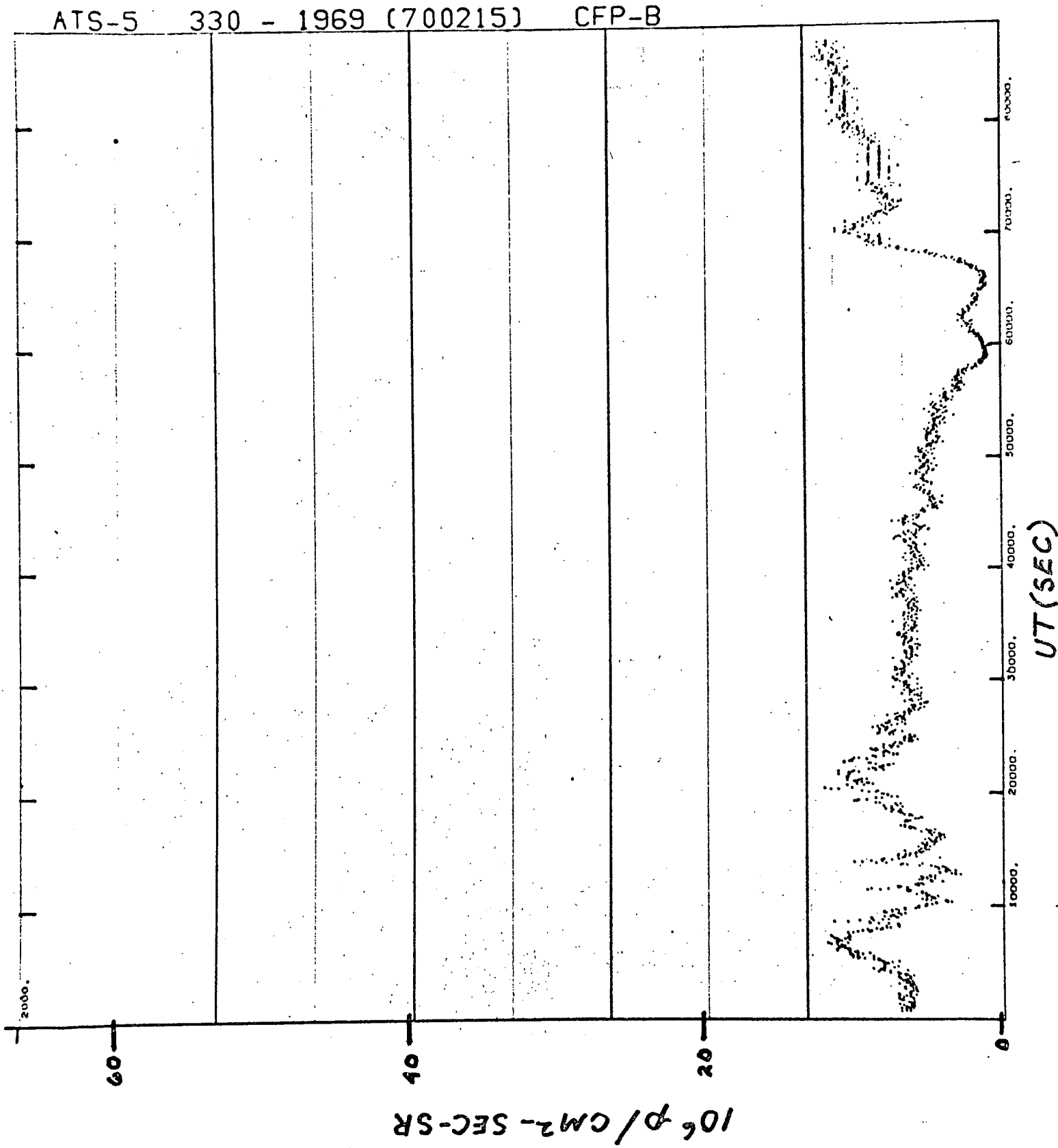
ATS-5 330 - 1969 (700215) CFP-B
60
40
20
0
2000.
10000.
20000.
30000.
40000.
50000.
60000.
70000.
80000.
UT (SEC)
10⁶ P/CM²- SEC-SR

Fig. 35

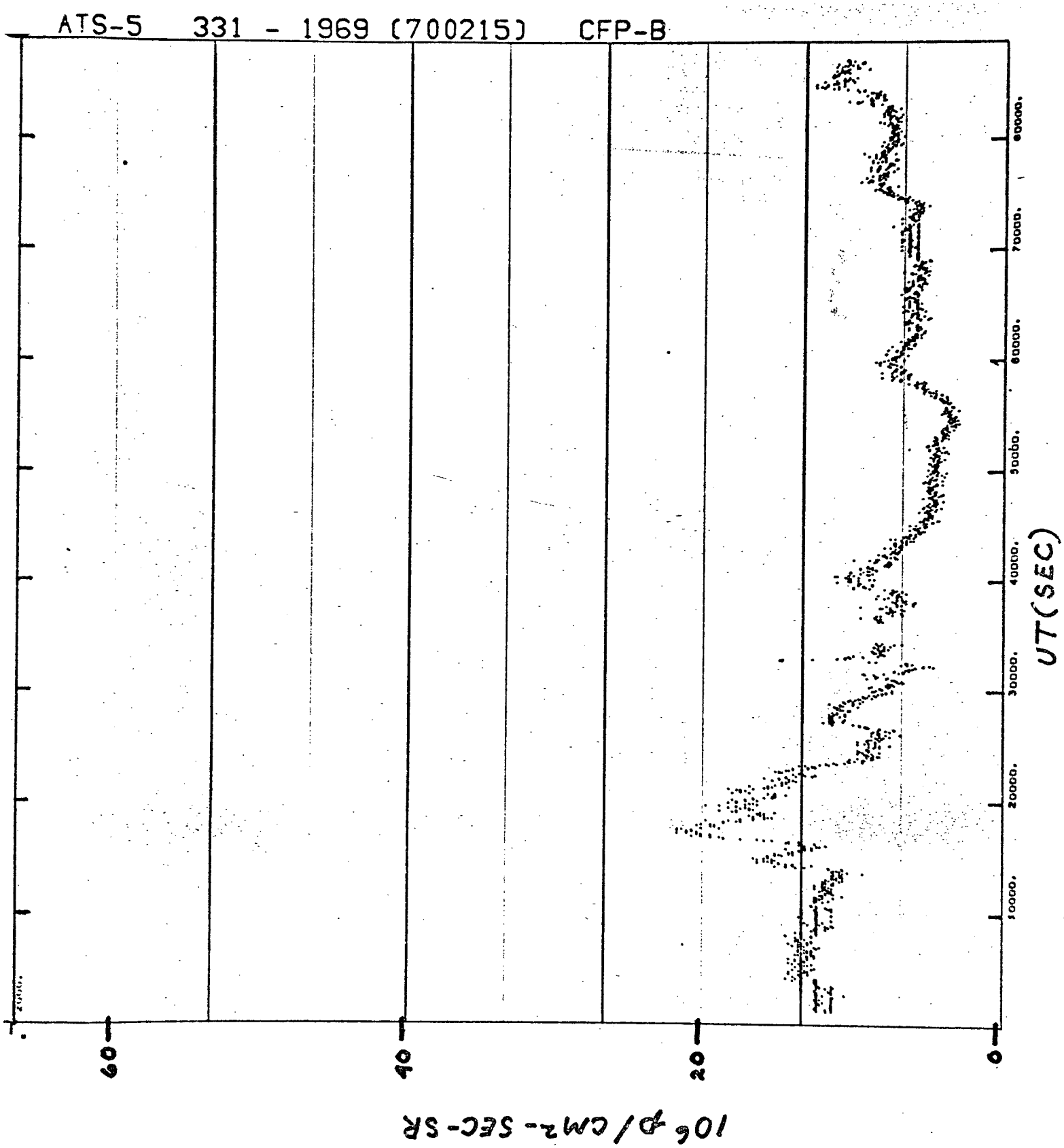
ATS-5 331 - 1969 (700215) CFP-B
60
40
20
0
10000.
20000.
30000.
40000.
50000.
60000.
70000.
80000.
UT(SEC)
10⁶ P/CM²-SEC-SR

Fig. 36

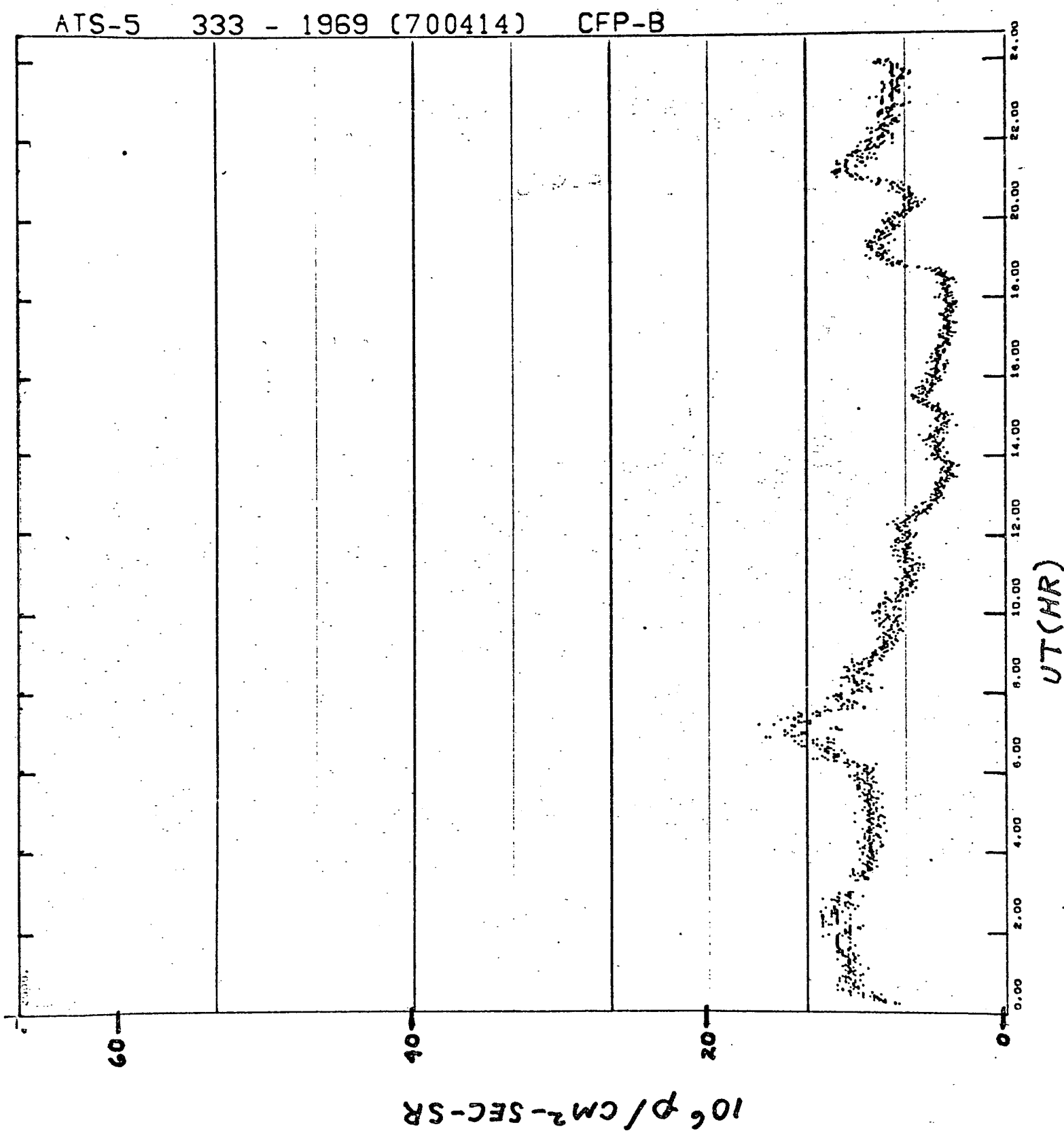
ATS-5 333 - 1969 (700414) CFP-B
60
40
20
0
10⁶ P/CM²-SEC-SR
0.00
2.00
4.00
6.00
8.00
10.00
12.00
14.00
16.00
18.00
20.00
22.00
24.00
UT(HR)

Fig. 37

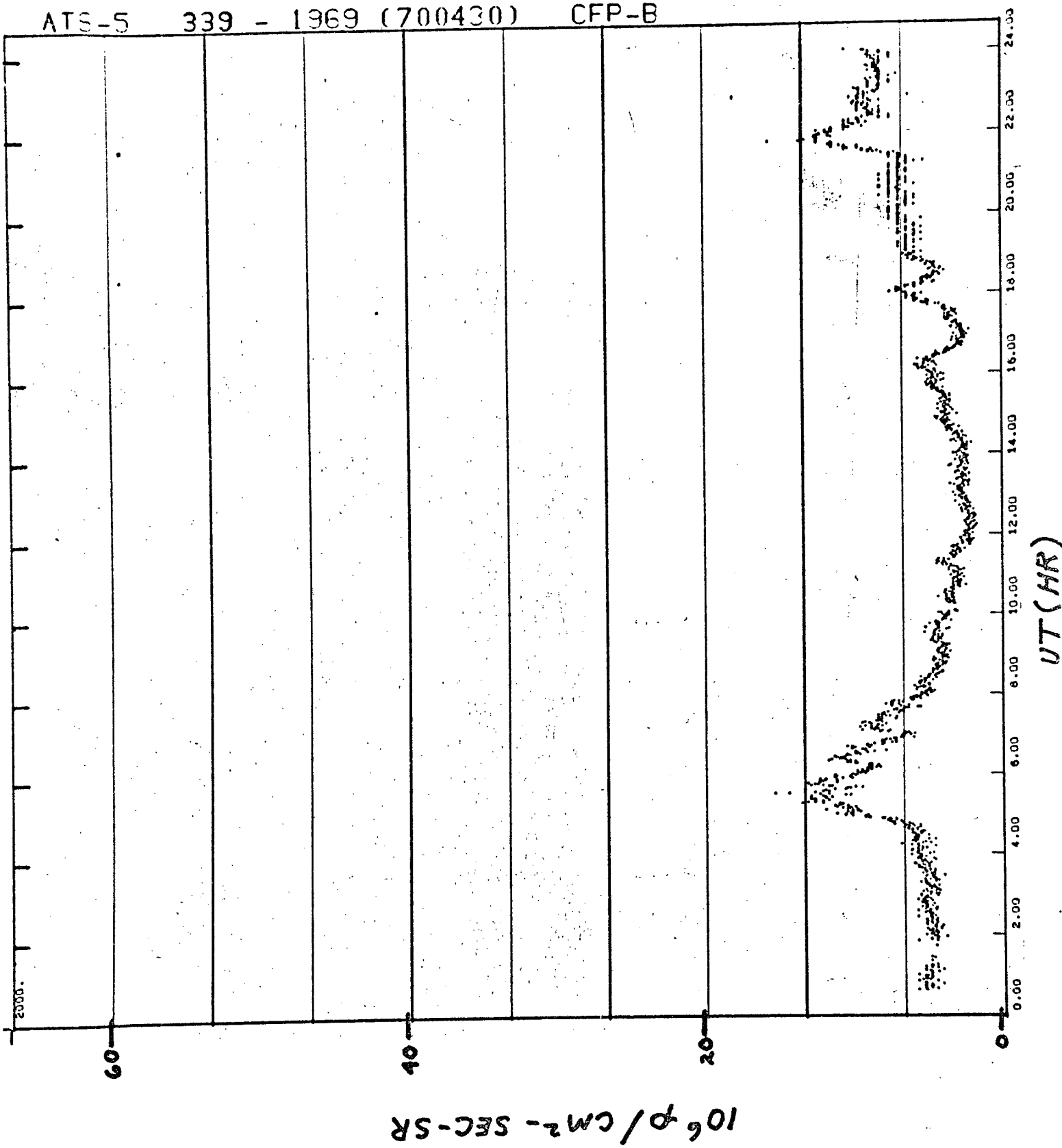
ATS-5 339 - 1969 (700430) CFP-B
2000.
60
40
20
0
0.00
2.00
4.00
6.00
8.00
10.00
12.00
14.00
16.00
18.00
20.00
22.00
24.00
UT (HR)
10⁶ P/CM²- SEC-SR

Fig. 38

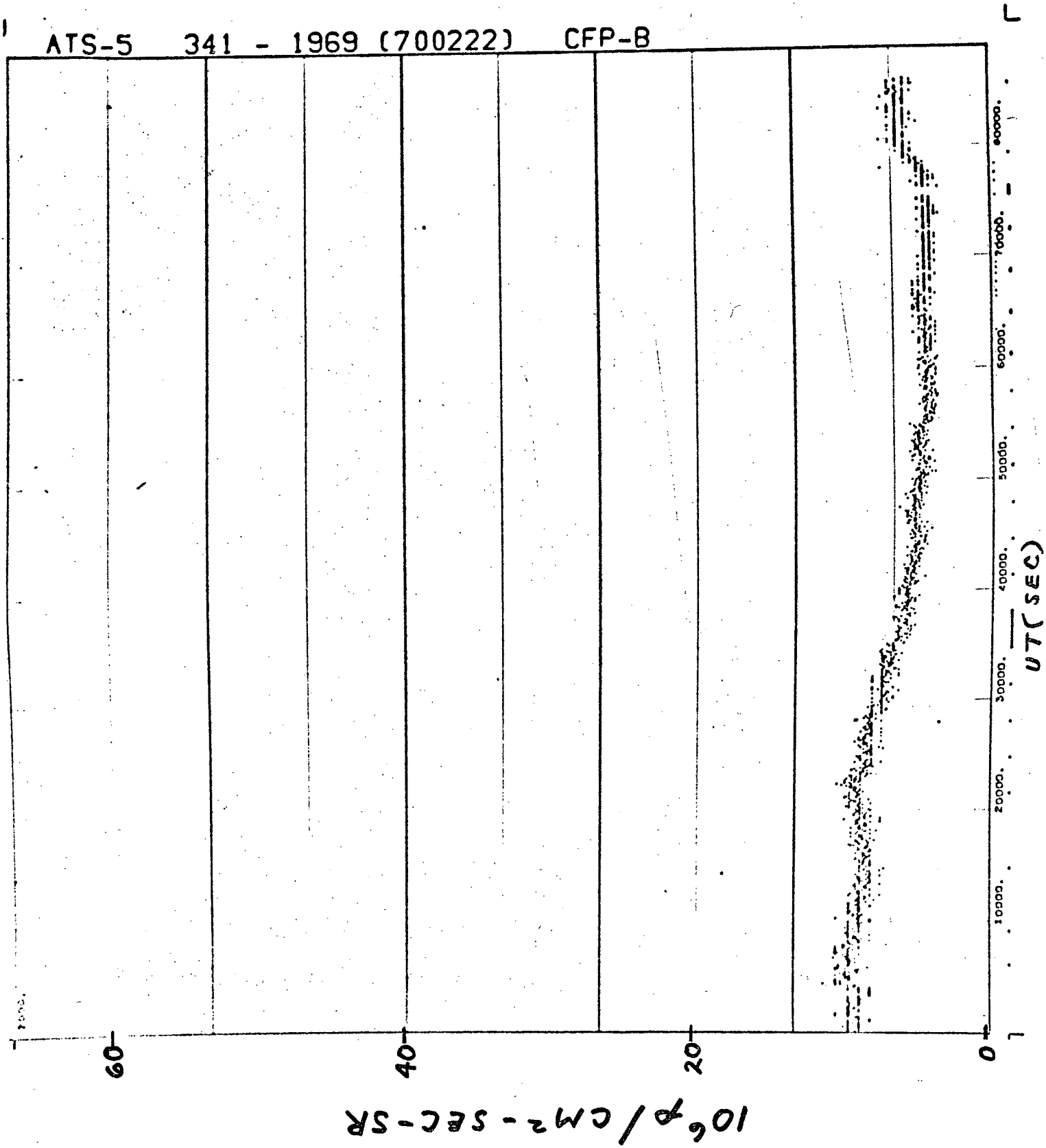

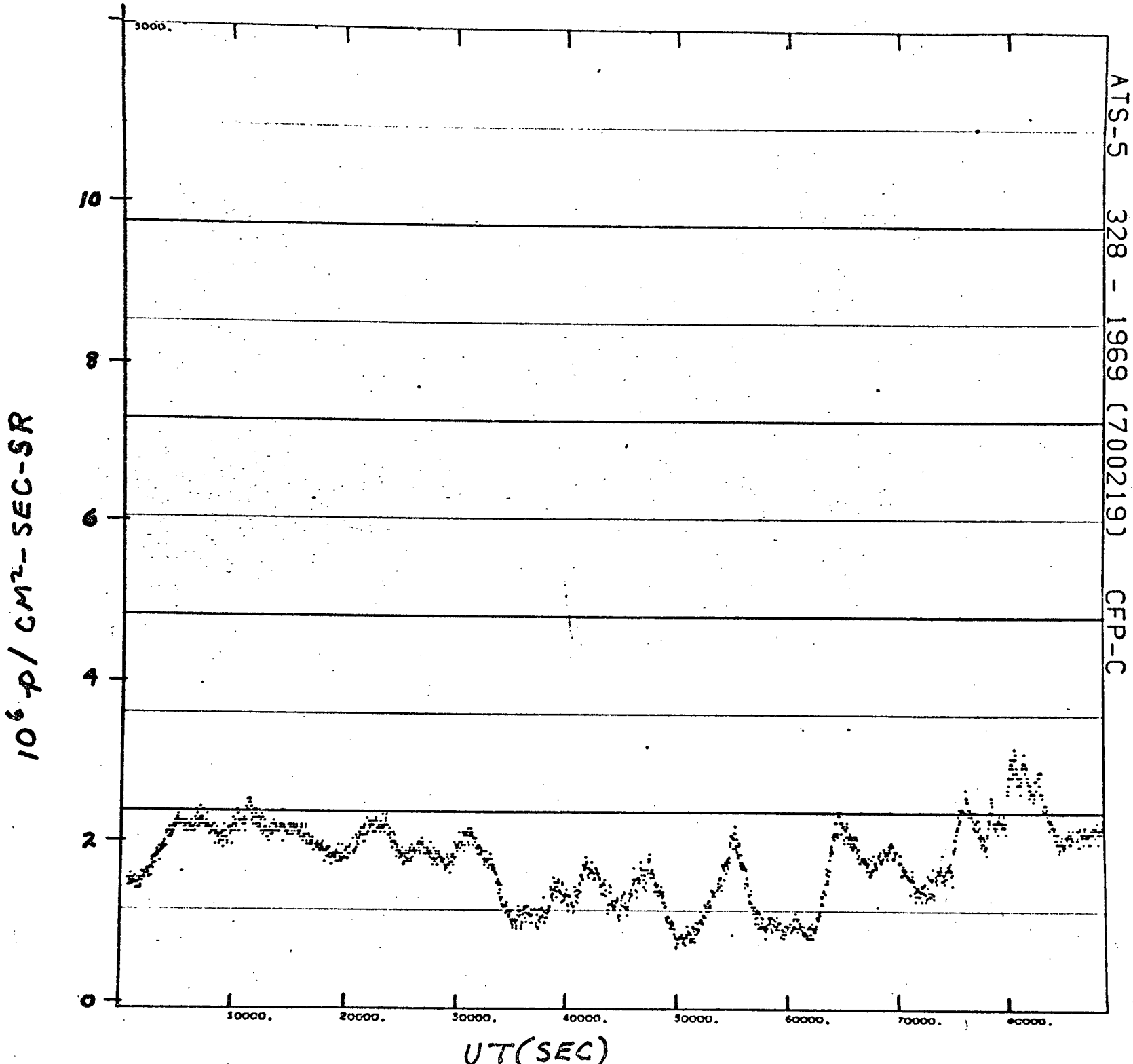
ATS-5 328 - 1969 (700219) CFP-C
10^6 p/CM^2-SEC-SR
UT(SEC)
0
2
4
6
8
10
10000.
20000.
30000.
40000.
50000.
60000.
70000.
80000.
3000.

Fig. 39

Fig. 40

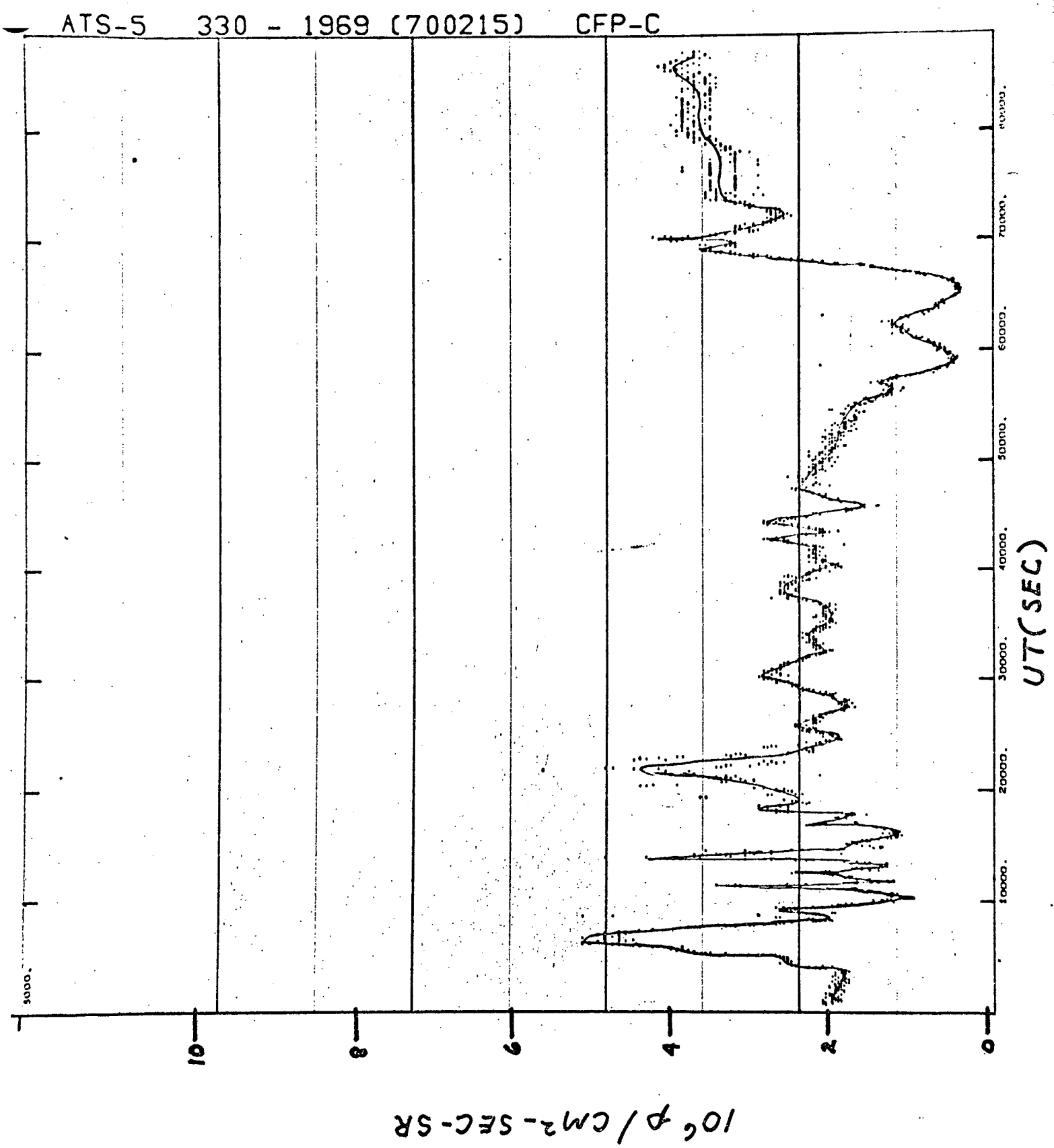

Fig. 41

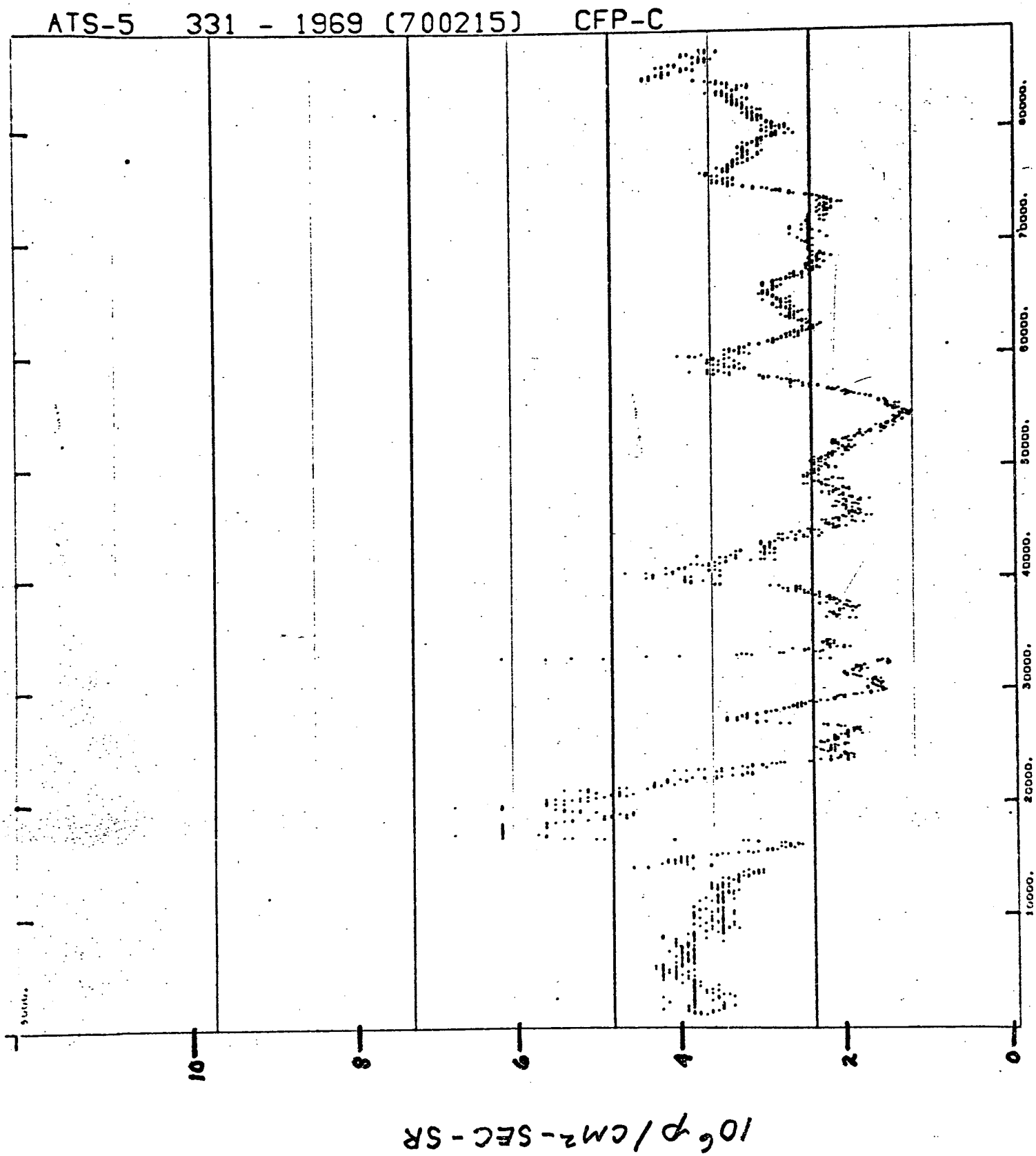
ATS-5 331 - 1969 (700215) CFP-C
10
8
6
4
2
0
10000.
20000.
30000.
40000.
50000.
60000.
70000.
80000.
UT (SEC)
10⁶ P/CM²-SEC-SR

Fig. 42

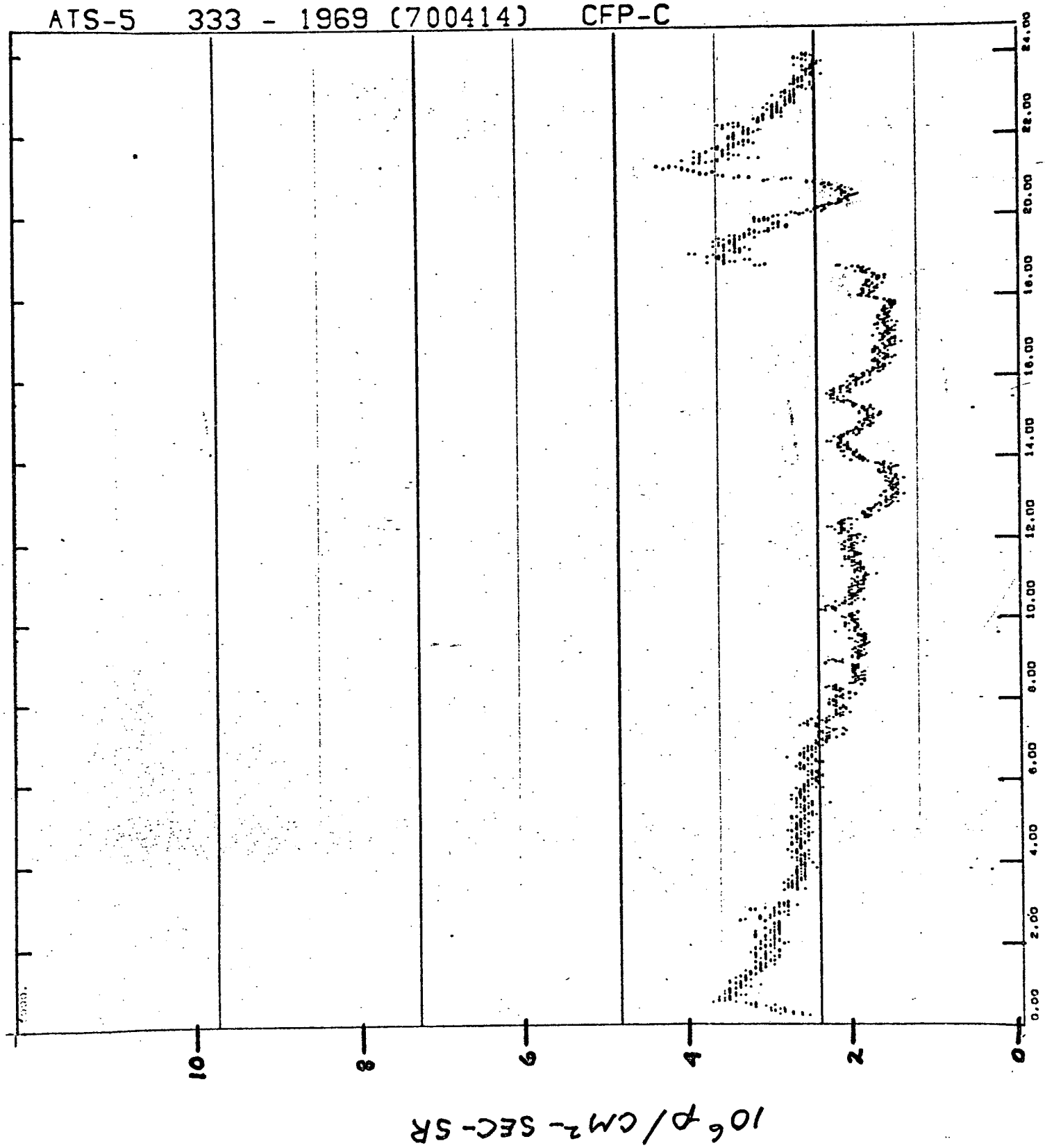

Fig. 43

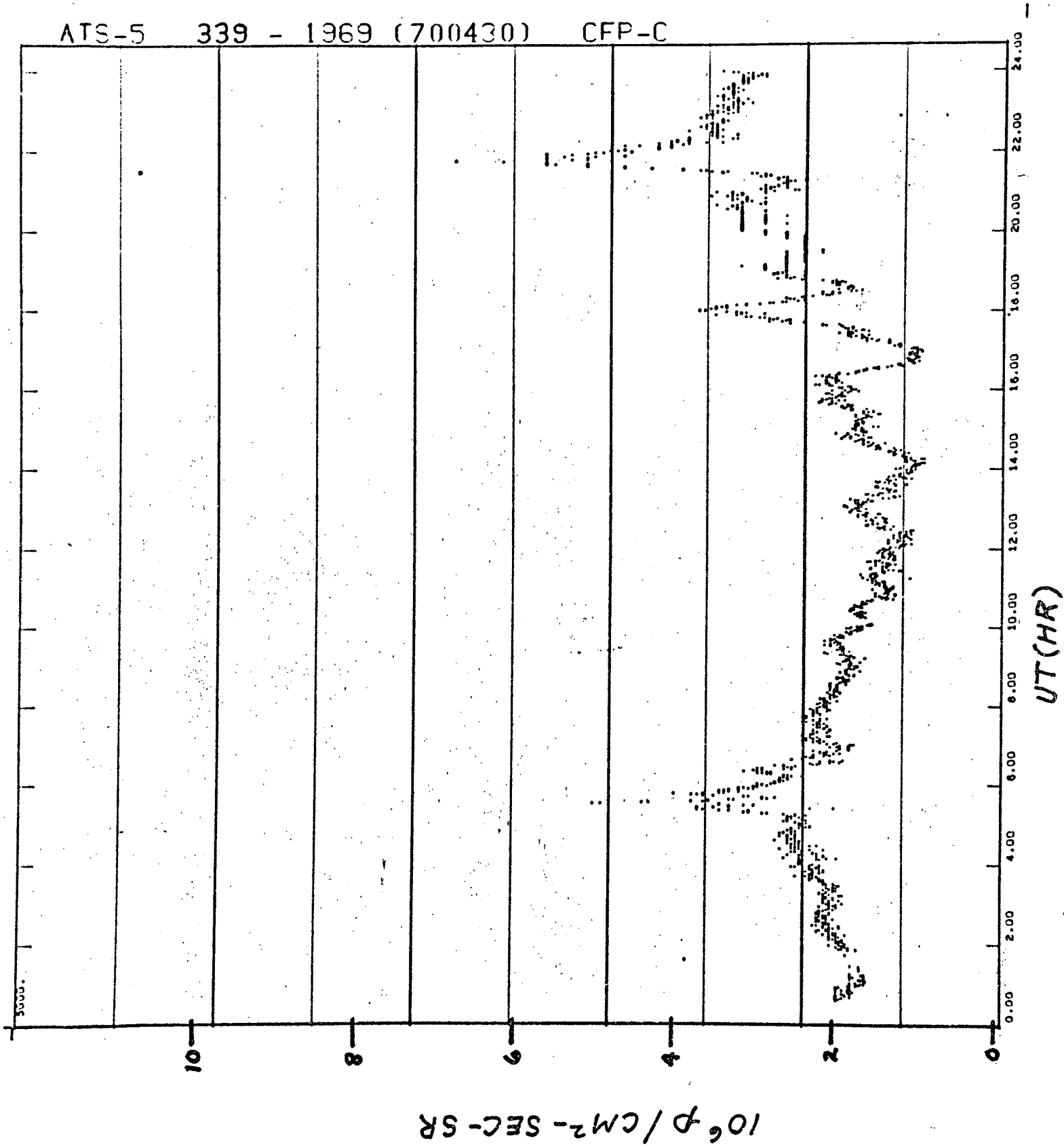
ATS-5 339 - 1969 (700430) CFP-C
10
8
6
4
2
0
0.00
2.00
4.00
6.00
8.00
10.00
12.00
14.00
16.00
18.00
20.00
22.00
24.00
UT(HR)
10⁶ P / CM²- SEC- SR

Fig. 44

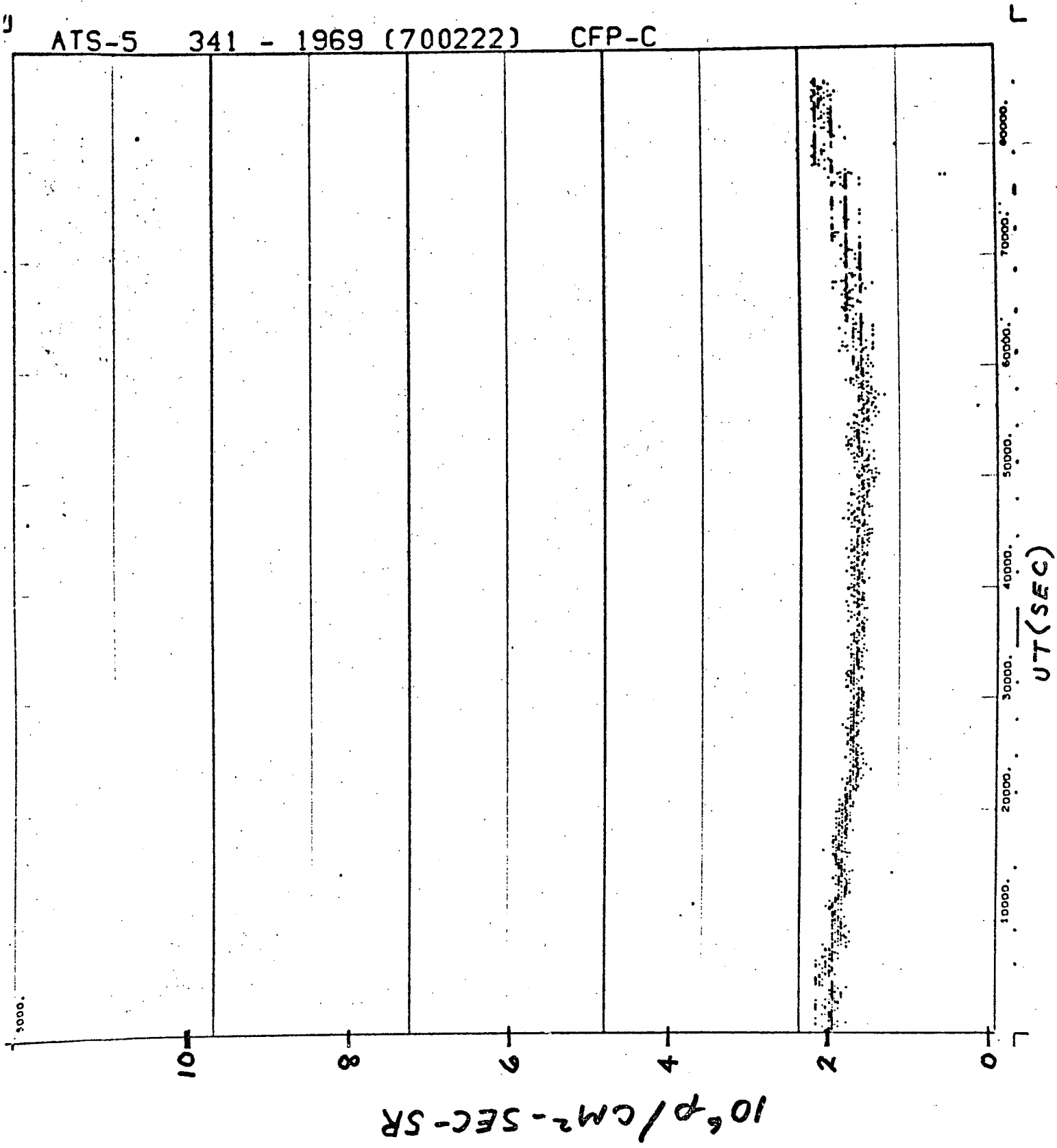
ATS-5 341 - 1969 (700222) CFP-C
UT(SEC)
10⁶ρ/CM²-SEC-SR
10
8
6
4
2
0
10000.
20000.
30000.
40000.
50000.
60000.
70000.
80000.

Fig. 45

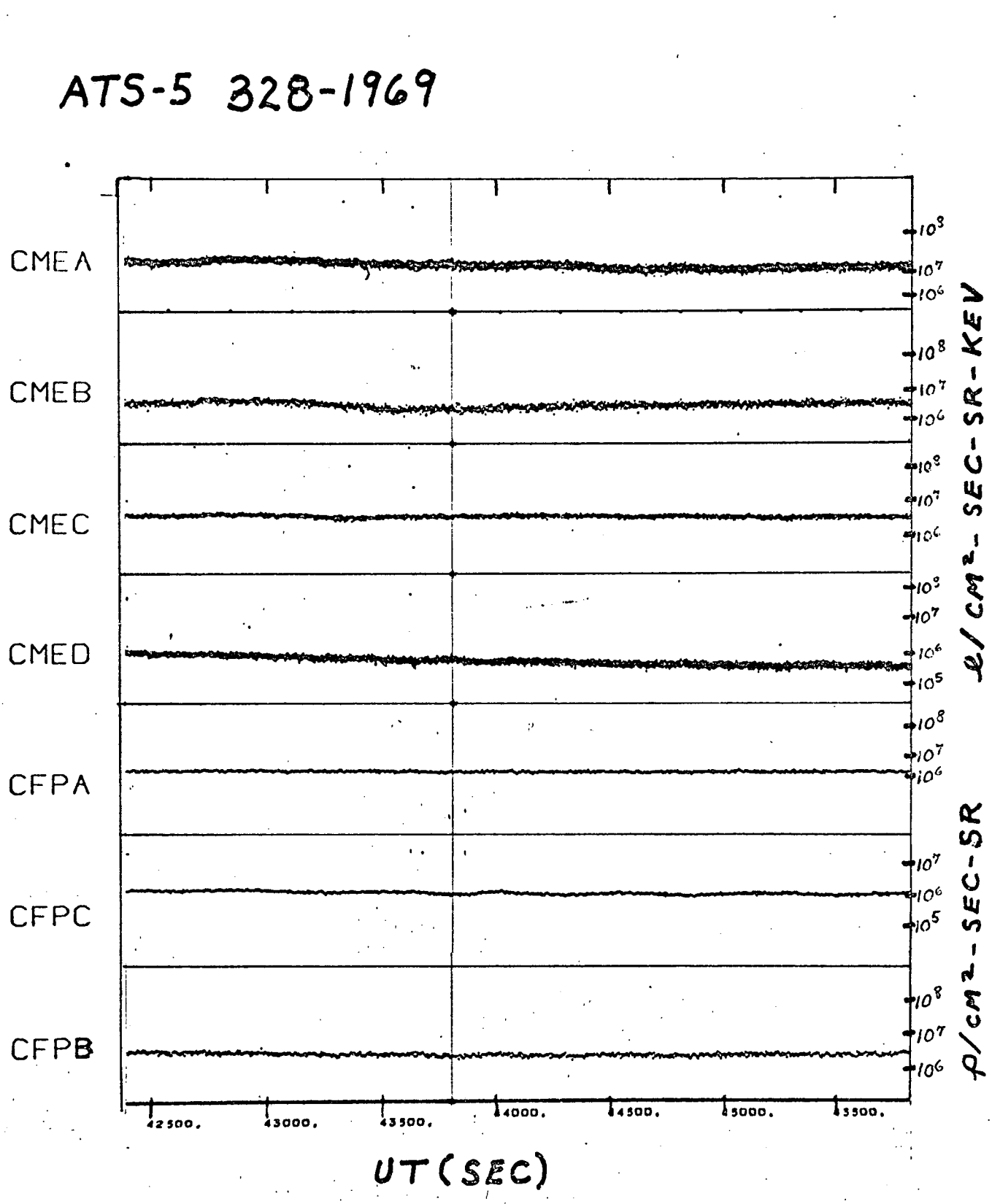
ATS-5 328-1969
CMEA
CMEB
CMEC
CMED
CFPA
CFPC
CFPB
10^8
10^7
10^6
10^5
42500.
43000.
43500.
44000.
44500.
45000.
45500.
UT (SEC)
e/cm²-sec-sr-kev
p/cm²-sec-sr

Fig. 46

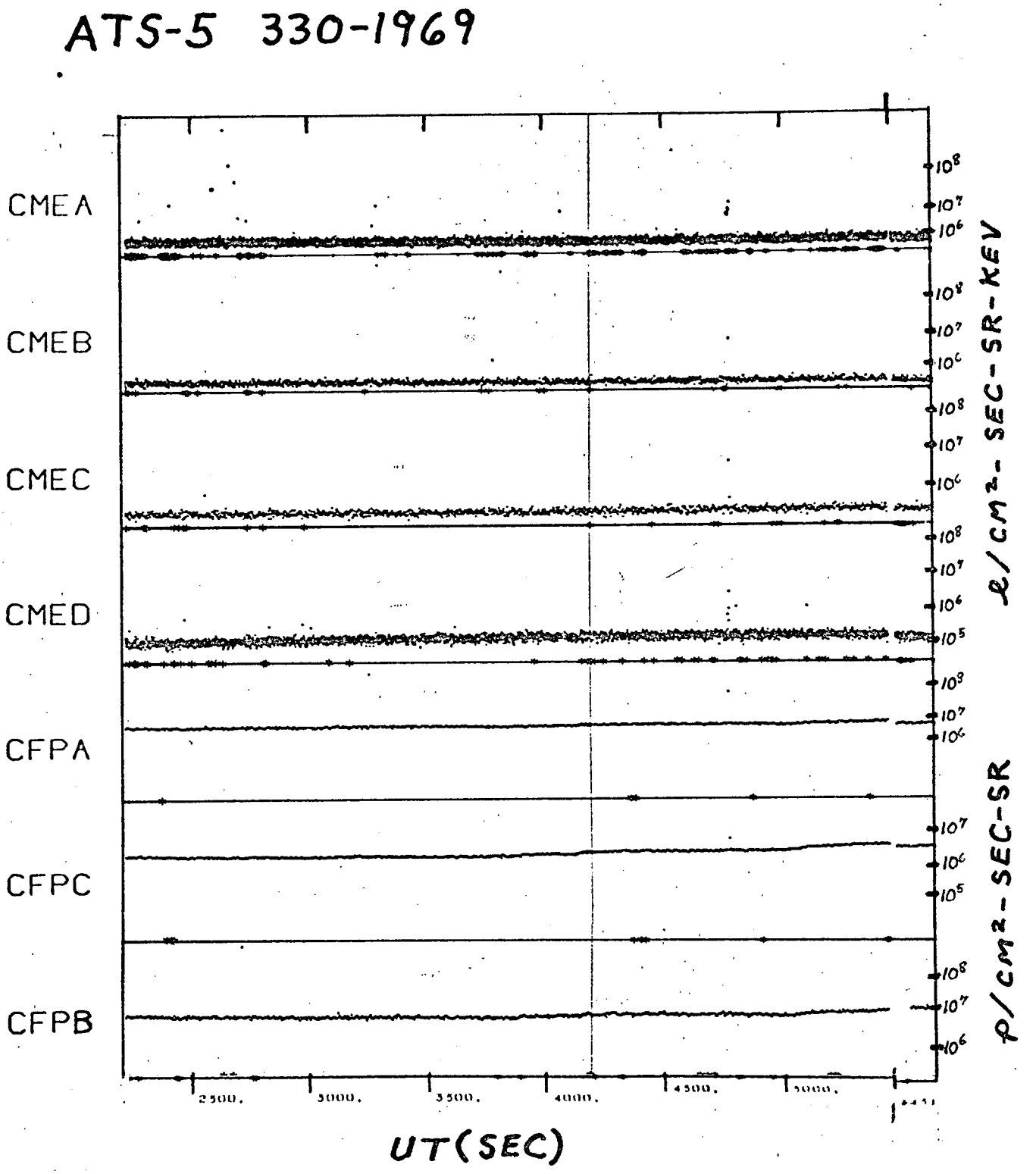
ATS-5 330-1969
CMEA
CMEB
CMEC
CMED
CFPA
CFPC
CFPB
10^8
10^7
10^6
10^5
10^9
10^4
2500.
3000.
3500.
4000.
4500.
5000.
UT(SEC)
e/cm²-sec-sr-kev
p/cm²-sec-sr

Fig. 47

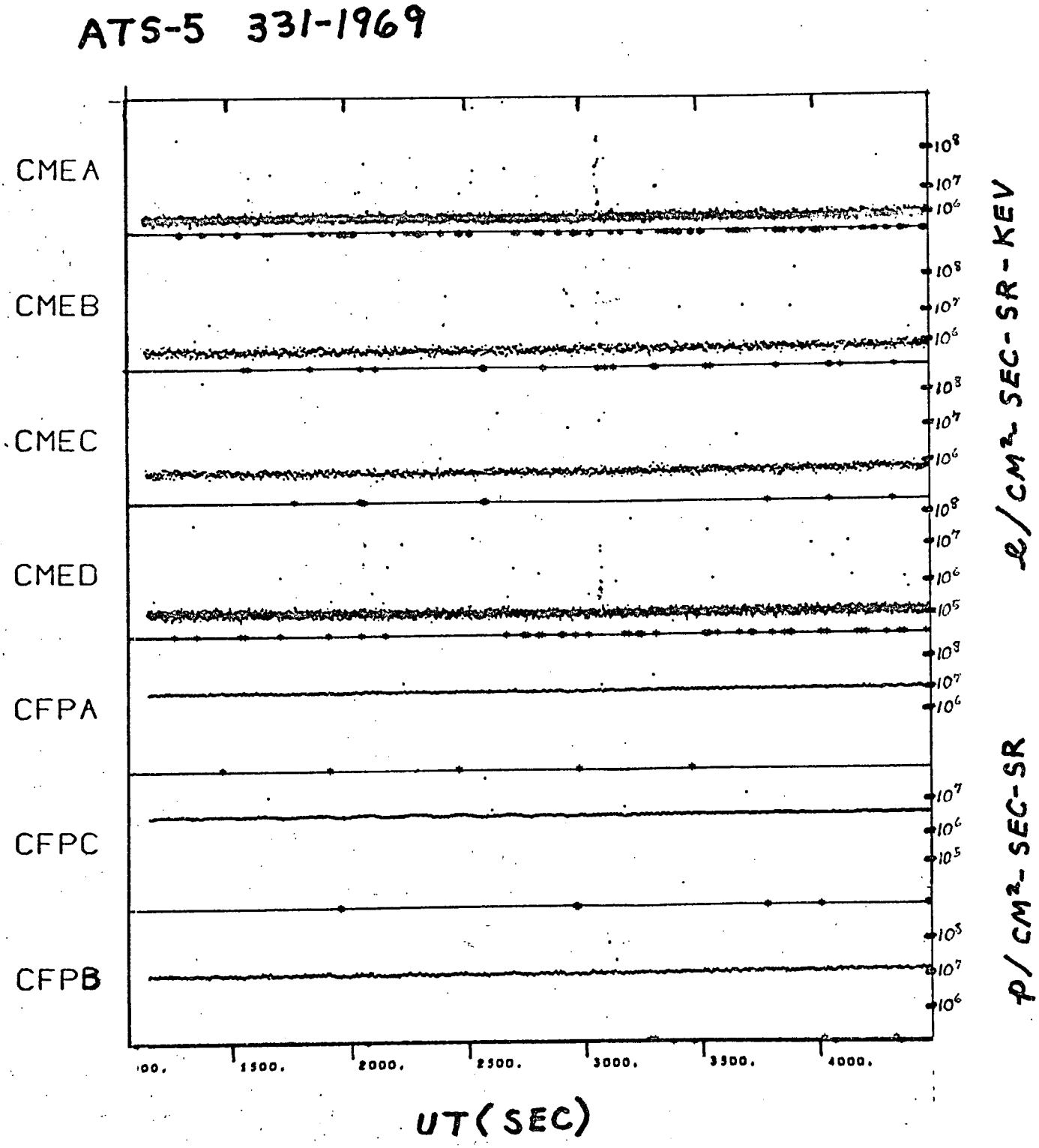
ATS-5 331-1969
CMEA
CMEB
CMEC
CMED
CFPA
CFPC
CFPB
10^8
10^7
10^6
10^5
e/CM²-SEC-SR-KEV
p/CM²-SEC-SR
1500.
2000.
2500.
3000.
3500.
4000.
UT(SEC)

Fig. 48

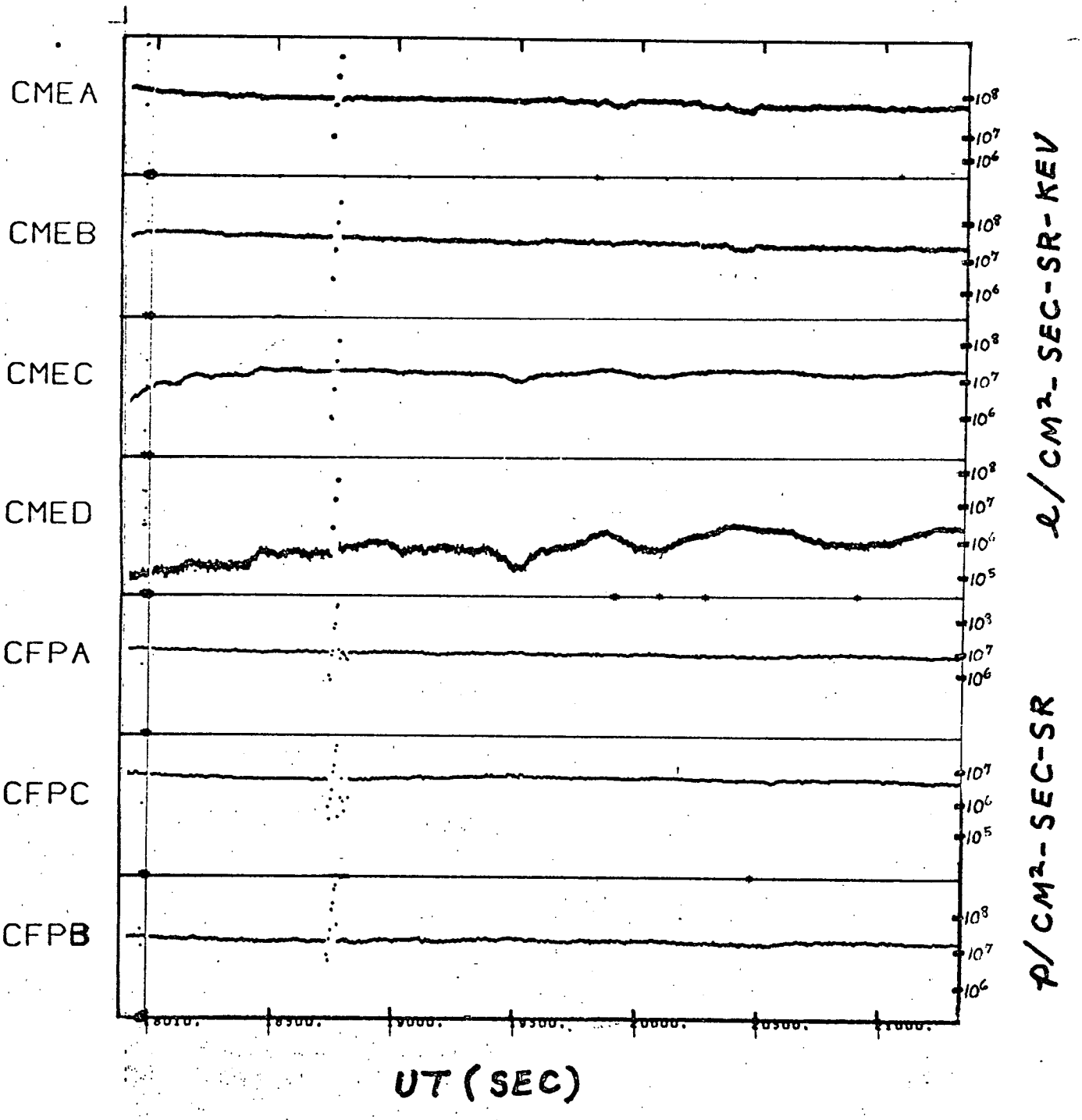
ATS-5 331-1969
CMEA
CMEB
CMEC
CMED
CFPA
CFPC
CFPB
10^8
10^7
10^6
10^5
10^3
UT (SEC)
e/CM²-SEC-SR-KEV
p/CM²-SEC-SR

Fig. 49

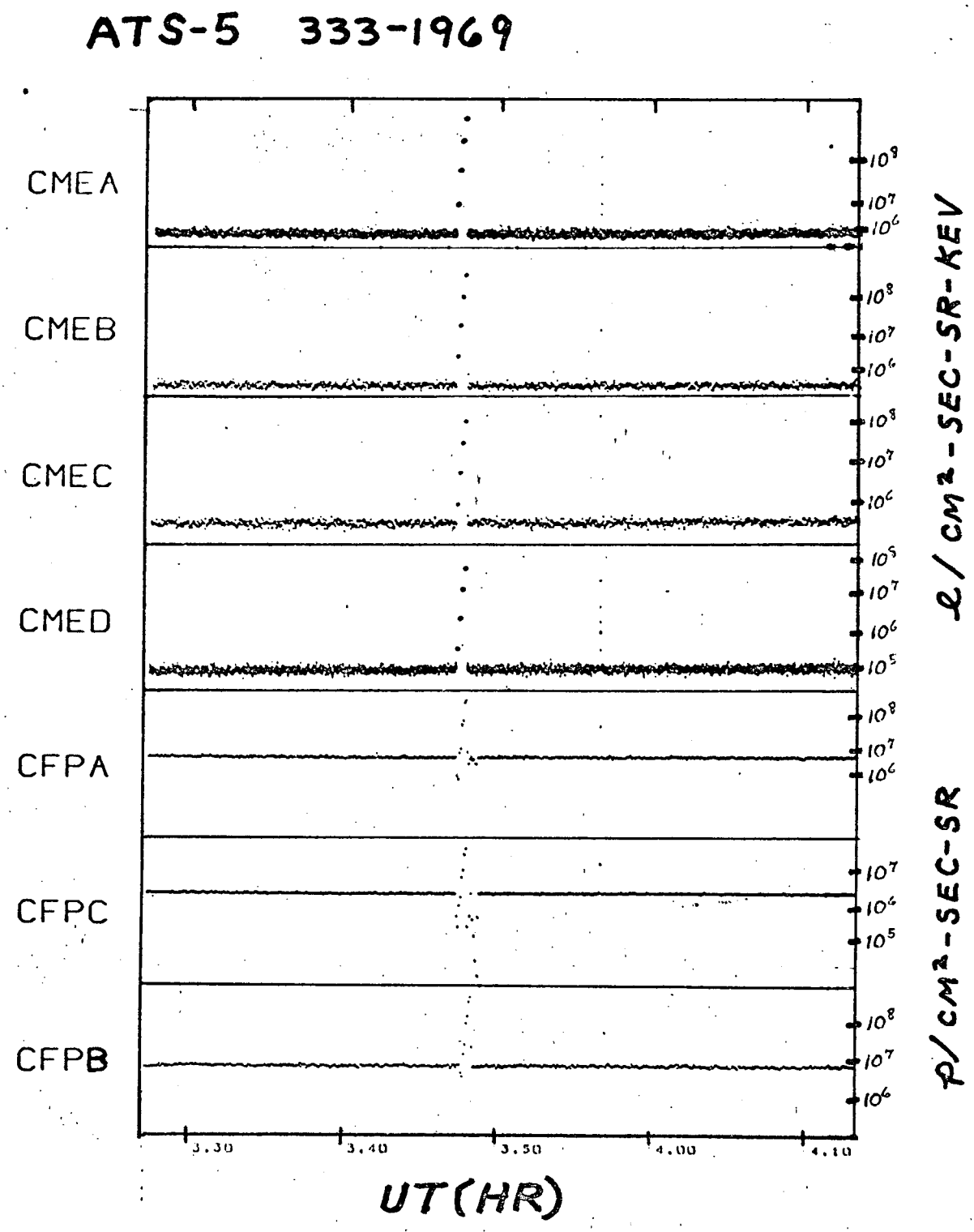
ATS-5 333-1969
CMEA
CMEB
CMEC
CMED
CFPA
CFPC
CFPB
10^9
10^7
10^6
10^8
10^7
10^6
10^8
10^7
10^6
10^5
10^7
10^6
10^5
10^8
10^7
10^6
10^7
10^4
10^5
10^8
10^7
10^6
3.30
3.40
3.50
4.00
4.10
UT(HR)
P/CM²-SEC-SR
P/CM²-SEC-SR-KEV

Fig. 50

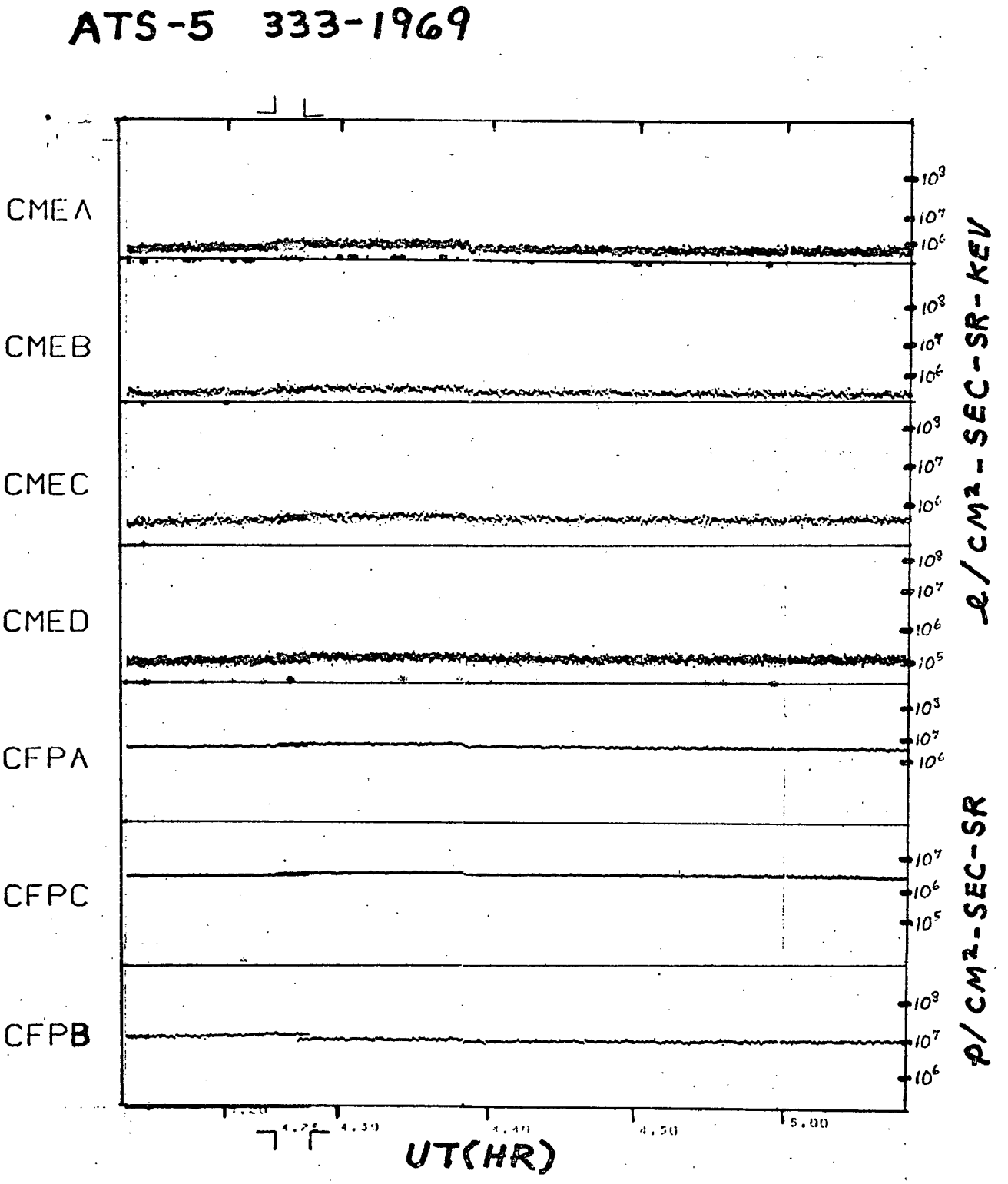
ATS-5 333-1969
CMEA
CMEB
CMEC
CMED
CFPA
CFPC
CFPB
10^9
10^7
10^6
10^8
10^5
e/CM²-SEC-SR-KEV
p/CM²-SEC-SR
4.30
4.40
4.50
5.00
UT(HR)

Fig. 51

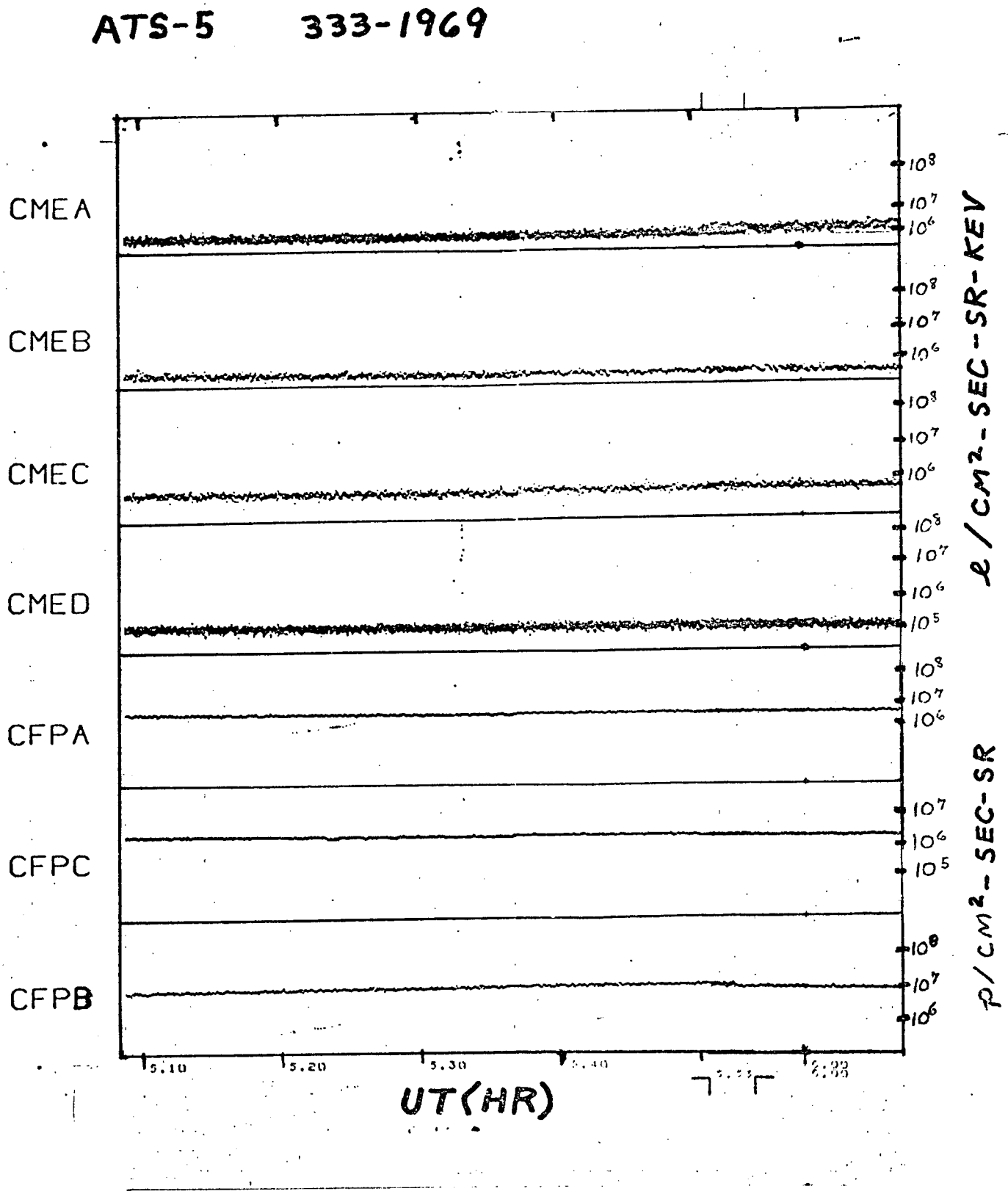
ATS-5 333-1969
CMEA
CMEB
CMEC
CMED
CFPA
CFPC
CFPB
10^8
10^7
10^6
10^5
e/CM²-SEC-SR-KEV
P/CM²-SEC-SR
5.10
5.20
5.30
UT(HR)

Fig. 52

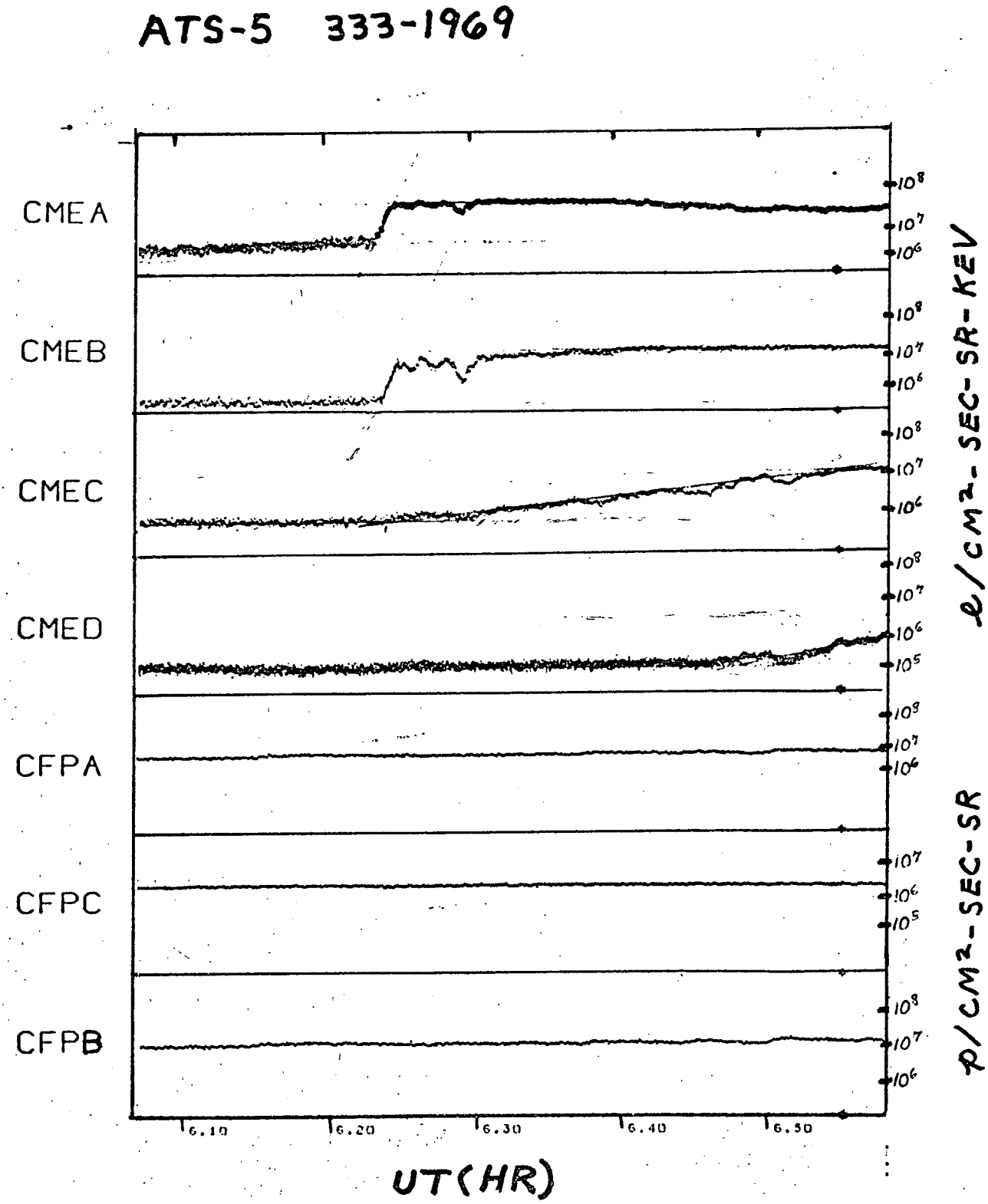
ATS-5 333-1969
CMEA
CMEB
CMEC
CMED
CFPA
CFPC
CFPB
10^8
10^7
10^6
10^5
10^9
6.10
6.20
6.30
6.40
6.50
UT(HR)
e/CM²-SEC-SR-KEV
p/CM²-SEC-SR

Fig. 53

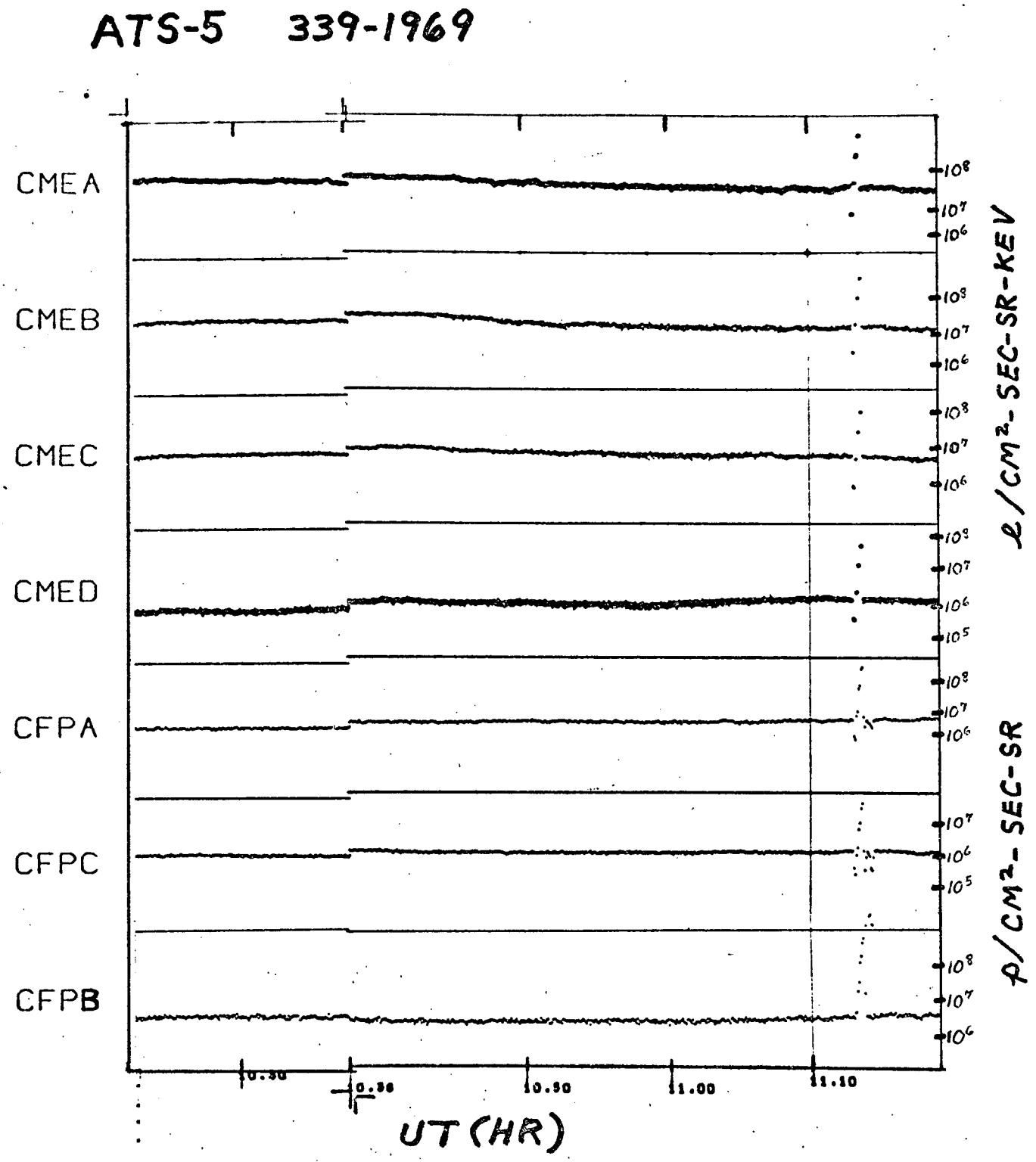
ATS-5 339-1969
CMEA
CMEB
CMEC
CMED
CFPA
CFPC
CFPB
10^8
10^7
10^6
10^5
P/CM²-SEC-SR-KEV
P/CM²-SEC-SR
0.30
0.50
1.00
1.10
UT (HR)

Fig. 54

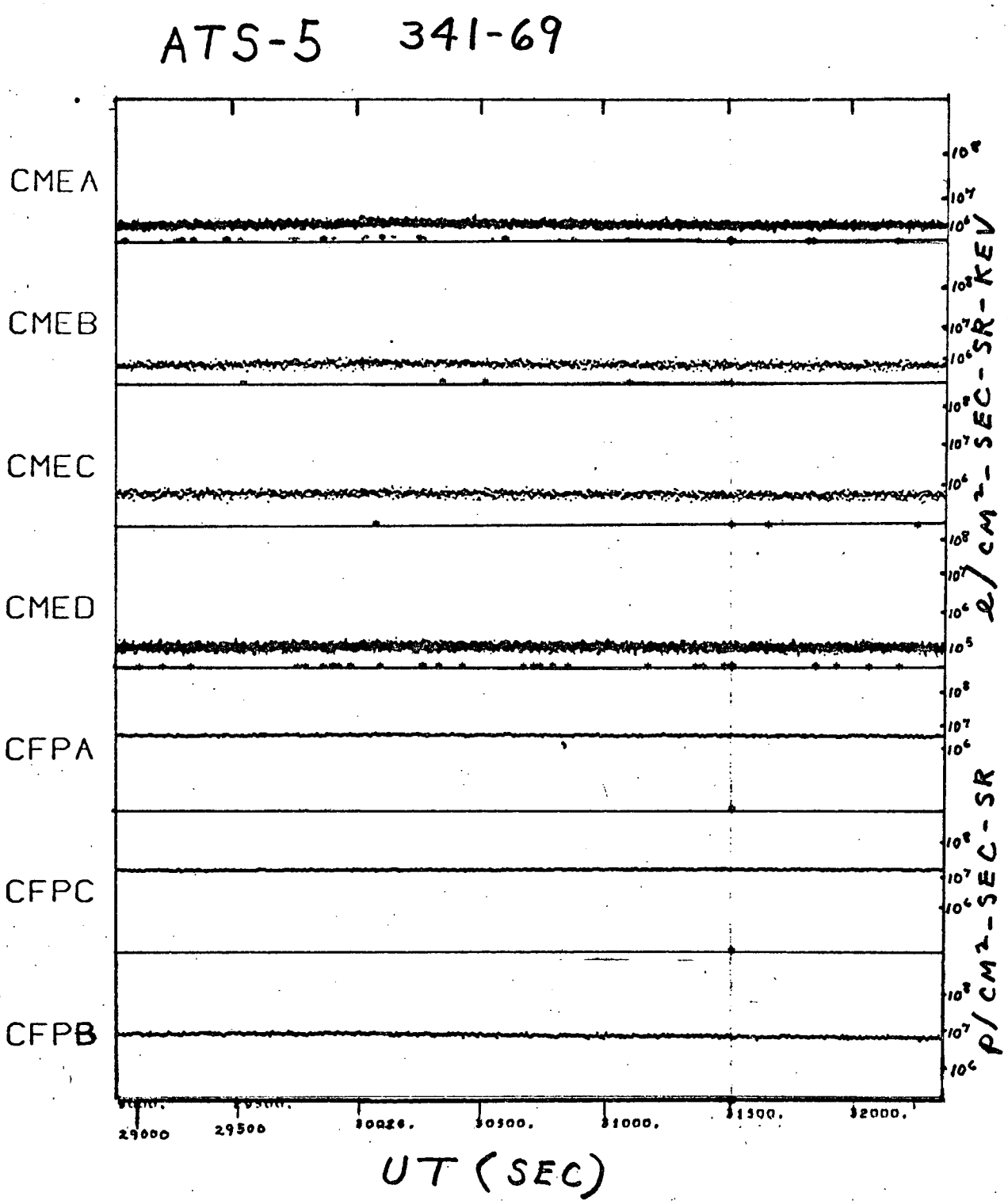
ATS-5 341-69
CMEA
CMEB
CMEC
CMED
CFPA
CFPC
CFPB
P/CM²-SEC-SR-KEV
P/CM²-SEC-SR
29000
29500
30000.
30500.
31000.
31500.
32000.
UT (SEC)

Fig. 55

HIGLO CME OUTPUTS GRP 1 ORBIT A4027

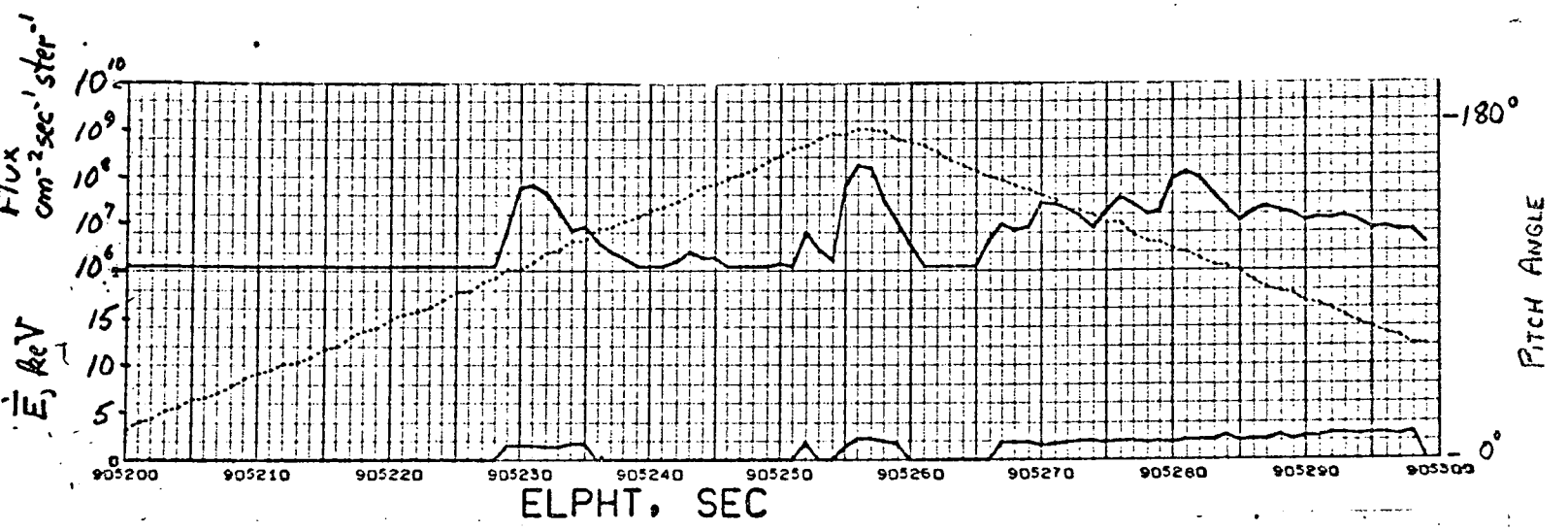

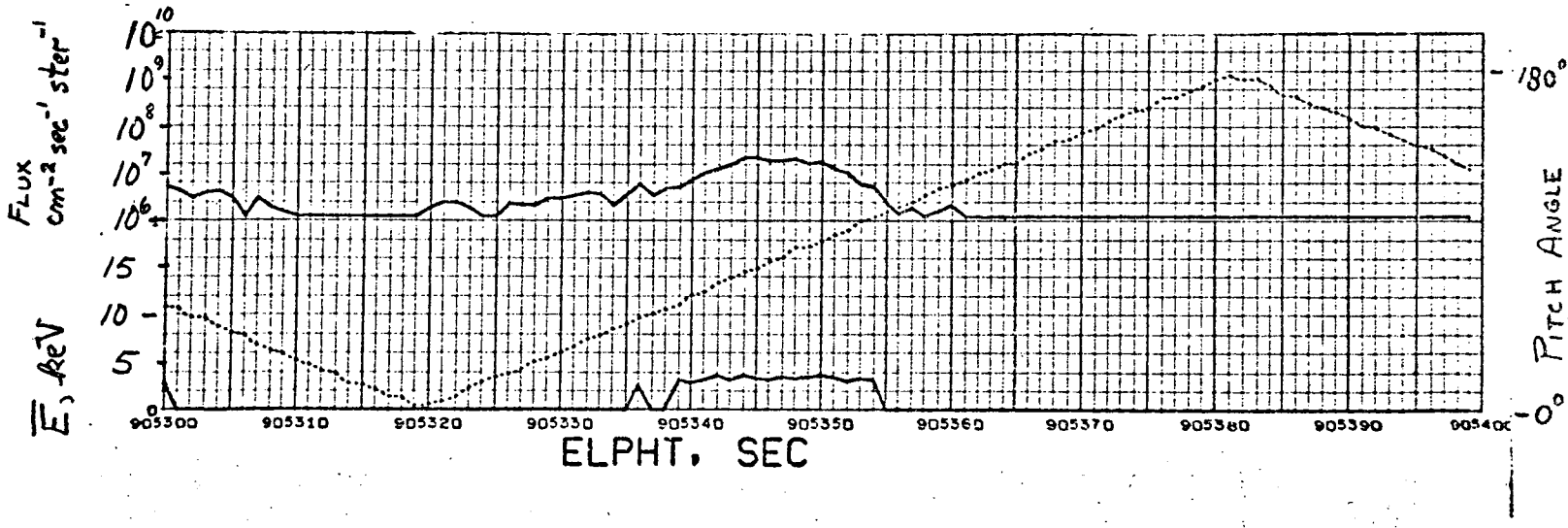

Fig. 56

HIGLO CME OUTPUTS GRP 2,3 ORBIT A4027

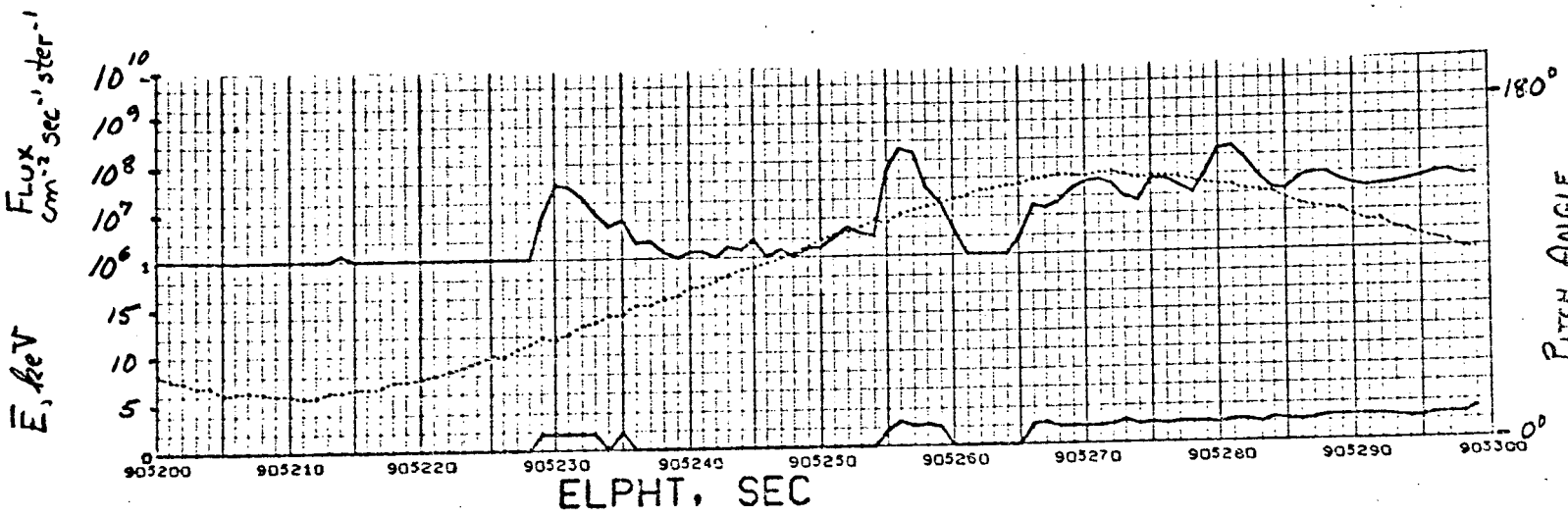

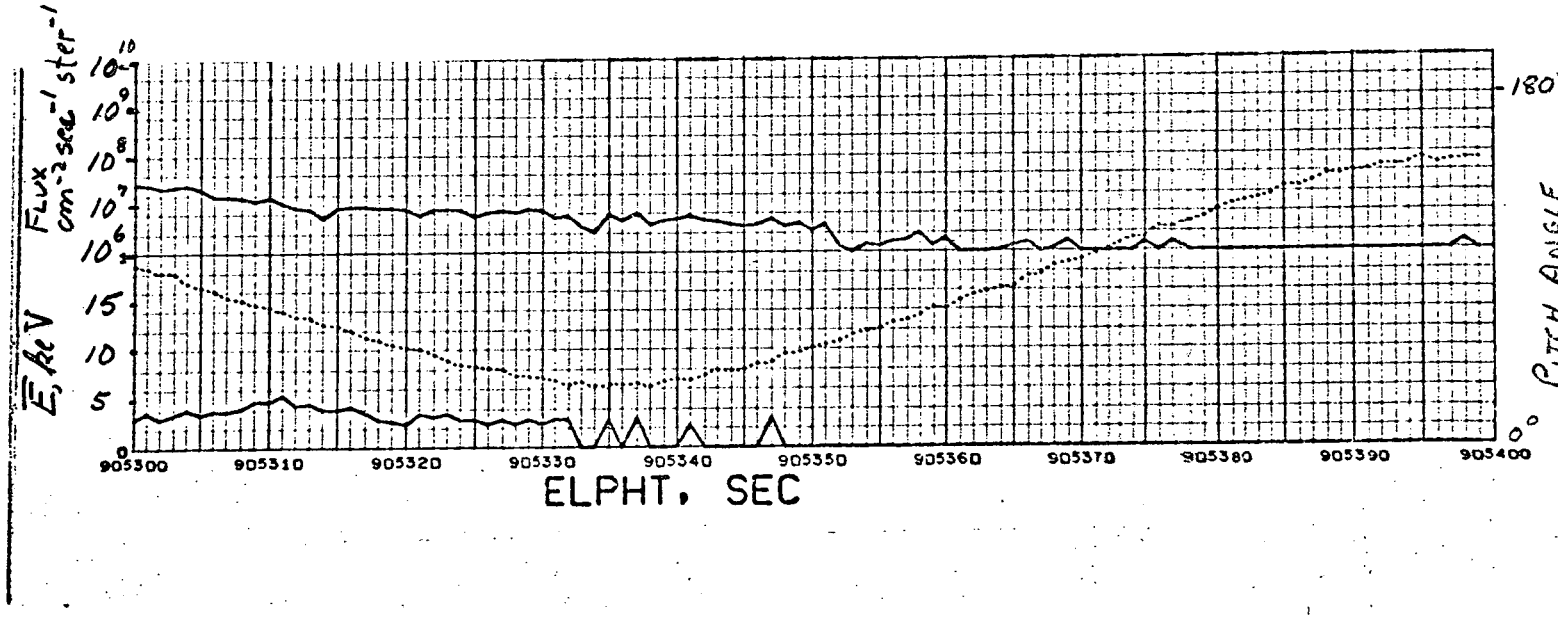

High Latitude Particle Precipitation, and Source Regions in the Magnetosphere

by

R. H. Eather* and S. B. Mende+

Presented at Advanced Study Institute on Magnetosphere-Ionosphere Interactions, Dalseter, Norway, April, 1971.

* Physics Department, Boston College, Chestnut Hill, Massachusetts 02167

+ Lockheed Research Labs, 3251 Hanover, Palo Alto, California 94304

HIGH LATITUDE PARTICLE PRECIPITATION, AND SOURCE REGIONS IN THE MAGNETOSPHERE

R. H. EATHER
Department of Physics
Boston College
Chestnut Hill, Massachusetts 02167

and

S. B. MENDE
Lockheed Palo Alto Research Labs.
3251 Hanover
Palo Alto, California 94304

Abstract

In this review we present averaged properties of precipitating auroral protons and electrons (as deduced photometrically) and compare these with direct satellite measurements of similar parameters. The various distinct types of precipitating particles are defined and related to their source regions in the magnetosphere.

There are two distinct types of proton precipitation. On the nightside, the proton aurora locates equatorward of electron aurora before midnight, and overlaps electron aurora after midnight. The most probable source region in the magnetosphere is the ring current, and gradient drift may sometimes extend this region through the dusk meridian and as far around as midday. There is a second, higher latitude zone of soft-proton precipitation on the dayside, which has its origin in magnetosheath plasma penetration through the cusp regions.

There are three distinct types of electron precipitation. On the nightside, there is a broad zone of soft (~1 keV) precipitation that extends from the equatorward side of the nightside oval and up to invariant latitudes of ~80°; the probable source region is the plasma sheet via loss-cone drizzle. The auroral oval on the nightside is generated by higher energy (~5 keV) electrons that superimpose on the low-latitude side of the soft zone. The most probable source region in the magnetosphere locates between the inner edge of the plasma sheet and the center of the plasma sheet (near neutral sheet) in the tail. Gradient drift of these electrons extends this region through the dawn meridian and past noon, resulting in a precipitation region locating just equatorward of the dayside oval. The third region of electron precipitation coincides with the high-latitude dayside protons and results from very soft magnetosheath electrons ($\lesssim$300 eV) penetrating the cusp regions. It is these soft dayside electrons that generate the dayside oval.

These multiple zones of particle precipitation, with their distinct and somewhat independent sources in the magnetosphere, comprise a much more complex picture than the simple concept of the auroral oval would suggest, but at the same time they provide a basis for a clearer understanding of high-latitude precipitation phenomena.

1. Introduction

This review describes how ground-based optical techniques may be used to determine the type, flux, and energy of precipitating auroral particles. Recent experiments along these lines are described, and we arrive at a number of new conclusions on precipitation patterns and source regions in the magnetosphere. Comparisons with satellite data facilitate the identification of these source regions.

This paper summarizes the essential features of a review talk given at the Magnetosphere-Ionosphere Interactions Conference.

2. Spectral-Photometric Measurements

Within certain limitations, ground based or airborne measurements of auroral emissions can be used to determine the type, energy, and flux of precipitating particles. The technique uses mainly 4861 Hβ, 4278 N_2^+ and 6300 OI measurements; the Hβ intensity is used to estimate the proton flux and the proton contribution to N_2^+ and OI excitation. The residual 4278 N_2^+ intensity then gives the total energy influx of precipitating electrons; at times when this residual is zero, airglow corrections can be made to the OI intensity. Finally the ratio 6300/4278 (proton corrected and airglow corrected) gives a measure of the average energy of the electrons.

There are certain precautions to observe in applying the procedure, such as van Rhijn and extinction corrections, perspective

effects, lifetime effects, etc; but one can obtain confirming data by measuring additional emissions such as 3914 N_2^+, 5577 OI and 5200 NI. Thus careful photometry can be a powerful technique to study the details of energetic particle precipitation.

Relevant conversion data from emission intensities to energy are shown in Figure 1. The conversion from 4278 N_2^+ intensity to total energy input would be independent of electron energy in a pure N_2 atmosphere (for electron energies ≥ 100 eV), but because the fractional abundance of N_2 varies with height, we must use the correction factor as a function of height (or electron energy) as shown in Fig. 1a. Figure 1b shows a theoretical curve (Rees, private communication) relating the 6300/4278 ratio to monoenergetic electron energy for an assumed model atmosphere. In practice, we have a distribution of precipitating electron energies, and the variation of 6300/4278 as a function of 4278 intensity (or total energy input) is shown in Figure 1c (theoretical curves, Rees, private communication), for various energy spectra peaked between 0.3 and 10 keV. Thus if we assume a spectral form and measure the 6300/4278 ratio and 4278 intensity (for electron excitation), we can uniquely define the parameter α giving the peak of the energy spectrum i.e. a measure of average electron energy.

3. Dayside Precipitation Patterns

Results from airborne experiments aboard the NASA Convair 990 have been published (Eather, 1969; Eather and Akasofu, 1969; Eather and Mende, 1971). Only four north-south passes were made near the midday sector, so statistics are limited. Averaged latitude distributions of 4278 N_2^+ and Hβ have been published (Eather and Mende, 1971), and are replotted as a function of oval co-ordinates (invariant latitude minus latitude of theoretical position of equatorward boundary of the auroral oval, see Eather and Mende, 1971) in Figure 2. Note first that the peak average 4278 intensity is only 70 R (which corresponds to subvisual aurora). 4278 intensities of ~300 R were observed in individual events, and such auroras were weak but visible. This average 4278 intensity is lower than nighttime averages by a factor of about 7. The peak Hβ average intensity (~8 R) is also less than nighttime averages but a factor of ~3; note too that the proton precipitation (Hβ) locates on the high-latitude half of a broader region of electron precipitation.

Figure 3 shows the 6300/4278 ratios (electron excitation) plotted in oval co-ordinates, and indicates a number of important results. There are two distinct types of dayside precipitation: a region equatorward of the equatorial boundary of the auroral oval where high energy ($\gtrsim$ 5 keV) electrons precipitate, and a region poleward of the equatorial boundary (i.e. in the position of the oval) where soft electrons ($\lesssim$ 200 eV) precipitate. (These energies

are derived from the ratios in Figure 3, the intensities in Figure 2, and the theoretical curves of Fig. 1c.) This same effect may be seen by looking at the details of particular north-south flights (Figure 4). It may be seen that for invariant latitudes less than about 77°, the 6300 intensity shows no relationship to the 4278 intensity, whereas above 77° the two curves show similar behavior. Both Figures 3 and 4 show that the division between the regions of hard and soft electron precipitation is very sharp and that there is little overlap of these regions.

The red auroras excited in the soft precipitation region have been photographed in color, and there is a clear distinction between these auroras and the more typical green aurora further equatorward (Akasofu, private communication).

Comparison of Figures 2 and 3 shows that the protons precipitate in the same region as the soft electrons. An examination of the Doppler profile of the emitted Hβ radiation shows that these protons are less energetic than on the nightside, so probably have energies $\lesssim$ 3 keV (Eather and Mende, 1971).

These deductions from photometric measurements agree very well with detailed particle measurements from the low-altitude satellite ISIS-1. Figure 5 shows spectrograms for electrons and protons plotted against invariant latitude (Heikkila and Winningham, 1971). The low-latitude, hard-electron precipitation, and high-latitude, soft-electron and proton precipitation, with a sharp transition at 73° (K_p = 5) are all clearly shown. For quiet times

(K_p ~ 0+1) the sharp transition occurs at higher latitudes (~ 77.5°) so that the soft precipitation of electrons and protons covers the Λ range ~78-81° (Winningham, 1970; Heikkila and Winningham, private communication).

The coincident precipitation of low-energy electrons and protons in a region adjacent to a lower-latitude region of hard electron precipitation led Heikkila and Winningham (1971) and Eather and Mende, (1971) to suggest that these particles may penetrate directly from the magnetosheath. Such a penetration through the dayside neutral points would imply that the lower-latitude, hard-electron precipitation occurs on closed field lines.

There are a number of recent satellite results associating high latitude precipitation of soft electrons and protons on the dayside with direct penetration of magnetosheath plasma through neutral points (or "polar cusp" or "cleft") (Heikkila and Winningham, 1971; Frank, 1971a). A summary of satellite observations of dayside precipitation, and a comparison with photometric results, is presented in Figure 6. Consideration of the experimental data (and remembering certain limitations on the energy coverage of some satellite detectors) leads to probable average energy influx of ~0.1 erg $cm^{-2}sec^{-1}ster^{-1}$ for soft electrons, and ~0.05 erg $cm^{-2}sec^{-1}$ $ster^{-1}$ for soft protons. The spectral peak seems to be typically 100-200 eV for electrons and ~300 eV for protons. A summary of the average features of dayside precipitation as shown in Figure 6 is presented in Table 1.

Table 1

Dayside Aurora

	Hard Zone	Soft Zone		
	Electrons	Electrons	Protons	Total
Average Energy Input (erg/cm^2sec ster)	0.1	0.1	0.05	0.15
4278 N_2^+ (R)	85	70	~30	100
5577 OI	~200	~250	~80	330
6300 IO	20	1250	~30	1280
4861 Hβ			10	10

The lower-latitude zone of hard electron precipitation has been discussed by Hoffman (1971) and indirectly by Frank (1971a). This is a broad, diffuse and steady region of precipitation occurring on closed field lines; the average energy flux being precipitated is similar to that in the soft zone (~0.1 erg $cm^{-2}sec^{-1}ster^{-1}$) and it seems clear that these electrons gradient drift from a nighttime source region (see full discussion by Hoffman, 1971). The width of the precipitation region is much broader before midday than after (Hoffman, 1971; Eather, Heikkila and Akasofu, private communications) and often extends only a few hours into the afternoon sector (Hoffman, 1971). This extent into the afternoon would probably be a function of the nightside source strength and the loss rate along the drift path.

It is interesting to note that early satellite results from the Lockheed group (Sharp and Johnson, 1969) showed a second zone of proton precipitation coincident with the hard electrons (Figure 7). This zone was not detected photometrically by Eather and Mende (1971), nor has it been reported by other satellite experiments. However it occurs in the same region as the trapped ring current in the dayside (Frank, 1971a) so it seems a likely explanation is that on some occassions, these trapped ring current protons do enter the loss cone. Indeed the second proton zone is probably entirely analogous to the hard electron zone in that it has as its source a gradient drift from a nightside source region. Such protons drift through the evening sector towards noon,

and their extent into the dayside would be a function of the nightside source strength and the loss rate along the drift path. Apparently the source strength and/or the loss rate near noon are only occasionally strong enough to give measureable precipitation.

It appears then that we have a quite satisfactory picture of dayside particle precipitation and the various source regions in the magnetosphere.

The only significant discrepancies between the satellite and photometric experiments listed in Figure 6 concerns the geometry of the polar cusp as a function of altitude. The low-altitude satellites and airborne photometric measurements show that the soft zone typically covers some 3° of latitude (i.e. ~300 km) and that the protons and electrons precipitate right across this region. Higher altitude measurements by Frank (1971a) indicate that the width of the soft precipitation region of protons, when projected to ionospheric heights, should be 10-200 km, with an average of ~100 km Frank (1971b), and that these protons precipitate in a sheet located poleward of the soft electron precipitation. An explanation of the narrower widths observed by Frank might involve the limited energy range he considers (700-1100 eV), or uncertainties in field-line projections. A more serious question is whether the protons precipitate separately and poleward of the electrons; this certainly is not the case at low altitudes and it is difficult to see how the situation could be different further up the field lines. Again Frank has compared limited energy ranges of protons (700-1100 eV) and electrons

(300-500 eV), so an energy variation with latitude could distort the picture, and if total number flux or total energy flux were considered, the situation may possibly be more in agreement with low altitude measurements. We must await a more detailed presentation of Frank's data to see if a problem really exists.

4. The Daytime Auroral Oval

The question arises as to what is meant by the auroral oval on the dayside. The oval has been determined from all-sky camera photographs, so represents aurora which exceed the sensitivity of the film used. Typically all-sky cameras will just detect about 500 R of 5577 OI, so respond to energy inputs ~0.1 erg/cm^{2}sec ster. In Table 1 we listed the energy inputs into the hard and soft zones and the expected optical emission intensities. Table 1 is based on average energy inputs. The normal, high-speed black and white films used in all-sky cameras (usually Tri-X, 2080, or equivalents) are panchromatic films and hence quite red-sensitive. Thus these films would respond preferentially to auroras in the soft zone (see Table 1), even though these may be as much or greater energy input into the hard zone. Even so, the average soft zone energy input is only just at the sensitivity limit of the film, so we must ask what is the statistical spread about the average energy input in both the hard and soft zones? The soft zone auroral forms show a lot of spatial structure and are often short-lived (Eather, 1969; Eather and Akasofu, 1969; Lassen, 1969) and this dynamic behavior

this also confirmed by satellite measurements (Hoffman and Evans, 1968 Burch, 1968; Heikkila and Winningham, 1971); in contrast, the hard zone seems much more steady. Indeed specific events would have to exceed the average by a factor of 4 to exceed all-sky camera sensitiving in the green. In the soft zone, the 6300 intensity on the average is near the all-sky camera sensitivity level.

We conclude that the presently accepted dayside auroral oval represents the soft-electron and proton precipitation, and Hoffman (this volume) has independently arrived at a similar conclusion. Fig. (3) confirms this as it shows the soft zone locates in a 3-5° band just above the equatorial boundary of the oval. However, hard electrons locating equatorward of the oval deposit as much or more energy into the atmosphere. As they probably result from a gradient drift of nighttime electrons, the concept of a continuous auroral oval might be more applicable to them. Thus we question the usefulness of the concept of a continuous auroral oval. It is a very artificial notion that only has meaning in terms of peak response of black and white all-sky camera film; this peak response evidently comes from "normal green" auroral on the nightside, and from "soft red" aurora on the dayside. These are two types of aurora have entirely different source regions in the magnetosphere, and there is no obvious topological connection between these regions.

We strongly recommend that the use of the auroral oval as a means of ordering high-latitude geophysical data on a 24 hour basis be discontinued, and that instead one keeps in mind the various different magnetosphere source regions of precipitating particles that are summarized at the end of this paper.

5. Nightside Precipitation Patterns

Statistical results from all NASA Convair expeditions in 1967-68 and 1969 (some 40 flights, each of ~6 hours duration) were used in this analysis. Figure 8 shows average 4278 N_2^+ (electron excited) and Hβ intensities in oval co-ordinates, and for night hours. Figure 9 shows the corresponding 6300/4278 ratio plot. (The difference between the two curves "average of ratios" and "ratio of averages" is discussed by Eather and Mende, 1971, but is not important in our present discussion.)

The previously reported nighttime soft zone (Eather, 1968, Eather and Mende, 1971) is evident in the peaking of the average 6300/4278 ratio above the oval position. The peak ratio of ~5.0 corresponds to about a 500 eV peak in the energy spectrum (Figure 1c). An alternate presentation (Figure 10) shows the percentage occurrence of peak energies of <1 keV and >5 keV - the >5 keV precipitation maximizes in the position of the auroral oval, whereas the <1 keV precipitation locates at much higher latitude - in fact ~90% of the occurrences of precipitation in the high-latitude soft zone are of <1 keV electrons. A plot of percentage occurrence of 4278 N_2^+ exceeding 0.5 and 50 R (Figure 11) shows, by comparison with Figure 10, that the soft precipitation is typically low intensity (<50 R). It is also interesting to note that there is a broad region centered on the oval where there is measurable precipitation virtually all of the time.

Various considerations led us to suspect that there may be a systematic relationship between the 6300/4278 ratio and the 4278 intensity i.e. between average energy and total energy precipitated. The ratio 6300/4278 are plotted versus mean 4278 intensity in Figure 12. The plotted numbers (1→1) represent 4° latitude intervals centered from 8° equatorward of the equatorial boundary of the auroral oval to 12° poleward of that boundary (so for example the numeral 6 represents the interval 0°-2° in oval co-ordinates). There are no points plotted unless the number of data points in the appropriate latitude-intensity box exceeded 5.

We have drawn a division line at an intensity level of 50 R, and note that for 4278 > 50 R, there is a reasonably systematic decrease of the 6300/4278 ratio with increasing 4278 intensity, for all latitudes. For 4278 < 50 R, it seems this relation breaks down, but a reasonably systematic increase in the ratio with increasing latitude becomes evident. We interpret these results as follows: (1) there is a low level (<50 R) of precipitation occurring in a very broad region from below the auroral oval position to well poleward of it. such that the average energy of precipitation softens with latitude (from ~1.5 keV to ≤ 500 eV).

(2) Higher intensity precipitation superimposes on this low level precipitation, and locates preferentially in the position of the oval. This precipitation is characterized by an increasing average energy as total energy input increases.

We conclude that the so-called "soft zone" does not just locate poleward of the auroral oval, but extends right across the auroral oval itself. There is a gradual softening with latitude throughout this broad region. Energetic electrons precipitation superimposes on the lower-latitude half of the soft zone, and gives rise to the visual auroral forms that make up the auroral oval. As the 4278 N_2^+ intensity in the oval increases from 50 R to up to ~10 kR, there is a systematic hardening of the electron spectrum.

The division of Figure 12 into two intensity division ($\gtrsim$50 R), and our interpretation in terms of two distinct particle observations, is not as arbitrary as it may seem. In Figure 13 we have plotted the occurrence frequency of α, where α is the parameter in the spectrum used in Figure 1c, and is a measure of the average energy. It may be seen that there is a definite indication of two separate particle populations, one between $\lesssim$200 eV and ~700 eV (our soft particle spectrum), and a wider distribution locating between ~1 and ~10 keV. Note that α exceeds 5 keV only 11% of all cases. However, if we exclude the low-α distribution, then for those more energetic electron spectra that excite visual aurora, α exceeds 5 keV some 25% of the time.

6. Variation of Total Energy Precipitated with Mean Energy

For this analysis, the energy spectrum parameter α (Figure 1c), and the total energy being precipitated were calculated. The resultant plot of total precipitated energy Φ (ergs/cm^{2}sec) versus peak energy of the spectrum α (keV) is given in Figure 14. (Note that average energy of spectrum = 2α.) The data have been average over all latitudes and times, for nightside data only.

If these particles had been accelerated by an adiabatic compression process with negligible sources and losses, then Lioville's theorem prodicts that if we plot Φ versus α on a log-log plot (as in Figure 14), then we should get a straight line with a slope of 3. On the other hand, if acceleration was by static electric fields, we would expect a slope of 1.0.

The plot of total energy precipitated versus α gives a reasonable straight line, though there seems to be a flattening out at lower energies. In this respect it is interesting to note that if we subtract a constant 0.15 ergs cm^{-2}sec^{-1} from Φ, a much better straight-line fit results (Figure 14). It is tempting to relate this 0.15 ergs cm^{-2}sec^{-1} (corresponding to ~40 R of 4278 N_2^+) with the average contribution of the soft precipitation, and then interpret the remainder as the harder, 'auroral' precipitation that superimposes on the soft zone. We do not claim to have proven this suggestion in Figure 14, but it is consistent with the rest of our results, and is aesthetically pleasing.

Figure 14 shows that for this particle population above about 0.5 keV, there is a quite linear relationship with a slope of

1.3 $\pm$ 0.15. We could argue that this is more consistent with an electric field acceleration mechanism, but other ad hoc explanations can explain with such a slope. For example, a combination of electric field acceleration and adiabatic compression, or adiabatic compression with strong losses of the higher energy particles, could give a slope in agreement with the experimental results.

In Figure 14 we have also drawn in the Φ versus α relationship for an electron flux of 3×10^8 $cm^{-2}sec^{-1}$. It is interesting to note that our results suggest that the number flux of precipitating electrons increases by less than 50% for two orders of magnitude increase in the total energy precipitated. The range plotted extends up to about 8 kR. We realize that there are times (especially at breakup) when very intense aurora are excited by much higher fluxes of 1-10 keV electrons. At those times fluxes in excess of $10^{10}cm^{-1}sec^{-1}$ have been reported. This must be a much more dynamic and transitory process than the lower-level, steady-state picture we invisage here, for IBC 1-2 auroras.

7. Comparison with Plasma Sheet Electrons

In Figure 15 we summarize plasma sheet data from 17 Re according to Hones (1968). We have plotted his data (originally published in tabular form) by performing averages as indicated and assuming equal weighting for his latitude-longitude boxes. In Figure 14A we see that the average energy of plasma sheet electrons decreases from about 1.2 keV at the center of the plasma sheet to some 0.4 keV near the edge. This has led us to associate these electrons with our soft precipitation zone, as it shows a similar softening with latitude. As the energies match fairly well, we believe that the soft precipitation represents a loss-cone drizzle of plasma sheet electrons, with no important acceleration processes involved. If we assume isotropy, the ~1° plasma sheet loss-cone maps down to the ionosphere and carries enough energy to excite some 10-50 R of λ4278 N_2^+ emission, in good agreement with energy inputs into the soft zone (Figures 4 and 12).

The data presented in Figure 15 were obtained for dipole tilts between $\pm$20°, so an effective broadening of the latitude extent of the plasma sheet results. Typically the latitudinal width of the plasma sheet near midnight is only ~$\pm$3 R_E, and the sheet thickens to perhaps double this value near the dawn and dusk meridians. According to Fairfield's (1968) model of the tail field, we would not expect the edges of the plasma sheet to map down to an invariant latitude that ever exceeds about 74°. But we observe soft precipitation up to about Λ = 79-80°, which we believe comes

from the edge of the plasma sheet. Certainly there are not sufficient fluxes of low-energy electrons in the high-latitude magnetotail to explain the observed precipitation. We are forced to conclude that the edges of the plasma sheet must map down to higher invariant latitudes in the ionosphere that would be expected from Fairfield's (1968) model. Independent studies of the thickening of the plasma sheet and poleward movement of the electrojet (Hones, et. al., 1970) also indicate that a given latitudinal interval in the plasma sheet near 17-18 R_E subtends a larger invariant latitude interval at the ionosphere then that indicated by Fairfield's model.

On the low-latitude side, our observations of aurora at invariant latitudes of 60° indicate, by comparison with Fairfield's model, that these aurora occur on closed field lines. Vasyliunas (1970a) has convincingly associated this equatorial boundary of aurora with the inner edge of the plasma sheet, which he also regards as being in a closed field line region.

We now consider the more energetic auroral precipitation (the >50 R side of Figure 12) that excite the visual auroral forms. Average energies are in the 1-10 keV range, and so exceed typical average energies in the plasma sheet. The average precipitated energy at the peak in Figure 8 is ~0.6 erg/cm^{2}sec ster, and this also exceeds typical plasma-sheet energy fluxes, though there are some discrepancies in reported fluxes. Hones (1968) and Vasyliunas (1968) agree on the electron mean energy (~0.2 - 2 keV, average ~1 keV) but the "most probable" energy density given by Vasyliunas

is a factor of ~3 higher than Hones' "average" values. In fact Hones' maximum energy flux (~0.3 erg/cm^{2}sec ster) is about the same as Vasyliunas' average. In either case, both the average energy and energy flux of plasma sheet electrons are significantly less than for the precipitated electrons in the auroral oval, and it is only the cases of very high plasma sheet energy fluxes (~1 erg/cm^{2}sec ster) that compare with average precipitated fluxes. Certainly the energy fluxes associated with commonly occurring IBC 2 aurora (~2 erg/cm^{2}sec ster) are almost never seen in the plasma sheet.

The variability of plasma-sheet energy spectra is illustrated in Figure 16A where we show a selection of published spectra; Figure 16B shows three schematic spectra derived from Figure 16A that represent typical "soft," "average," and "hard" spectra. The energy carried by each of these spectra is .06, 0.3, and 1.0 erg/cm^{2}sec ster respectively. The "typical" spectrum published by Vasyliunas (1970b) seems to be nearer to the hardest of published spectra.

The photometric data presented in this paper, together with arguments presented earlier by Vasyliunas (1970b) and Frank (1971), seem quite convincing in associating the harder, auroral-oval precipitation with a magnetospheric source region locating from the inner edge of the plasma sheet and extending down the centre of the plasma sheet. We maintain that some acceleration is required between the plasma sheet at ~18 R_E and the auroral zone, and note

that a simple adiabatic compression would be entirely adequate to provide the required energization (of about a factor of 5). We note that harder plasma sheet spectra in Figure 16A were all measured close to the earth (9-11 R_E) than the Vela orbit (17-18 R_E).

We are somewhat in disagreement with Vasyliunas (1970b), who also views the auroral oval as an extension of the plasma sheet to ionospheric heights, but he requires no energization in the process. (We believe that loss-cone drizzle does occur, but gives rise only to the soft zone.) Vasyliunas (1970a, b) cites the contention of Chase (1969) that the electron energy spectrum in post-breakup auroral closely resembles, in both shape and intensity, the spectrum within the plasma sheet. We have examined Chase's (1969) published comparison (his Fig. 2), and note: the total energy in the plasma sheet spectrum is ~0.3 erg cm^{-2}sec, whereas that in the auroral spectrum is ~2.0 erg cm^{-2}sec; the auroral spectrum has a peak between 5 and 10 keV that carries 2/3 of the total energy, and has no counterpart in the plasma sheet spectrum. Thus we conclude there is little reason to contend these spectrums are similar (even though they may appear so in a figure that plots 7 1/2 orders of magnitude of flux in a space of just one inch, Chase (1969). A few more detailed comparison of plasma sheet and auroral spectrum (Hones et. al., 1971) reveals that the plasma sheet spectrums are typically softer than auroral spectrums, especially in that they do not show peaks in the 5-10 keV range as are often observed by rockets; and plasma sheet fluxes are typically an order of magnitude less than auroral fluxes as measured by rockets.

Vasyliunas also compares the averaged precipitated electron flux in the auroral oval (Sharp et. al., 1969) with three OGO-1 passes in the plasma sheet. We again feel the "agreement" is not convincing. First there is the problem of matching the plasma-sheet data (at various estimated distances from the neutral sheet) with satellite data at various invariant latitudes; we have discussed above evidence that a given distance above the neutral sheet should correspond to higher latitude than indicated by Fairfield's mode. Second, Vasyliunas energy fluxes (~0.3 erg/cm^2sec ster) are about three times Hones' average, and Sharp et. al. peak average flux (~0.3 erg/cm^2sec ster) are about half of Eather and Mende's average. So if we compare data fron Hones and Eather and Mende, we would conclude there was a discrepancy of a factor of six. This argument reduces to the question of which data to believe, so is not particularly profitable. But we feel the argument concerning the differences in average energy of plasma-sheet and auroral particles is quite convincing.

A few final comments should be made on the character of the auroral precipitation. Figure 11 shows that there is always measurable precipitation in the position of the oval, but that the energy flux only exceeds .06 erg/cm^2sec ster about 50% of the time. At higher latitudes where mainly soft precipitation locates, emissions are detectable only ~50% of the time and exceed 50 R only 5-10% of the time. Thus in neither case is there a <u>continuous</u>

There are, however, short-lived (few minutes) structured (spatially) bursts of precipitation across the polar cap. Eather and Akasofu (1969) showed from photometric data that the emissions were excited by soft (≤1 keV) electrons. Heikkila and Winningham (1970) and Hoffman and Evans (1968) see similar features from satellites. From the geometry of the magnetosphere, it seems these electrons must come from the high-latitude magnetotail, though we know of no reports of isolated plasma "clouds" in that region.

10. Precipitation Patterns and Source Regions

We have tried to summarize the basic precipitation patterns in Figure 17, for both electrons and protons. Figure 17A shows the electron patterns, displayed on an invariant latitude - magnetic time grid, with the auroral oval for quiet times (Q = 1) added for reference. As discussed in Section 4, the oval on the dayside locates in the soft zone and results from direct penetration of low-energy electrons from the magnetosheath. Immediately adjacent to it and on the equatorward side are the higher energy electrons that have gradient-drifted from the nightside. Hoffman (1971) associates these with Sandford's mantle aurora. The dayside precipitation of these electrons does not seem to extend much past noon, where it is thinner (in latitude) and less intense. On the nightside, the auroral oval precipitation is shown, and has it's origin in the region bounded by the inner edge of that plasma sheet and the region of the plasma sheet

close to the neutral sheet. The wide, soft zone is shown extending right through the oval and up to latitudes of 79-80°, and we believe this is a consequence of loss-cone drizzle of plasma sheet electrons.

We know of no published data that allows us to connect the dayside and nightside soft zones, though Frank (1971b) has published a model showing a topological connection between the associated source regions. The question marks in the figure indicate the uncertainties in that respect, and the uncertainties in how far the dayside hard zone extends into the morning hours. This extension is probably very dependent on source and loss functions, and hence on magnetic activity.

Figure 17B shows the proton patterns. The nightside proton aurora has been discussed in detail by Eather (1967), Montbriand (1969) and Eather and Mende (1971). It locates equatorward of electron aurora in the evening hours, with the separation decreasing towards midnight. In the morning hours, electron and proton aurora overlap, and as magnetic activity increases, the electron aurora maximum may move equatorward of the proton aurora maximum (Montbriand, 1969). We believe the proton aurora has its source in the ring current, and the ring current is filled by adiabatic compression of plasma-sheet protons. The extent of the proton aurora (with a ring-current source) in the morning hours is not clear. Gradient drift carries the protons to the evening side and under quiet conditions they extend at least to the dusk meridian. Occasional observations of ~10 keV proton precipitation near midday indicates

that gradient drift may at times carry precipitation around to the noon meridian, but this does not seem to be a regular occurrence. We know of no experimental data that allows the connection of the proton aurora at dusk to the hard proton precipitation at midday, so we have dashed the connection in Figure 17B and indicated uncertainty with a question mark.

The soft-proton precipitation from the magnetosheath gives the main zone of proton aurora on the dayside. We classify this as the main zone as it is a regular feature of the daytime precipitation pattern, whereas the zone of harder precipitation seems transitory. The azimuthal extent of this soft proton precipitation has not been established though it clearly does not extend into the evening sector at high latitudes. Gradient drift could take these protons to the dawn sector and confuse the picture there, though for these low energies we suspect the proton lifetime could be considerably shorter than the drift time.

If Figures 17A and 17B were superimposed, then one can obtain an idea of the complexity of auroral precipitation. With two particle types, and a number of source regions and precipitation processes, it is clear than any well designed experiment (either photometric, rocket, or satellite) must measure a wide variety of parameters to obtain the complete picture.

Our Figure 17A (for electrons) is considerably different from the Hartz and Brice model, as modified recently by Hartz (1971). Hartz implies continuous (24 hour) zones of "splash" and "drizzle"

type of precipitation, with the superposition of the magnetosheath precipitation near midday (Figure 18). We would associate his low intensity "drizzle" on the nightside with our soft zone (and point out that it should extent up to higher latitudes ~79°), but on the dayside we would associate his higher intensity drizzle with our dayside hard zone. As we invisage different source mechanisms, we would not connect these two regions. We would associate his high intensity "splash" on the nightside with the auroral oval precipitation, and his low intensity splash on the dayside with the high latitude soft zone, and again we see no evidence to connect these regions into a 24 hour pattern, as they have separate source regions. We would prefer to connect the high intensity nightside splash with the high intensity dayside drizzle as we believe the latter results from the former, via gradient drift.

Finally, both photometric and satellite data show the dayside soft and hard zones are adjacent to each other, and not separated by a region of low or zero precipitation as indicated in the Hartz model (Fig. 18).

In Figure 19, we have drawn a model of the magnetospheric source regions, in the noon-midnight plane. This model is similar to recent magnetospheric models (O'Brien, 1966; Vasyliunas, 1970b; Frank, 1971a) though different from all of them in some respects. The salient features of Figure 19 have all been discussed in the preceeding text, so will not be further elaborated.

Acknowledgements: This review was written with the support from grant NGR 22-003-018 from the National Aeronautics and Space Administration, Airborne Sciences Office.

Figure Captions

Fig. 1: a) Fraction of the total ionization cross-section presented by N_2 in the Jacchia (1964) atmosphere, as a function of height, and corresponding 4278 N_2^+ emission per 1 erg/cm^2 sec ster of electron energy deposited at that height.

b) Theoretical 6300/4278 ratios (column integrated) as a function of 4278 intensity for monoenergetic electrons, for a fixed flux of 10^9 elec/cm^{2}sec. (Rees, private communication).

c) Theoretical 6300/4278 ratios (column integrated) for an assumed form of the electron energy spectrum, with different peak energies α, as a function of 4278 intensity.

Fig. 2: Average 4278 N_2^+ and Hβ intensities as a function of "oval co-ordinates" (see text), for dayside auroras.

Fig. 3: 6300/4278 ratios as a function of oval co-ordinates, for dayside auroras.

Fig. 4: 4278 N_2^+, 6300 OI, and 4861 Hβ intensities throughout a north-south meridian flight near noon.

Fig. 5: Satellite measurements of electron and proton energy spectra for a crossing of the dayside auroral region. The density of the trace qualitatively indicates the spectral energy density as a function of particle energy and time. (Heikkila and Winningham, 1971).

Fig. 6: Summary of measurements of proton and electron energy fluxes, and mean energies, in the polar cusp.

Fig. 7: Lockheed measurements of the location of peak particle precipitation; plotted are the number of auroral-zone crossings with peak response in the 1° interval centered on θ_L (Johnson et. al. 1966).

Fig. 8: Average 4278 N_2^+ and Hβ intensities as a function of "oval co-ordinates" (see text), for nightside aurora.

Fig. 9: 6300/4278 ratios as a function of oval co-ordinates, for nightside auroras.

Fig. 10: Percentage occurrence of precipitation with mean electron energy <1 keV and >5 keV, as a function of oval co-ordinates.

Fig. 11: Percentage occurrence of 4278 N_2^+ exceeding 0.5 R (limit of detection) and 50 R, as a function of oval co-ordinates.

Fig. 12: The mean ratio 6300/4278 plotted as a function of mean 4278 intensity, for 10 latitude intervals. The plotted numbers (1→11) represent 4° intervals centered every 2° from 8° equatorward of the equatorial boundary of the oval to 12° poleward of that boundary (eg. the numeral 6 represents 9-2° in oval co-ordinates).

Fig. 13: Number of cases of occurrence of a given α (defined in Figure 1c, and is a measure of peak energy for the spectrum), per unit energy interval. Two separate particle distributions are indicated.

Fig. 14: Summary of Hones (1968) plasma-sheet electron properties at 17 R_E. The 180° curve is for the midnight sector, and 120° and 240° for the dusk and dawn sectors. A. Average energy B. Energy density C. Energy flux and resultant 4278 N_2^+ emission if this flux was isotropic over the atmospheric loss-cone.

Fig. 15: Total energy precipitated ϕ (ergs/cm^{2}sec) as a function of energy spectrum parameter α, for nightside data. The relation for a constant number flux of 3×10^8 electrons/cm^2 sec is also shown.

Fig. 16: A) A selection of published plasma-sheet electron energy spectra. 1-4 at 18 R_E (Hones et. al. 1971); 5-15.9 R_E, 6-10.5 R_E, 7-15.3 R_E, 8-19.7 R_E, 9-13.5 R_E, 10-10.1 R_E, (Frank, 1967); 11-9.8 R_E (Schield and Frank, 1970); 12- Vasyliunas (1970) "typical" spectrum.

B) Schematic representation of typical "soft" (1) "average" (2), and "hard" (3) plasma-sheet electron energy spectra.

Fig. 17: A) Electron precipitation patterns.

B) Proton precipitation patterns.

Fig. 18: Auroral precipitation patterns after Hartz (1971). Triangles indicate zones of discrete or splash precipitation, and dots indicate diffuse or drizzle precipitation. Precipitation of magnetosheath plasma is indicated by stars. Intensity is indicated by symbol density.

Fig. 19: Source regions in the magnetosphere for the precipitation regions depicted in Fig. 17. (noon-midnight plane).

References

Burch, J.L., Low-energy electron fluxes at latitudes above the auroral zone. J. Geophys. Res., 73, 3585, 1968.

Chase, L.M., Evidence that the plasma sheet is the source of auroral electrons, J. Geophys. Res., 74, 346, 1969.

Cornwall, J.M., F.V. Coroniti, and R.M. Thorne, Turbulent loss of ring-current protons, J. Geophys. Res., 75, 4699, 1970.

Eather, R.H., Auroral proton precipitation and hydrogen emissions, Reviews of Geophysics, 5, 207, 1967.

Eather, R.H., Latitudinal distributions of auroral and airglow emissions: the "soft" auroral zone, J. Geophys. Res., 74, 153, 1969.

Eather, R.H. and Syun-I Akasofu, Characteristics of polar cap auroras, J. Geophys. Res., 74, 4794, 1969.

Eather, R.H. and S.B. Mende, Airborne observations of auroral precipitation patterns, J. Geophys. Res., 76, 1746, 1971.

Eather, R.H. and R.L. Carovillano, The ring current as a source region for proton auroras, Cosmic Electrodynamics, 2, 105, 1971.

Fairfield, D.H., Average magnetic field configuration of the outer magnetosphere, J. Geophys. Res., 73, 7329, 1968.

Frank, L.A., Initial observations of low-energy electrons in the earth's magnetosphere with OGO3, J. Geophys. Res., 72, 185, 1967.

Frank, L.A., Further comments concerning low-energy charged particle distributions within the earth's magnetosphere and its environs in "Particles and Fields in the Magnetosphere," edited by Billy M. McCormac, D. Reidel, Dordrecht, Holland, 319, 1970.

Frank, L.A., Plasma in the earth's polar magnetosphere, J. Geophys. Res., 76, 1971a.

Frank, L.A., Comments on a proposed magnetospheric model, J. Geophys. Res., 76, 2512, 1971b.

Hartz, T.R., Particle precipitation patterns, paper at NATO Advanced Study Institute, Kingston, Ontario (August, 1970). To be published in proceedings, Billy M. McCormac, editor, 1971.

Heikkila, W.F., and J.D. Winningham, Penetration of magnetosheath plasma to low altitudes through the dayside magnetic cusps, J. Geophys. Res., 76, 883, 1971.

Hoffman, R.A., Auroral electron drift and precipitation: cause of the mantle aurora, J. Geophys. Res., 76, , 1971.

Hoffman, R.A. and D.S. Evans, Field-aligned electron bursts at high latitudes observed by OGO-4, J. Geophys. Res., 73, 6201, 1968.

Hones, E.W., Review and interpretation of particle measurements made by Vela satellites in the magnetotail, in "Physics of the Magnetosphere," edited by R.L. Carovillano, J.F. McClay, H.R. Radoski, Reidel, Dordrecht-Holland, 1968.

Hones, E.W., S.-I. Akasofu, P. Perreault, S.J. Bame and S. Singer, Poleward expansion of the auroral oval and associated phenomena in the magnetotail during auroral substorms, 1. J. Geophys. Res., 75, 7060, 1970.

Hones, E.W., J.R. Askbridge, S.J. Bame and S. Singer, Energy spectra and angular distributions of particles in the plasma sheet and their comparison with rocket measurements over the auroral zone, J. Geophys. Res., 76, 63, 1971.

Lassen, K., Polar cap emissions, in "Aurora and Airglow," edited by Billy M. McCormac, Reinhold, New York, 1969.

Montbriand, L.E., Morphology of auroral hydrogen emission during auroral substorms, Thesis, Univ. of Saskatchewan, 1969.

Sandford, B.P., Aurora and airglow intensities variations with time and magnetic activity at southern high latitudes, J. Atmos.Terrest. Phys., 26, 749, 1964.

Sandford, B.P., Variations of auroral emissions with time and magnetic activity and the solar cycle, J. Atmos. Terrest. Phys., 30, 1921, 1968.

Schield, M.A. and L.A. Frank, Electron observations between the inner edge of the plasma sheet and the plasmasphere, J. Geophys. Res., 75, 5401, 1970.

Sharp, R.D., and R.G. Johnson, Distribution with invariant latitude of electron and proton precipitation close to noon and midnight, in "Aurora and Airglow," edited by Billy M. McCormac, Reinhold, New York, 1969.

Sharp, R.D., D.L. Carr and R.G. Johnson, Satellite observations of the average properties of auroral particle precipitations: Latitidinal variations, J. Geophys. Res., 74, 4618, 1969.

Vasyliunas. V.M., A survey of low-energy electrons in the evening sector of the magnetosphere with OGO1 and OGO3, J. Geophys. Res., 73, 2839, 1968.

Vasyliunas, V.M., Magnetospheric plasma, Review paper presented at STP Symposium, Lenningrad, U.S.S.R., 1970a.

Vasyliunas, V.M., Low energy particle fluxes in the geomagnetic tail, in "The Polar Ionosphere and Magnetospheric Processes," edited by G. Skovli, Gorden and Breach, New York, 1970b.

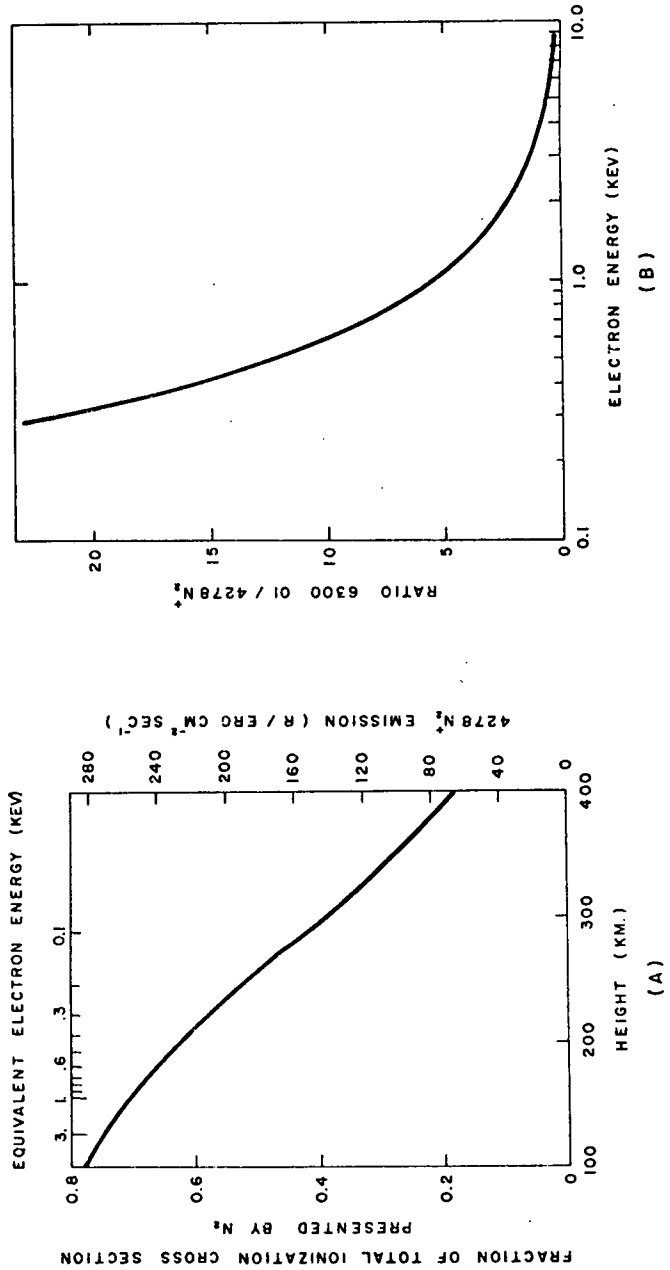

Fig. 1

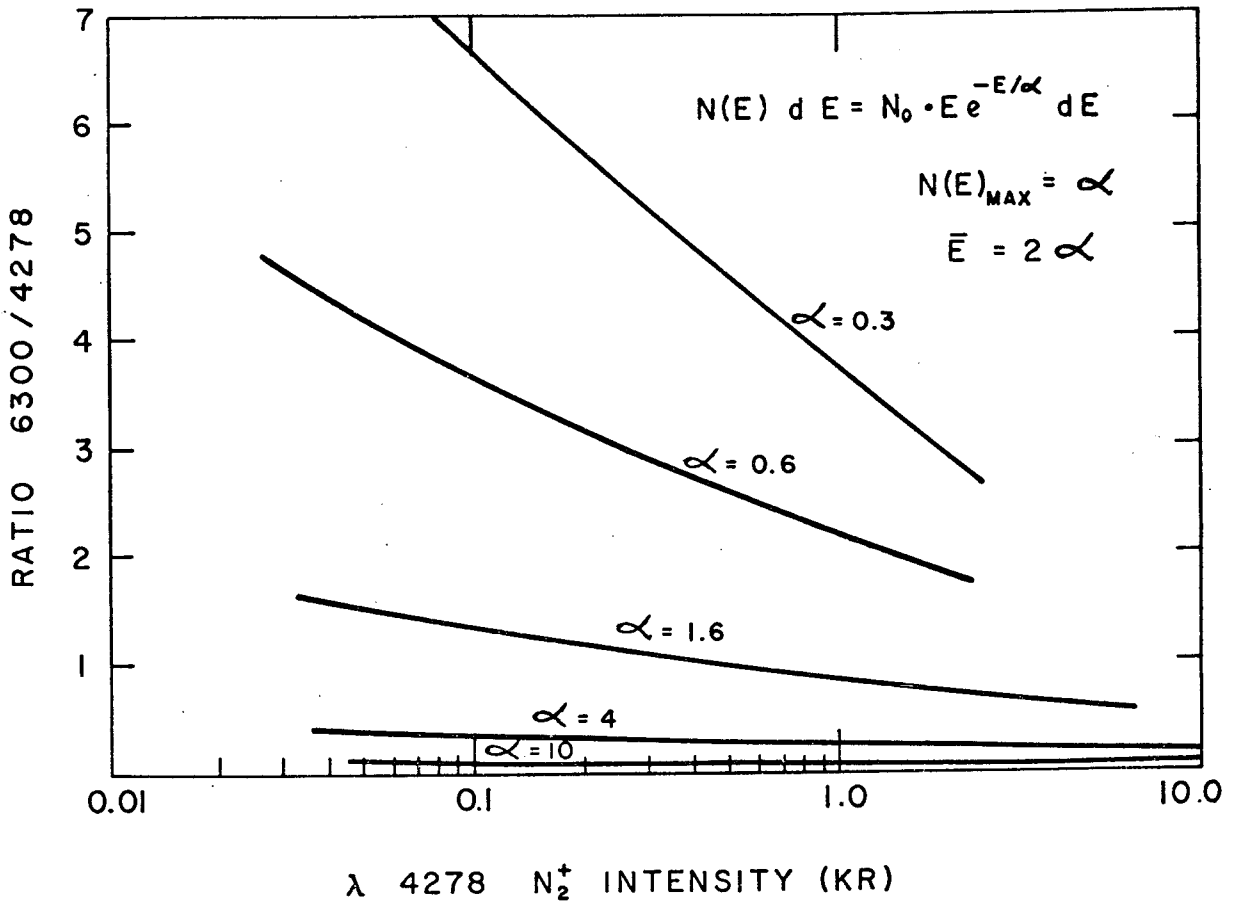
RATIO 6300/4278
7
6
5
4
3
2
1
N(E) d E = N₀ · E e^(−E/α) dE
N(E)MAX = α
Ē = 2α
α = 0.3
α = 0.6
α = 1.6
α = 4
α = 10
0.01
0.1
1.0
10.0
λ 4278 N₂⁺ INTENSITY (KR)

Fig. 1c

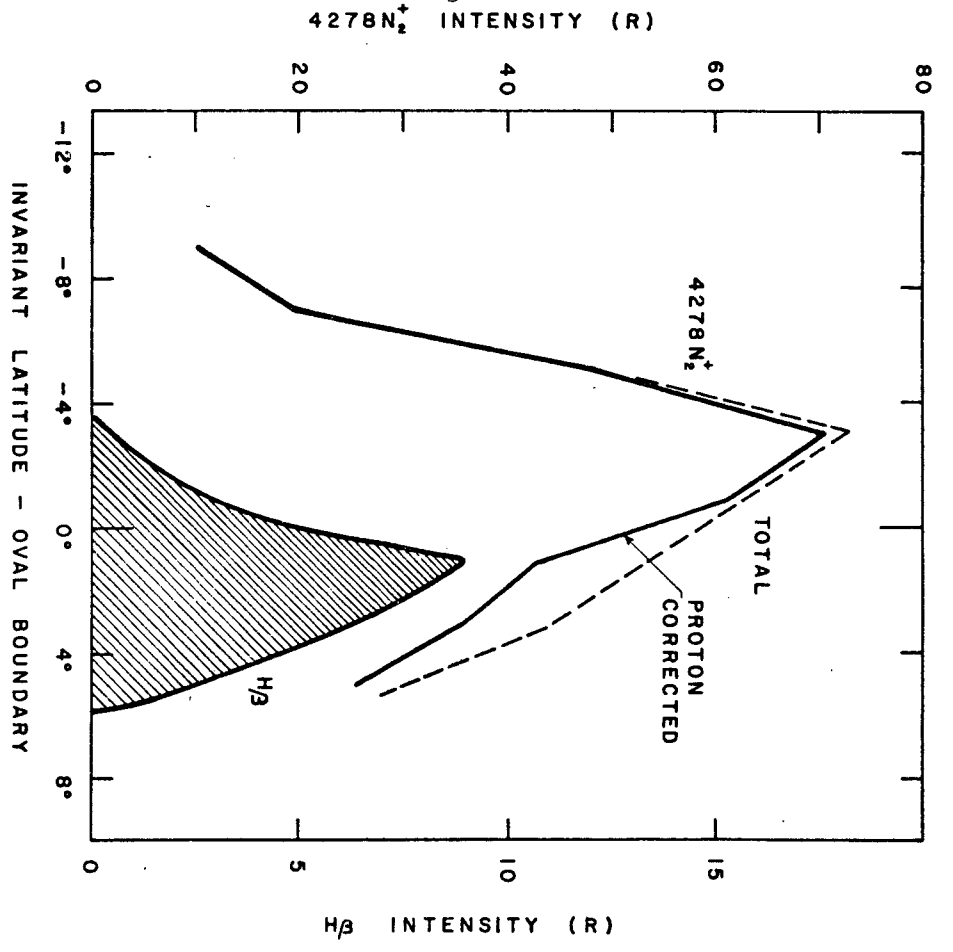
4278N₂⁺ INTENSITY (R)
0
20
40
60
80
INVARIANT LATITUDE - OVAL BOUNDARY
-12°
-8°
-4°
0°
4°
8°
4278N₂⁺
TOTAL
PROTON CORRECTED
Hβ
0
5
10
15
Hβ INTENSITY (R)

Fig. 2

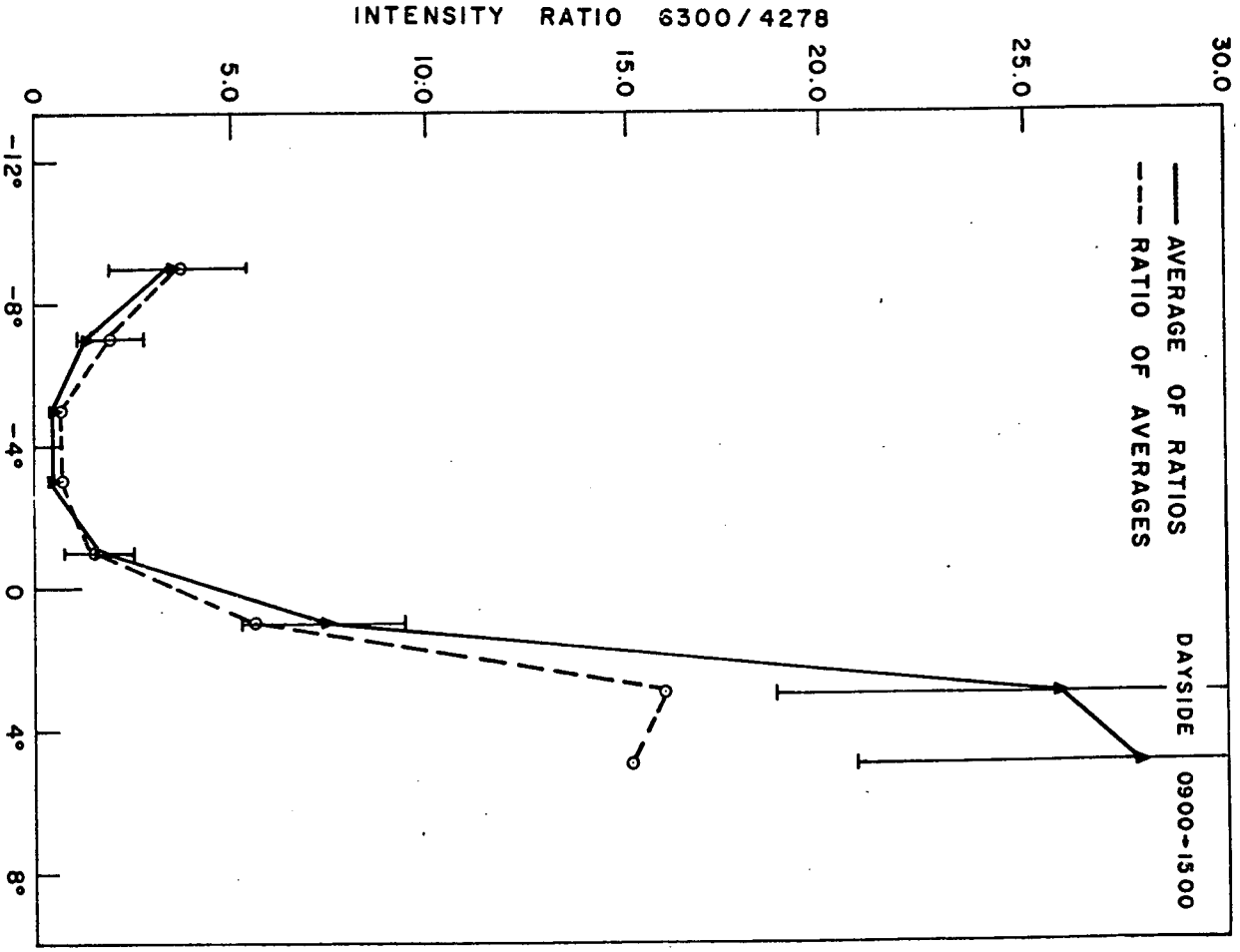
INTENSITY RATIO 6300/4278
0
5.0
10.0
15.0
20.0
25.0
30.0
-12°
-8°
-4°
0
4°
8°
INVARIANT LATITUDE - OVAL BOUNDARY
AVERAGE OF RATIOS
RATIO OF AVERAGES
DAYSIDE
0900-1500

Fig. 3

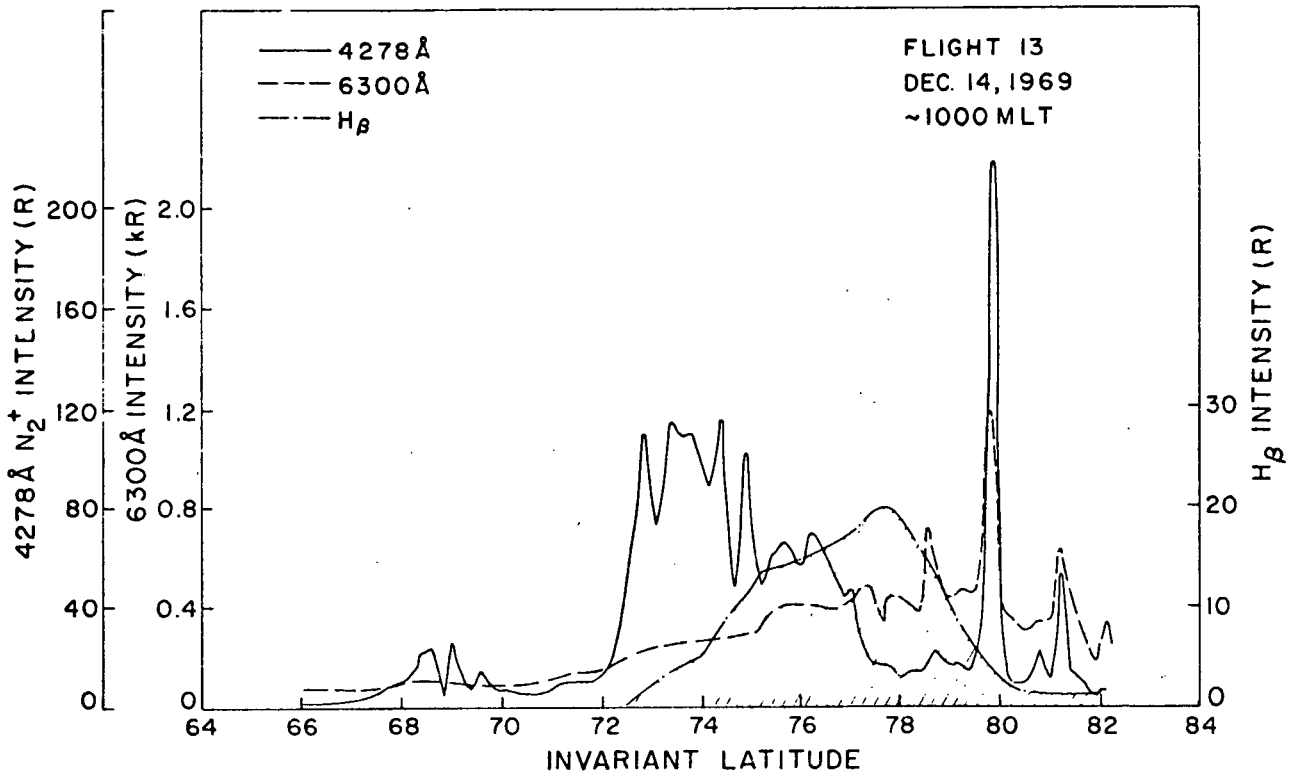
4278Å
6300Å
Hβ
FLIGHT 13
DEC. 14, 1969
~1000 MLT
4278Å N2+ INTENSITY (R)
6300Å INTENSITY (kR)
Hβ INTENSITY (R)
INVARIANT LATITUDE
64
66
68
70
72
74
76
78
80
82
84

Fig. 4

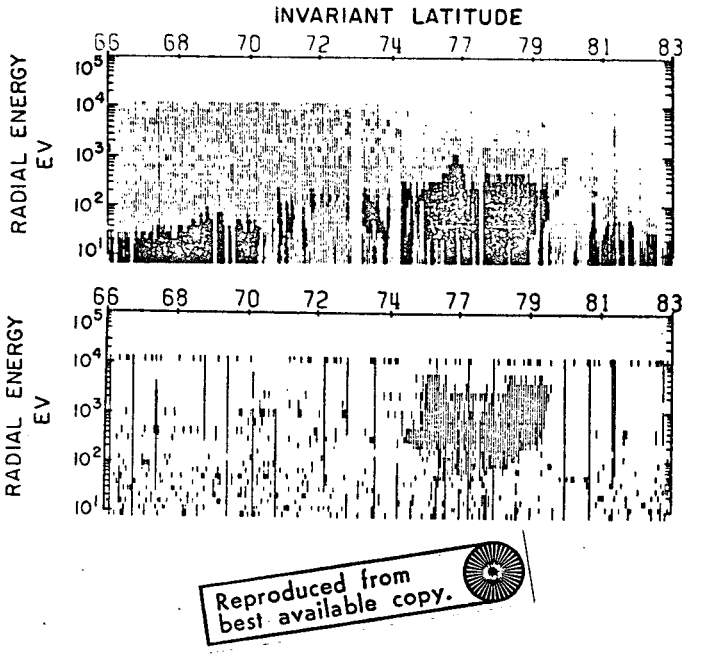

Reproduced from best available copy.

Fig. 5

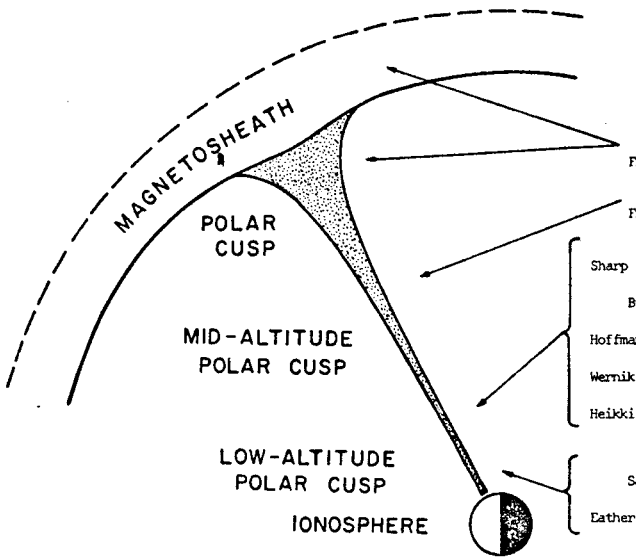

REF.	SOFT ELECTRONS TOTAL ENERGY (erg/cm² sec ster)	SOFT ELECTRONS SPECTRAL PEAK (eV)	SOFT PROTONS TOTAL ENERGY (erg/cm² sec ster)	SOFT PROTONS SPECTRAL PEAK (eV)
Frank (1970)	≤ .05	< 150	~ .06	~ 300
Frank (1970)			~ .04	~ 700
Sharp & Johnson (1968)	≤ 0.1+	≤ 1000*	> .02+	< 4000*
Burch (1968	.06 → .3	≤ 100		
Hoffman & Berko (1970)	.06 → .2+	< 700*		
Wernik et. al. (1970)	.03 → .3	~ 140		
Heikkila & Winninham (1970)	~ 0.2	100-200	.01 → .1	~ 300
Sandford (1964)	≥ .1			
Eather & Mende (1970	.03 (av.) .2 (peak)	100-200	.05	≤ 1000
PROBABLE AVERAGES:	0.1	100-200	0.05	~ 300

* Significant precipitation below this lower energy limit.

\+ Probably contains significant contribution from higher energies.

Fig. 6

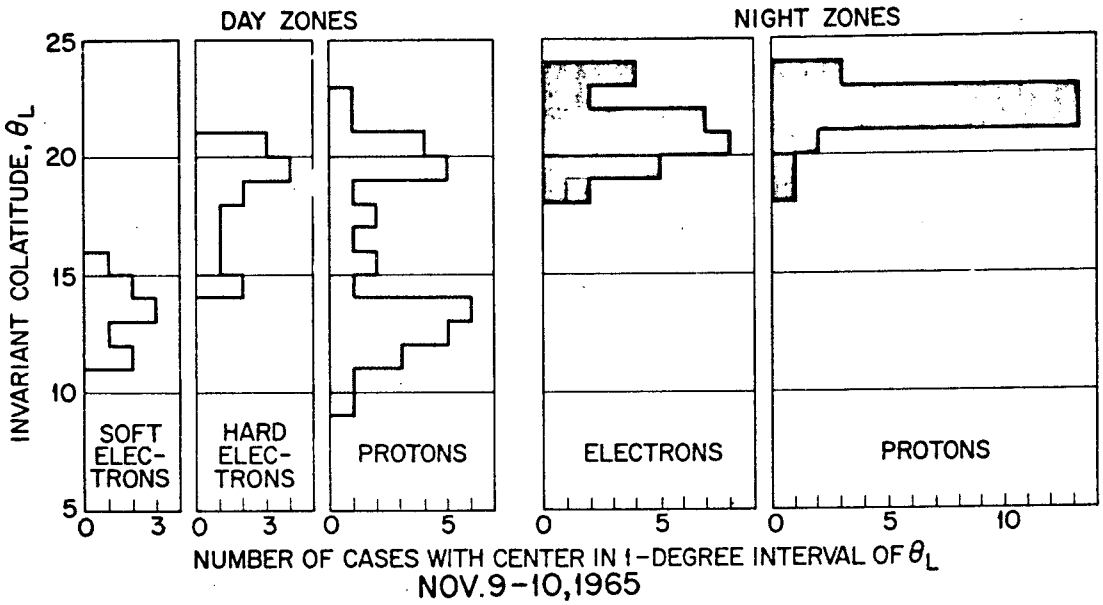
DAY ZONES
NIGHT ZONES
INVARIANT COLATITUDE, θ_L
25
20
15
10
5
SOFT ELEC-TRONS
HARD ELEC-TRONS
PROTONS
ELECTRONS
PROTONS
0 3
0 3
0 5
0 5
0 5 10
NUMBER OF CASES WITH CENTER IN 1-DEGREE INTERVAL OF θ_L
NOV. 9-10, 1965

Fig. 7

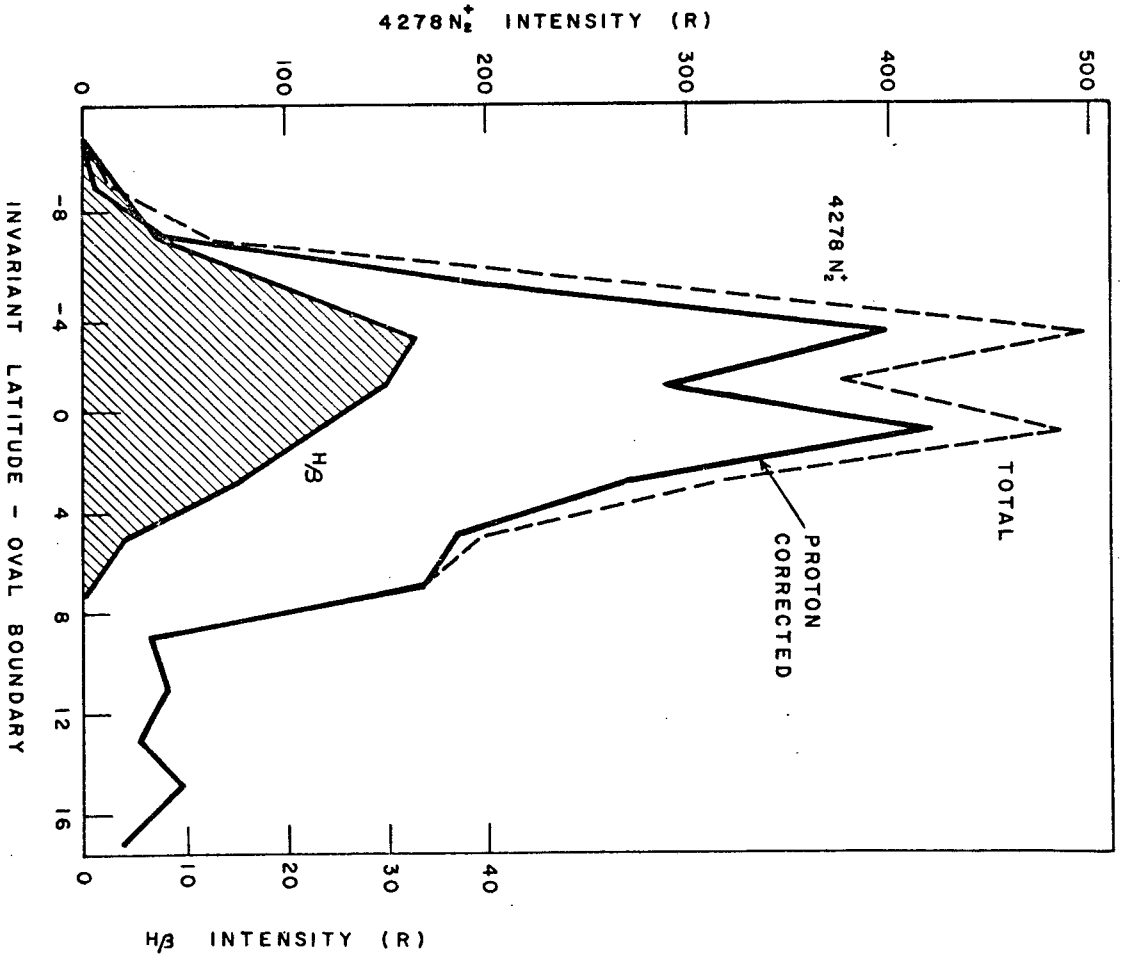
4278 N_2^+ INTENSITY (R)
0
100
200
300
400
500
INVARIANT LATITUDE - OVAL BOUNDARY
-8
-4
0
4
8
12
16
4278 N_2^+
Hβ
TOTAL
PROTON CORRECTED
0
10
20
30
40
Hβ INTENSITY (R)

Fig. 8

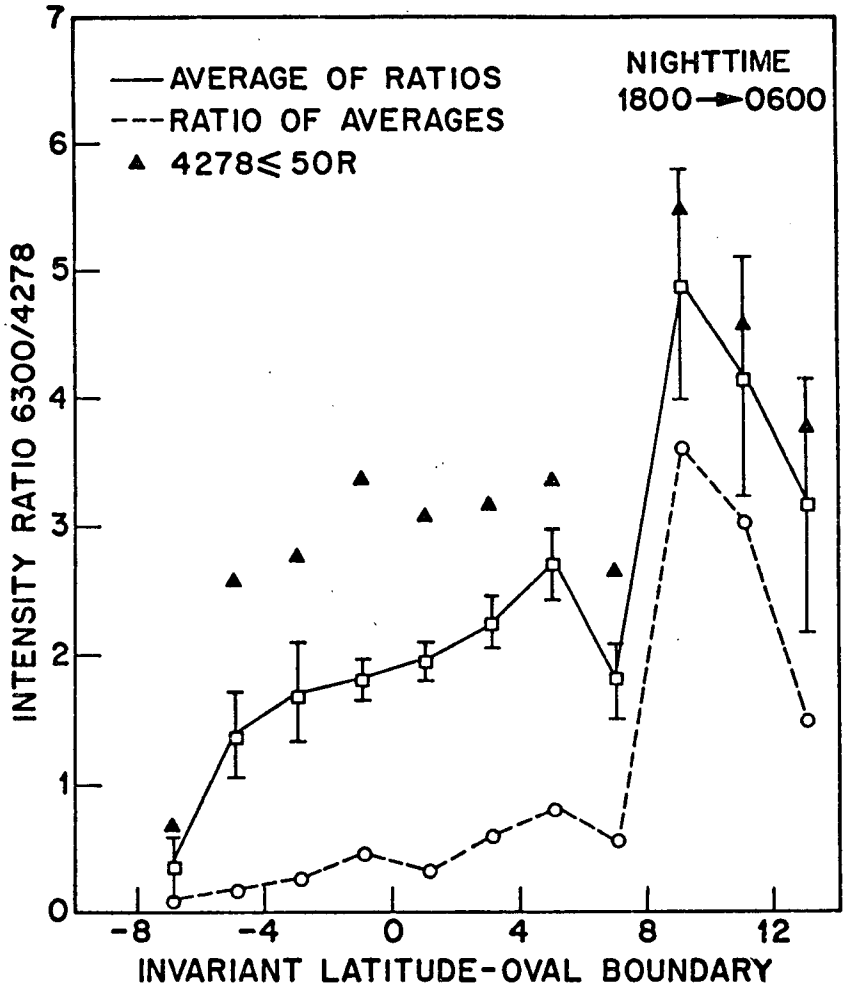
AVERAGE OF RATIOS
RATIO OF AVERAGES
▲ 4278≤50R
NIGHTTIME
1800→0600
INTENSITY RATIO 6300/4278
INVARIANT LATITUDE-OVAL BOUNDARY
0
1
2
3
4
5
6
7
-8
-4
0
4
8
12

Fig. 9

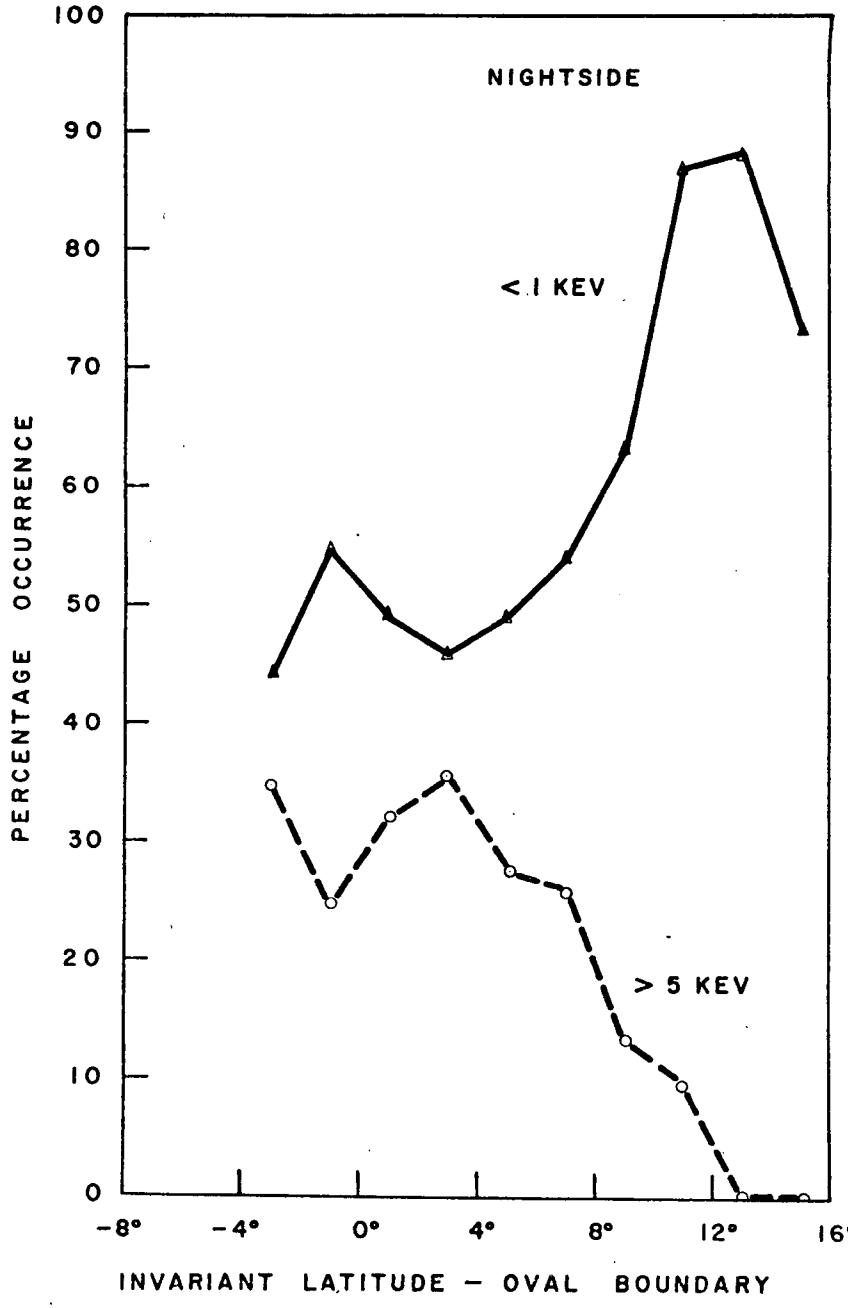
NIGHTSIDE
< 1 KEV
> 5 KEV
PERCENTAGE OCCURRENCE
INVARIANT LATITUDE - OVAL BOUNDARY
0
10
20
30
40
50
60
70
80
90
100
-8°
-4°
0°
4°
8°
12°
16°

Fig. 10

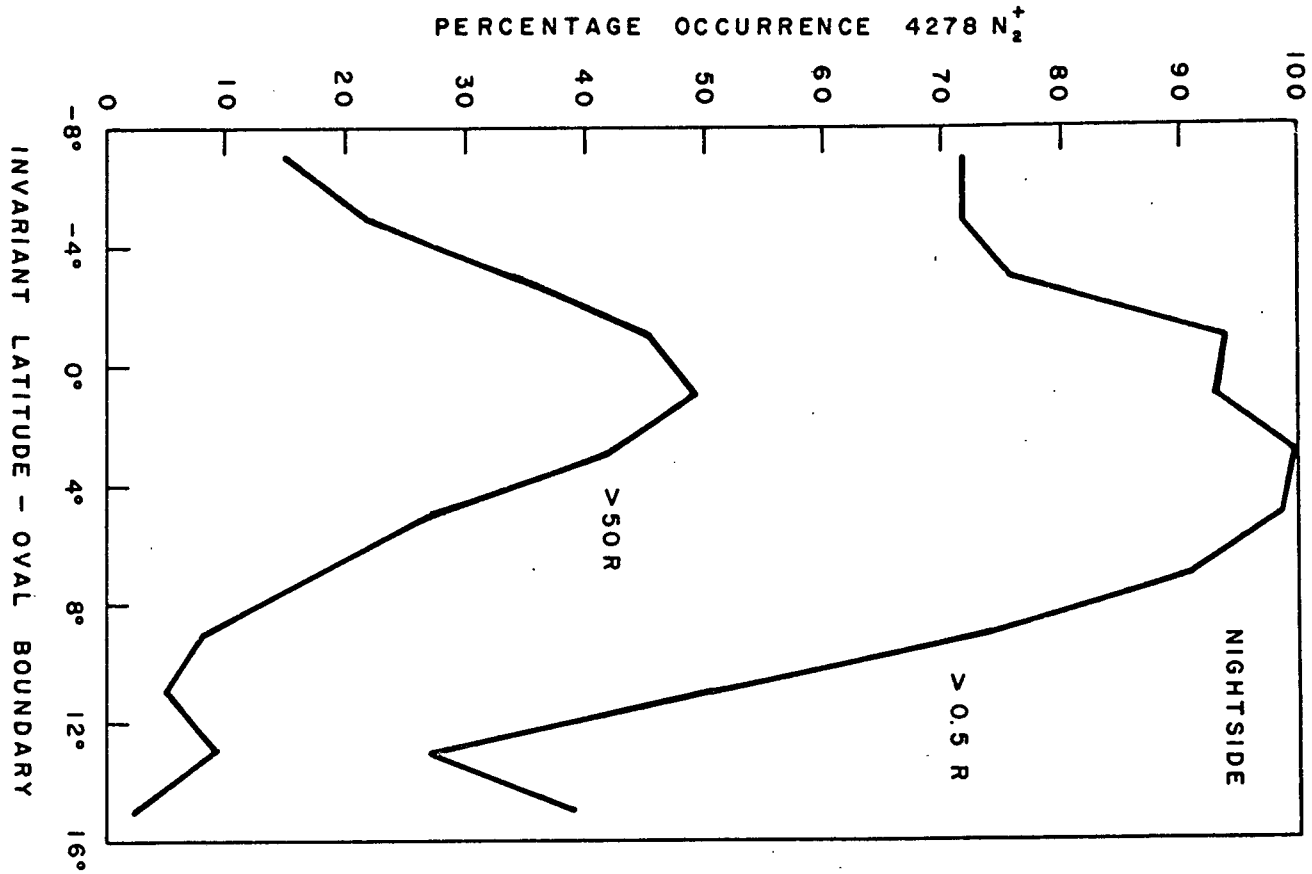
PERCENTAGE OCCURRENCE 4278 N_2^+
0
10
20
30
40
50
60
70
80
90
100
-8°
-4°
0°
4°
8°
12°
16°
INVARIANT LATITUDE - OVAL BOUNDARY
V 50 R
V 0.5 R
NIGHTSIDE

Fig. 11

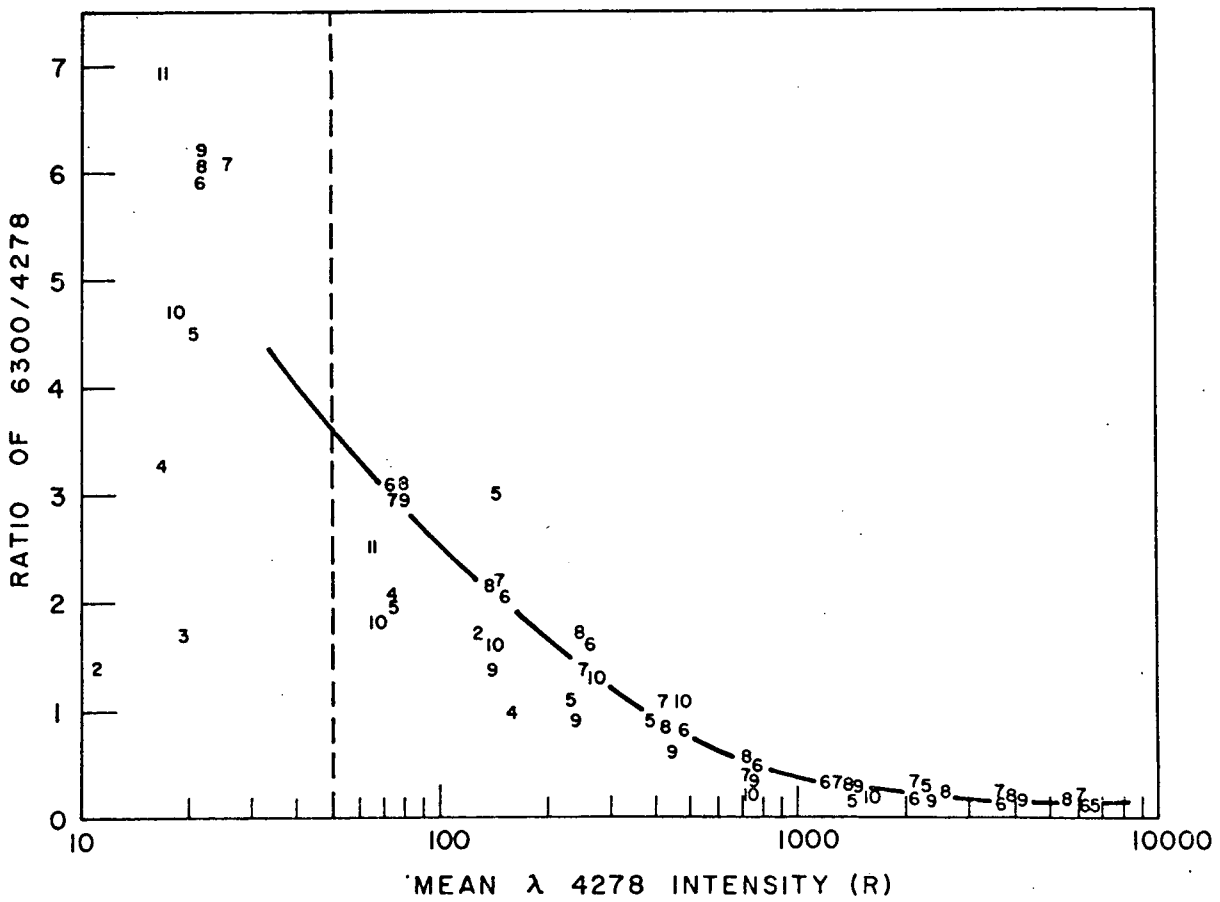
RATIO OF 6300/4278
0
1
2
3
4
5
6
7
10
100
1000
10000
MEAN λ 4278 INTENSITY (R)

Fig. 12

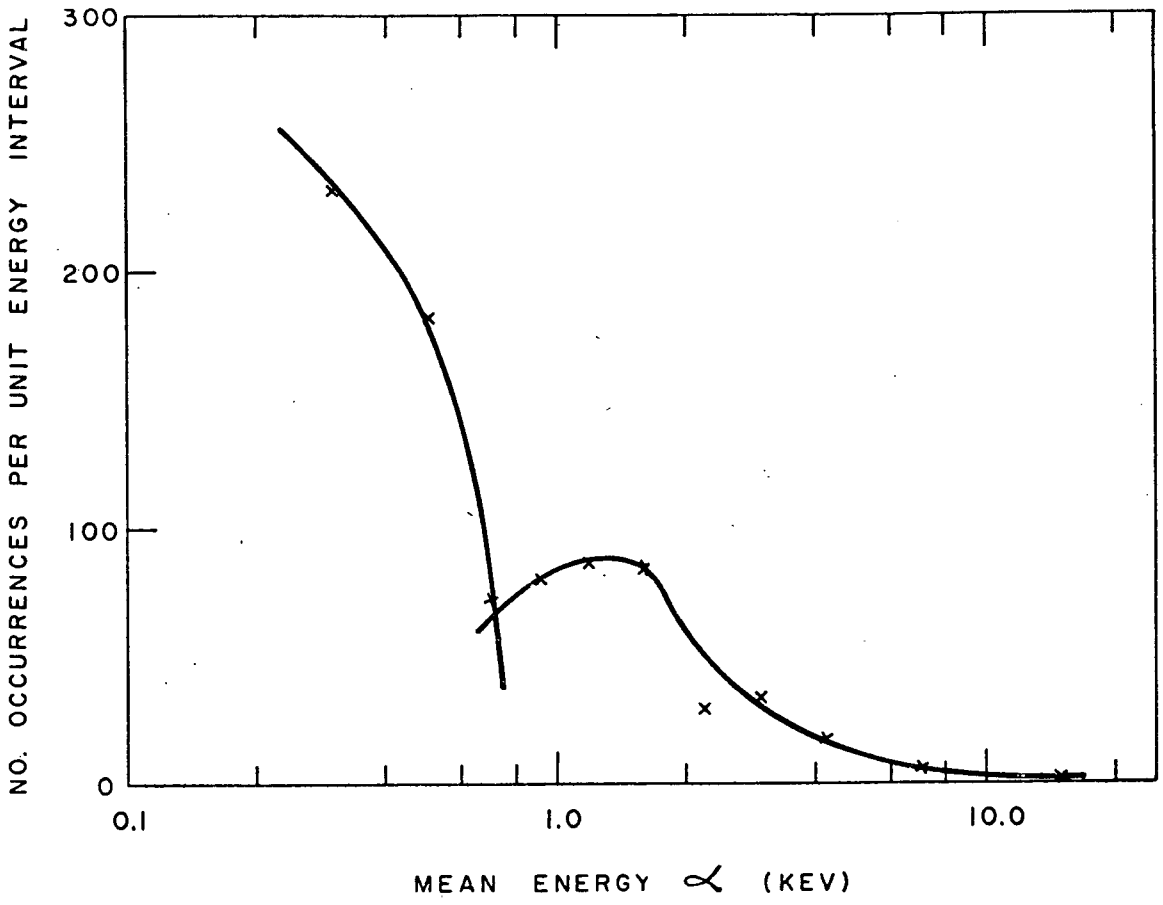
NO. OCCURRENCES PER UNIT ENERGY INTERVAL
300
200
100
0
0.1
1.0
10.0
MEAN ENERGY α (KEV)

Fig. 13

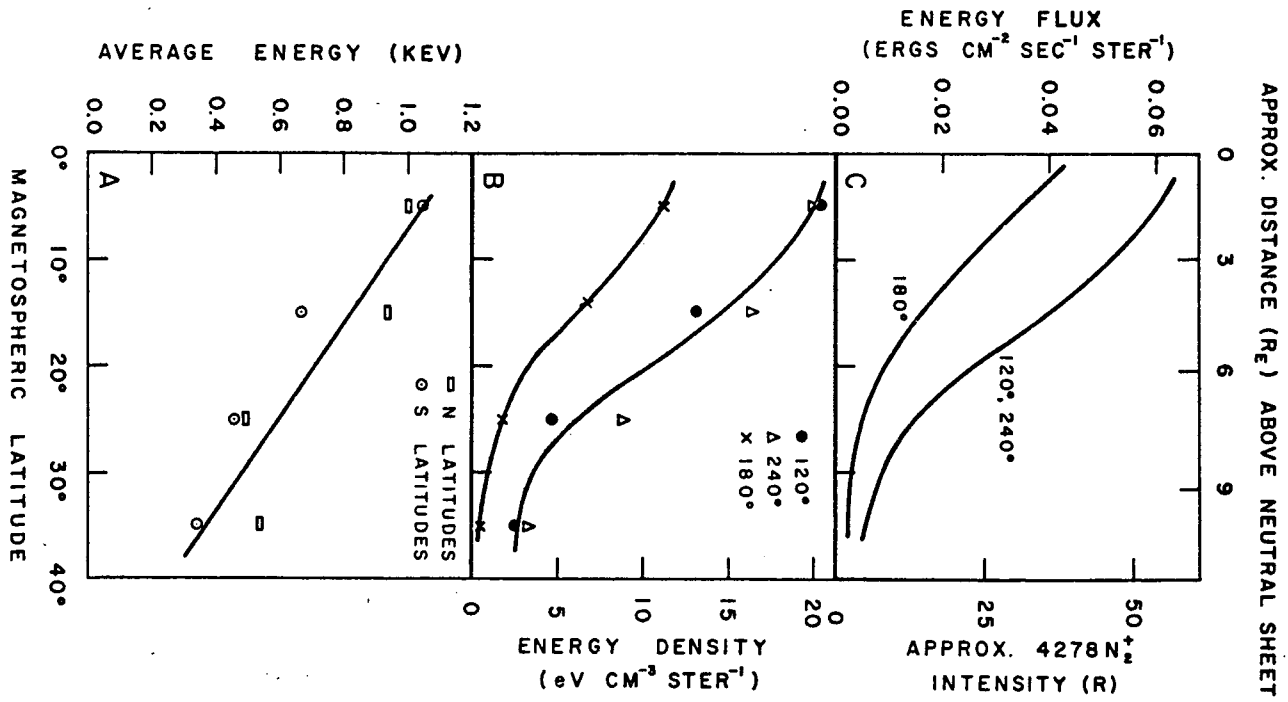
AVERAGE ENERGY (KEV)
0.0
0.2
0.4
0.6
0.8
1.0
1.2
ENERGY FLUX
(ERGS CM⁻² SEC⁻¹ STER⁻¹)
0.00
0.02
0.04
0.06
A
B
C
MAGNETOSPHERIC LATITUDE
0°
10°
20°
30°
40°
□ N LATITUDES
○ S LATITUDES
● 120°
Δ 240°
× 180°
180°
120°, 240°
0
5
10
15
20
25
50
ENERGY DENSITY
(eV CM⁻³ STER⁻¹)
APPROX. 4278N₂⁺
INTENSITY (R)
APPROX. DISTANCE (R_E) ABOVE NEUTRAL SHEET
0
3
6
9

Fig. 14

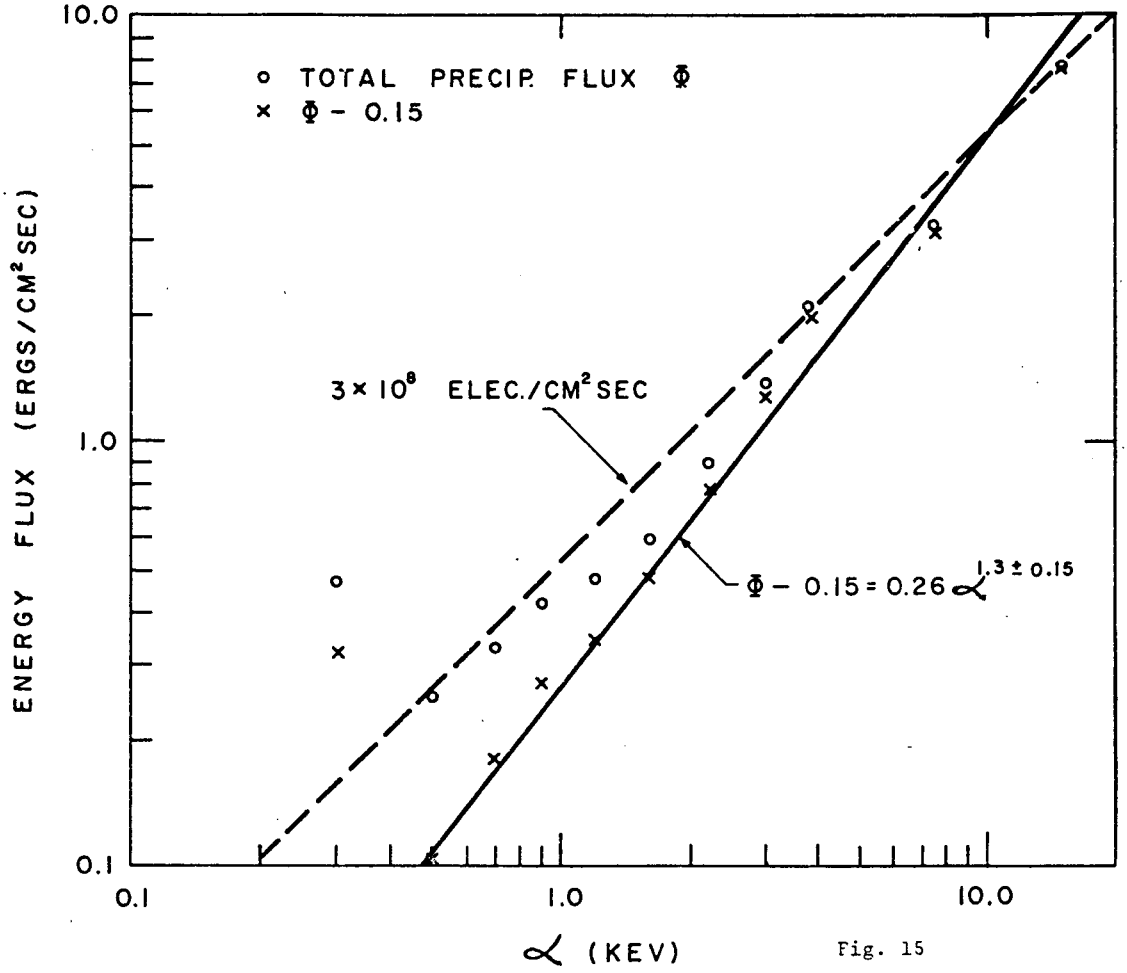

Fig. 15

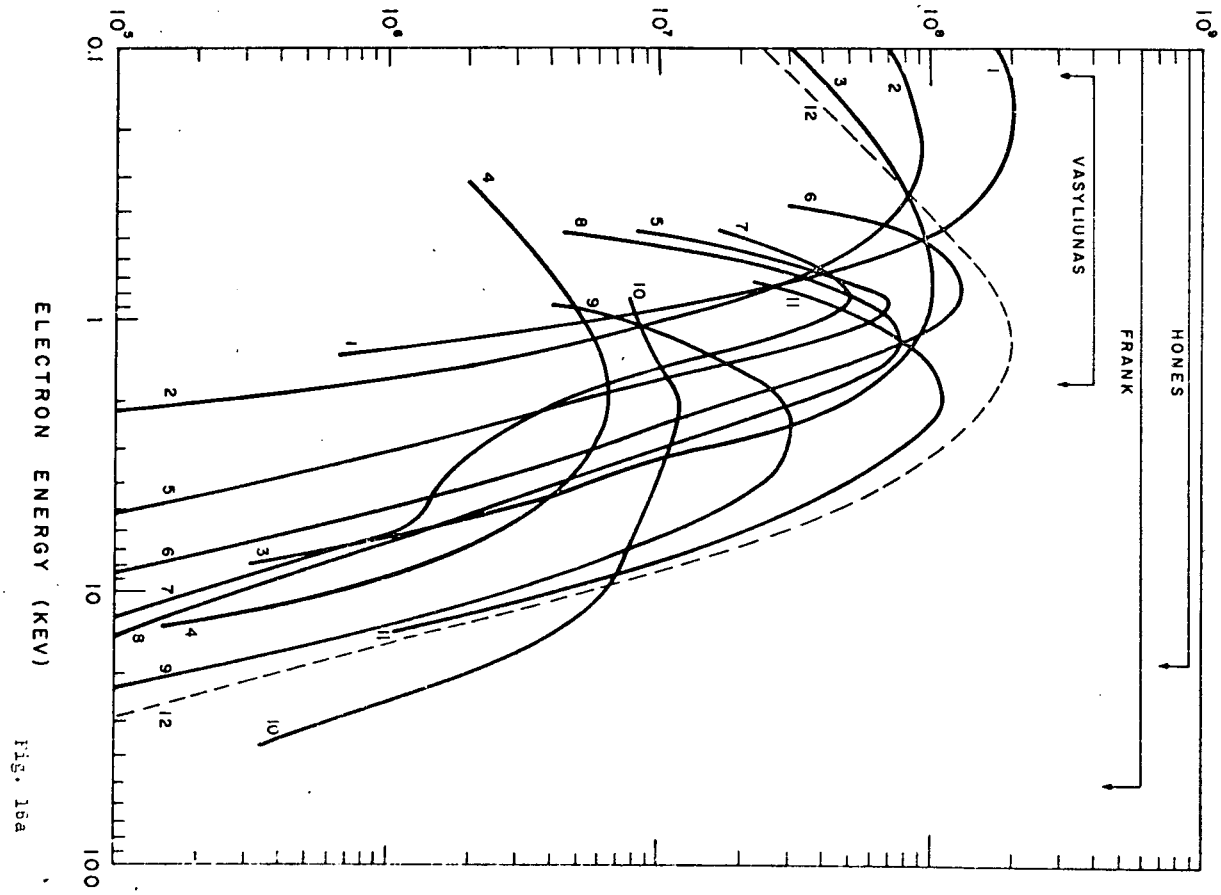

Fig. 16a

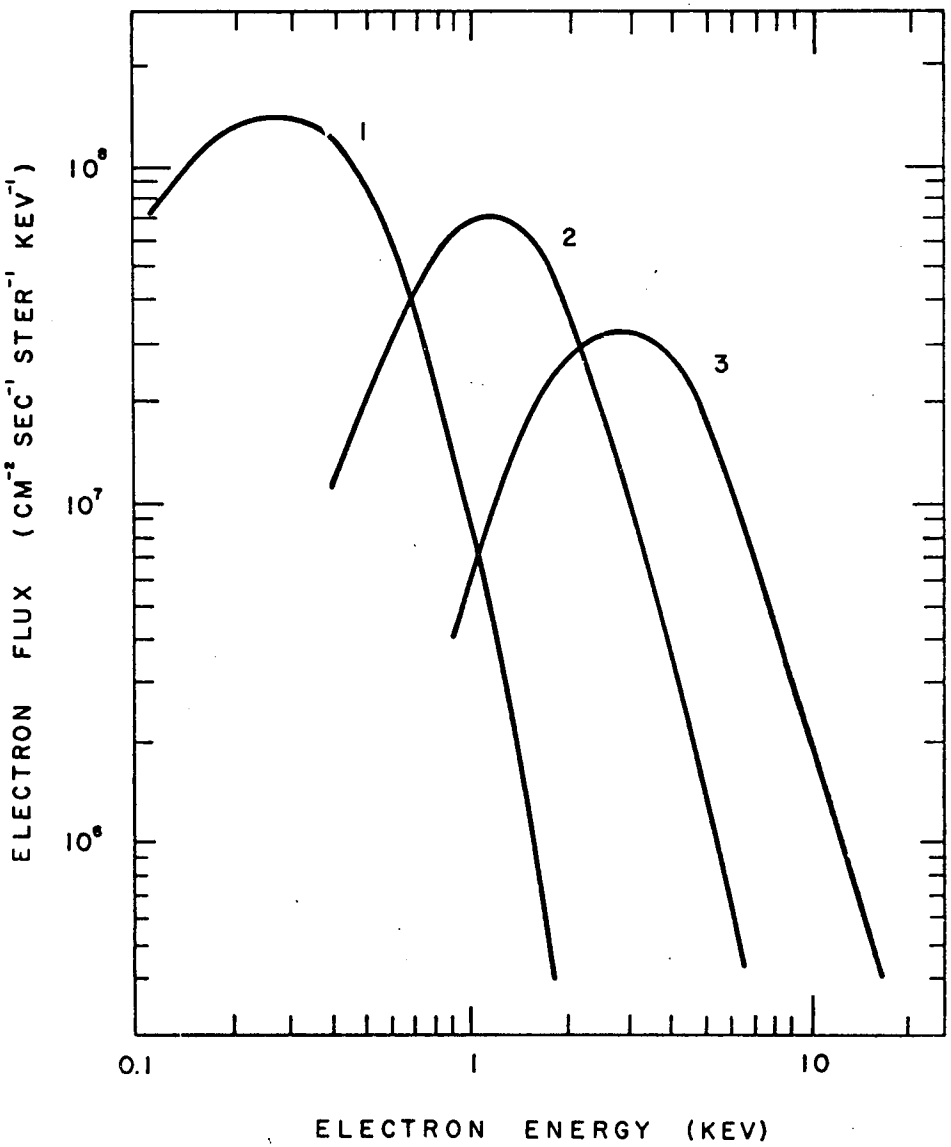

Fig. 16b

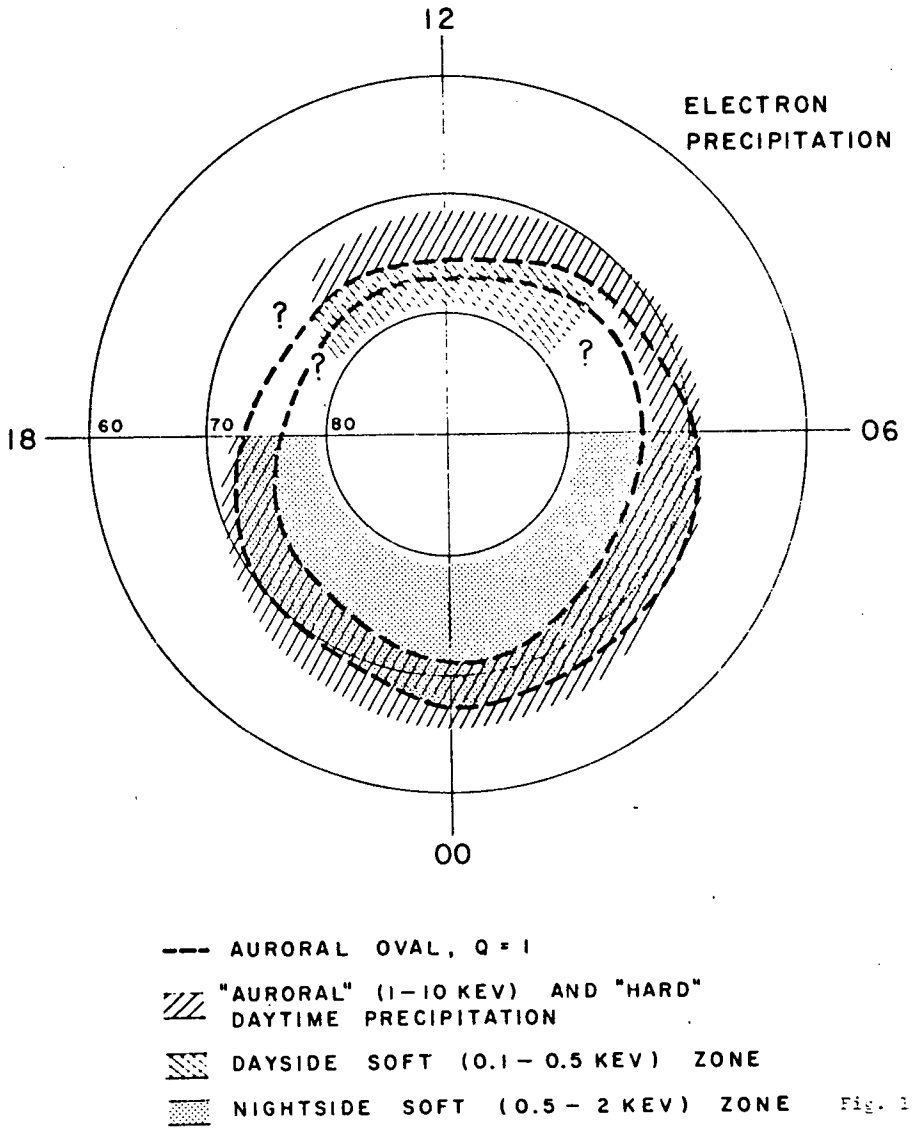

Fig. 17a

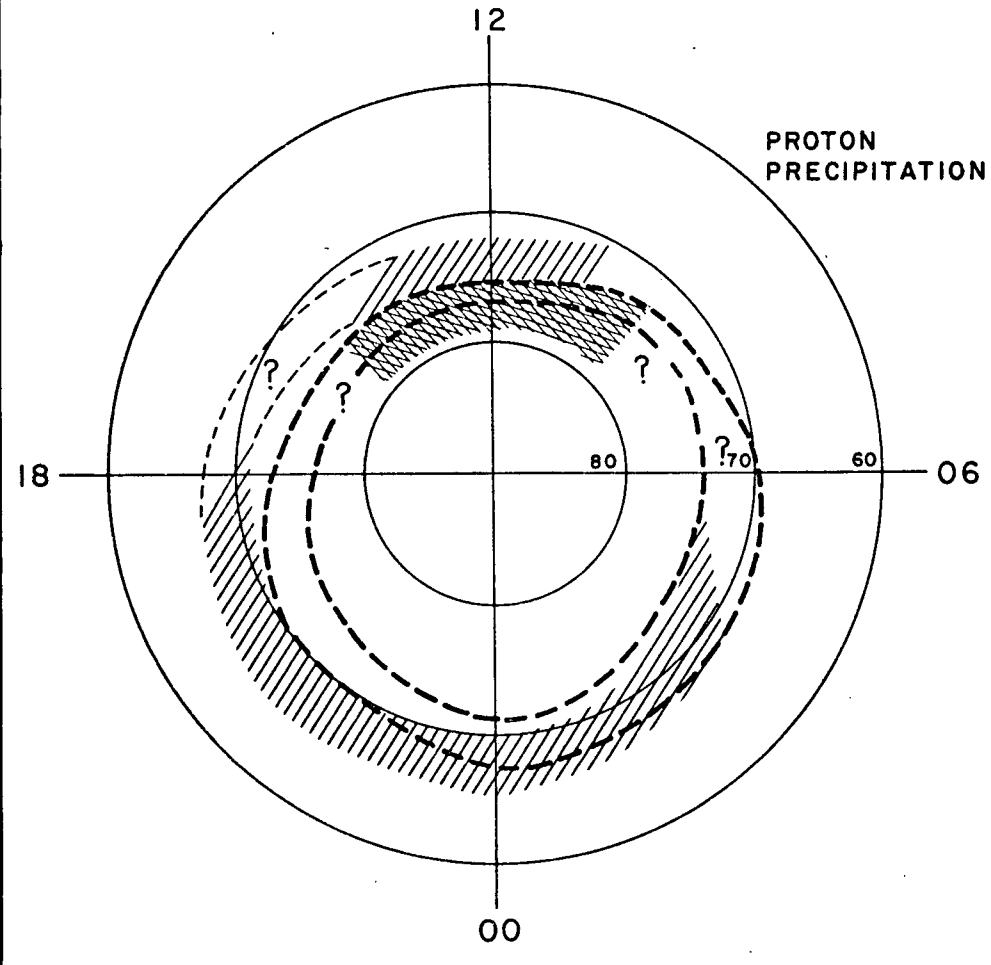

--- AURORAL OVAL, Q = 1

"AURORAL" (1–20 KEV) AND "HARD" DAYTIME PRECIPITATION

DAYSIDE SOFT (≲ 1 KEV) ZONE

Fig. 17b

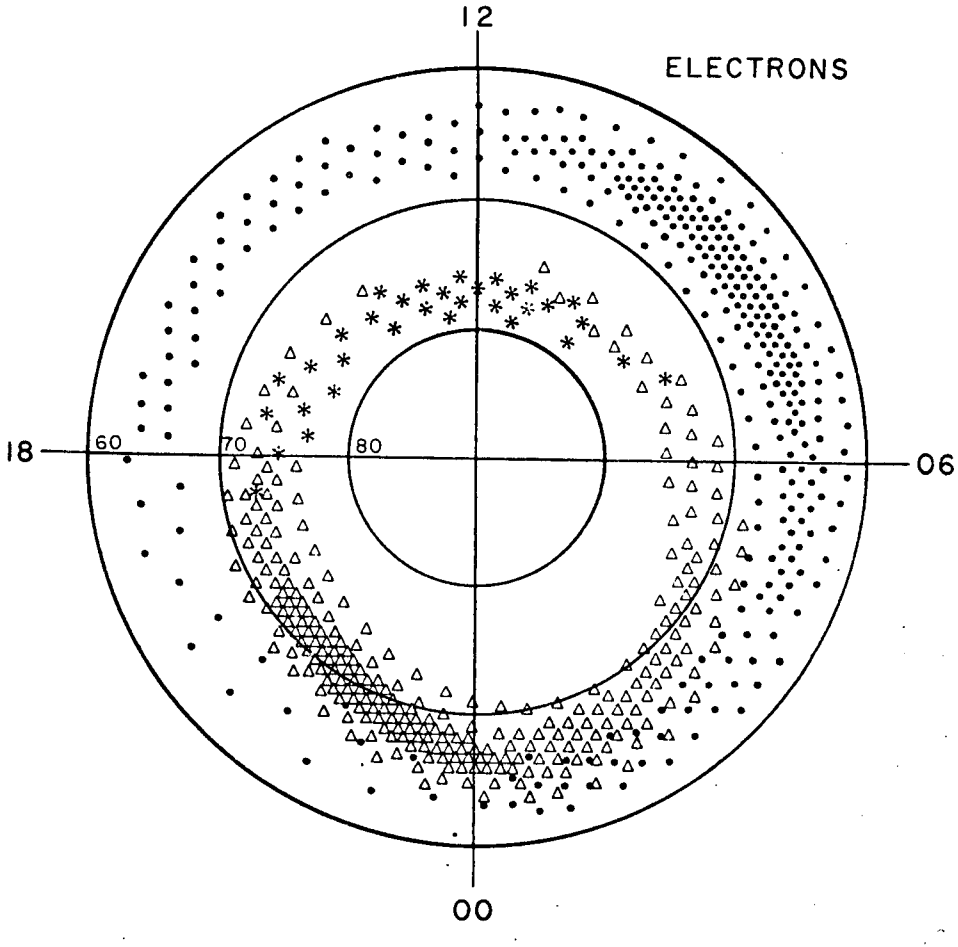

Fig. 18

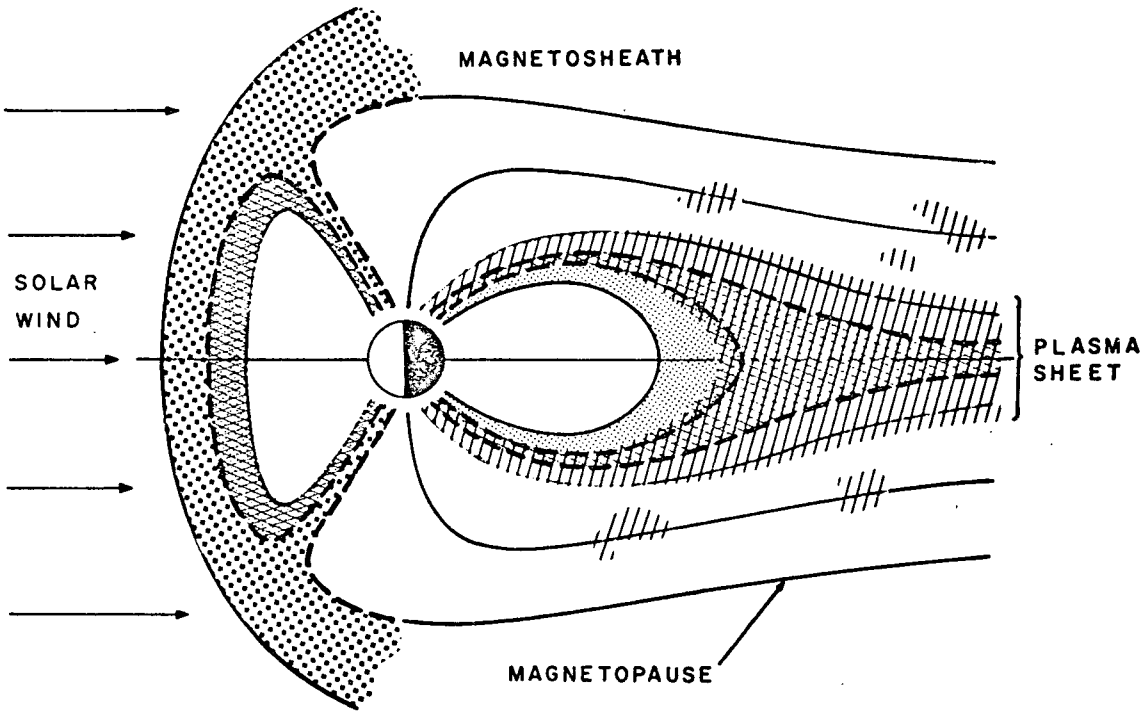

BOUNDARIES OF AURORAL OVAL

"AURORAL" (1 — 10 KEV) AND "HARD" DAYTIME PRECIPITATION

NIGHTSIDE SOFT (0.5 — 2 KEV) ZONE

PROTON RING CURRENT

DAYSIDE SOFT ZONE
ELECTRONS 0.1 — 0.5 KEV
PROTONS $\lesssim$ 1 KEV

(PATCHES) — POLAR CAP AURORA?

Fig. 19